NTNU – Trondheim
Norwegian University of
Science and Technology

Structural resistance of polar ships and FPSO´s to ice loading

Md. Mosfiqur Rahman

Marine Technology
Submission date: June 2012
Supervisor: Jørgen Amdahl, IMT

Norwegian University of Science and Technology
Department of Marine Technology

NTNU
Norwegian University of Science and Technology
Department of Marine Technology

Abstract

Due to the substantial increase in oil and gas activities in Polar areas the demand for ice strengthened vessel has increased greatly. This increase in demand has highlighted the importance of designing ice strengthened ship structures that are more producible and maintain adequate safety and integrity. In order to encounter these new challenges, the international association of classification societies (IACS) has developed unified regulations for the designing of ice strengthened ship. In addition to these requirements, most of the classification societies have their regulation for design of polar ships.

Stiffened plates are the basic structural building blocks of ships. So, the study mainly explores the plastic response of stiffened plate subject to lateral ice loads. The Non Linear Finite Element Method (NLFEM) is extensively used to study the plastic behavior of stiffened plates. The Abaqus non linear finite element program is used in this study.

The aims of the study are to investigate the validity of the limit state equation employed in the IACS new Unified Requirements for Polar Ships, investigate the membrane effect at large deformation, determine the ALS design load, and assess limit loads when fracture in plating likely to take place. The study also focuses on the warping effect of unsymmetrical sections and the effect of end brackets on the lateral load carrying capacity of the stiffener. The effect of mid-span tripping bracket on the load deflection behavior of L and T stiffeners is also studied. In particular, the study focuses on the behavior of inclined T and L stiffener.

As ships move forward by crushing ice, sides of ships' bow come across with ice initially. To design ice strengthened vessel, it is very important to understand the behavior of ships' side structure subjected to ice loads. So, this study extensively focuses on the non-linear finite element analysis of ships' side structure subjected to ice loads. Normally ship design rules are based on the behavior of single frame subjected to loads. It is reasonable to consider frames singly under the uniform loading but in case of ice loading which is non uniform, the behavior of the structure obtained from single frame based design does not accurately represent the true behavior of the structure. The load-deflection characteristic of frames in isolation, frames as part of a ½+1+½ frames and frames as part of a grillage subjected to unsymmetrical loading is studied. As stiffeners in the side structure of ships' bow are not normally perpendicular with shell plate, the lateral capacity of frames as part of a ½+1+½ frames and as part of a grillage is obtained for inclined stiffener.

The analyses in this study cover the full range of stiffener behavior from elastic, through yield, through the formation of initial mechanisms, through large deformations. The parameters considered for the analyses are:

- frame profile: Angle, Tee
- frame span

- load length: patch (transverse), uniform (longitudinal)
- web thickness
- end brackets: with, without
- inclination angle of stiffener web with the plate flange
- Tripping bracket at mid span

By observing the load-deflection characteristic of L and T frames for 45 degree to 80 degree inclination of stiffener web, it is found that L frames exhibit higher capacity at large deformation. In the elastic region and onset of plastic deformation no significant difference in lateral load carrying capacity is observed, when stiffener web of L frame has sufficient strength to counteract the warping effect.

Preface

This master thesis is carried out for the partial fulfillment of the requirements for Master of Science degree program at the department of Marine Technology, Norwegian University of Science and Technology (NTNU) in Trondheim, Norway.

The work of the thesis is performed in spring 2012. In the time frame of this thesis, some of the items given in the problem text had to be omitted in consultation with supervisor Professor Jørgen Amdahl.

I would like to express my profound gratitude to my honorable supervisor Professor Jørgen Amdahl for his advice and unique support throughout this study.

Trondheim, 10th of June 2012

Md. Mosfiqur Rahman

Contents

Table of Figures

Table of Tables

Nomenclature

A_f	Stiffener Flange Area
Aw	Stiffener Web area
AR	Aspect ratio
b	Patch load length
b_w , Wf, b_f	Width of stiffener flange
C_o	*Mass reduction coefficient*
CF_c	Crushing class factor
CF_D	Patch class factor
CF_F	Flexural class factor
D_{ship}	Ship displacement
E_{crush}	Ice crushing energy
E_s	Secant modulus
E_T	Tangent modulus
F_n	Normal force
h_w	Stiffener web height
h_{ice} , h_i	Ice thickness
h_{fc}	Height of stiffener measured to the center of the flange area
K	stiffness
K_I	Tangent stiffness or increment stiffness
KE_n	Normal Kinetic Energy
L	frame length
M	Bending moment
M_e	effective mass
M_p	Plastic bending moment
M_{pfo}	Bending moment relative to the flange edge
M_{pr}	Reduced Plastic bending moment
M_{ship}	Ship mass
M_{pw}	Bending moment at mid-span in the flange
P	Pressure
P_0	Class dependent ice pressure
P_{3h}	IACS UR limit state load for 3 hinge collapse
Q	Line load
R	External load
r	displacement
S	Stiffener spacing
T	Shear
t_f	Flange thickness
t_p	Plate thickness
t_w	Stiffener web thickness
UR	IACS unified requirment
Ux	Translation in x direction
Uy	Translation in y direction
Uz	Translation in z direction
URx	Rotation about x axis
URy	Rotation about y axis
URz	Rotation about z axis

V_{ship}	Ship velocity
V_n	normal velocity
Z, Zp	Plastic section modulus
Zw	Plastic section modulus of stiffener web
σ	stress
σ_f , σ_y	Yield stress
ϵ	strain
δ	Normal ice penetration, deflection
φ_w	Angle between the shell plate and the flange side of web

Chapter 1

1 Introduction

The cold and severe Arctic climate is expected to be a major challenge for future development of hydrocarbons, since a lot of the remaining reservoirs are located just in such areas. Many oil companies are involved in projects regarding exploration of oil and gas in ice infested water, and a lot of money is invested. Because the Arctic is covered with ice in large parts of the year it is necessary to design both ships and platforms to withstand the loading from ice interaction. The importance of a proper set of rules for dimensioning is not just due to safety for personnel and structures, but an oil spill in these areas will also be very unfortunate for the vulnerable wildlife and nature.

This report mainly contains:

1. Literature review of polar classes, design ice loads, ice pressure-contact area relationship, IACS & DNV framing rule requirements, theory behind non-linear finite element analysis, Abaqus non-linear finite element analysis.
2. Modeling procedures of ships' side frames in Abaqus.
3. Simulations and Analysis of ships' side frames in Abaqus and compare the results with IACS UR limit state loads.

Background of polar classes, design ice loads and ice pressure-contact area relationship presented in chapter 2 were studied to gain extensive knowledge about how the ice loads act on the ships' structure and varies with the contact area and what factors govern the different polar classes. IACS and DNV rules requirements for framing presented in chapter 3 were studied to understand the collapse mechanisms of frame used in developing the rule requirements for framing for the respective classification societies. To gain insight about the solution technique, convergence of solution of non-linear finite element analysis, finite element discretization technique of structure and how non-linearities arise when structure subject to loads were studied and described in chapter4 and chapter5. In chapter 6, modeling technique of ships' side structure in Abaqus has been described briefly.

Simulations and analysis of ships' side frames and panels have been presented in chapter 7. Load-deflection characteristic of frames in isolation and frames as part of a ½+1+½ frames and as part of a grillage has been described. The effect of end brackets, mid-span tripping bracket, web inclination, web thickness, frame span length and patch load length on the load deflection characteristic of different frame sections has also been described.

Chapter 2

2 Background to Ice Classes, Ice design loads and Ice pressure area relationship

2.1 Introduction

When designing a ship to operate in polar area, the designer needs knowledge of how ice is acting on the ship and how this interaction is modeled. Ice conditions, ice environment and ice strength were studied in order to gain insight about how ice is acting on the ship and magnitude of ice force exerted on the ship. The definition of different polar classes is based on these parameters. For example, polar classes defined in the IACS [6] have been shown in Table 1. The derivation of ice load from the ship-ice interaction is described followed by the description of ice load dependency with contact area in this chapter.

Table 1 Polar classes

POLAR CLASS	ICE Description (based on WMO sea Ice Nomenclature)
PC 1	Year round operation in all Polar Waters
PC 2	Year round operation in moderate multi-year ice conditions
PC 3	Year round operation in second year ice which may include multi-year ice inclusions.
PC 4	Year round operation in thick first year ice which may include old ice inclusions.
PC 5	Year round operation in medium first year ice which may include old ice inclusions.
PC 6	Summer/Autumn operation in medium first year ice which may include old ice inclusions.
PC 7	Summer/Autumn operation in first year ice which may include old ice inclusions.

2.2 Overview of the different IACS POLAR classes

All of the major classification societies have their own set of rules intended for ships operating in polar waters. DNV [12] has mainly divided the ice requirement into two major parts, one is covering Baltic equivalent areas and another one is covering the Arctic and Antarctic waters as mentioned above. For ships intended to operate in Baltic waters or in areas with similar ice conditions, the rules are mainly built in accordance with the Finnish-Swedish Ice Class rules. This division of Baltic and Arctic classes is recognized in the rules of many societies, among others American Bureau of Shipping (ABS) and Lloyds Register (LR). However, both the RS and IACS ice requirements offer only one set covering both Baltic and Polar conditions, where the lowest classes are assumed capable of meeting the structural requirements given in the Baltic codes. According to [15], PC7 and PC6 are equivalent to the Finnish Swedish ice class 1A and 1A super respectively.

In the development of the UR IACS rules, a lower and an upper bound class were decided. The lower bound was set such that the ship should be sufficiently strength to meet the ice conditions in the Baltic. This class is PC7 described in Table 1. PC1 acts as an upper bound that covers ships which can operate in all polar waters at any time of the year. IACS has selected a set of seven classes, which is in accordance with many of the other systems existing today [15]. For ships which may be exposed to repeated ramming an additional set of rules must be applied than that of PC1.

2.3 IACS ICE DESIGN LOADS

Ice Design load is based on Design scenario of ship ice interaction. The design scenario that form the basis of the ice loads for plating and framing design is a glancing collision on the shoulders of the bow [16] (see figure 1). The ship is assumed to be moving forward at the design speed, striking an angular ice edge as it penetrates the ice and bounds the ice away. The ship speed, ice thickness and the ice strength are assumed to be class dependent. The maximum force is found by equating kinetic energy with the energy used to crash the ice. The ice crushing force cannot exceed the force required to fail the ice in bending. The combination of angles, ice strength and thickness determine the force limit due to bending.

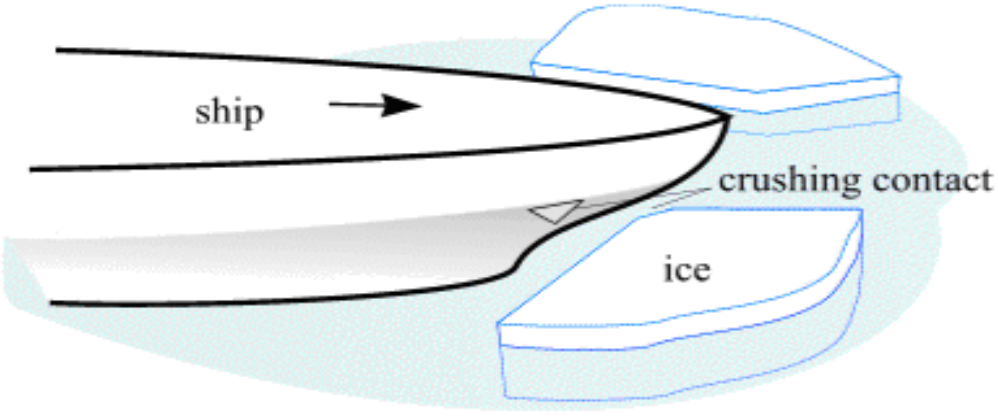

Design scenario 1 - glancing collision on shoulder

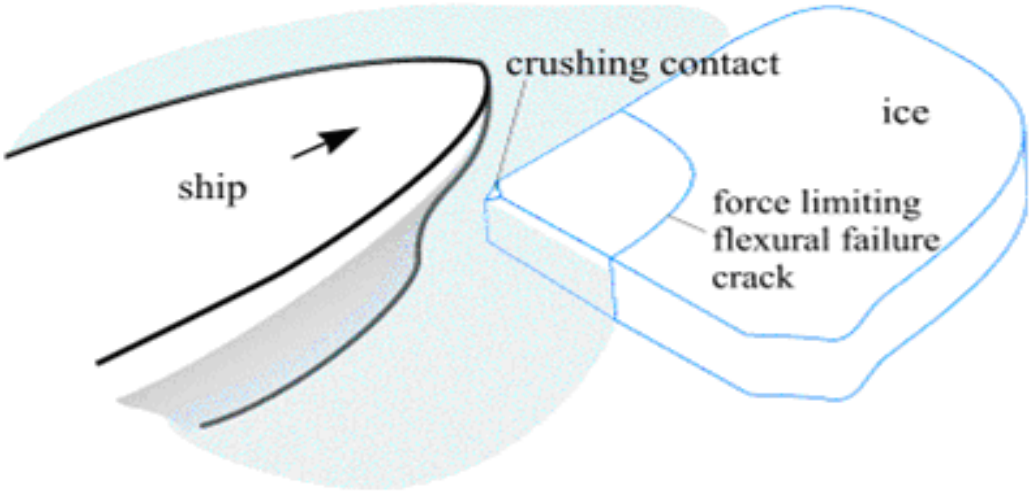

Design scenario 2 - flexural failure during glancing collision

Figure 1 Design scenario, flexural failure during glancing collision

The design scenario described above is strictly valid for the bow region, and for the stern of double acting ships. Loads on the other hull areas are set as a proportion of the bow area by using empirical hull area factors. The loads on other hull areas not strongly dependent on bow angles, and so bow loads are normalized using a 'standard' set of bow angles before being applied elsewhere [16].

The design loads are developed in several stages. First, the load is found as the minimum of the crushing and flexural limiting loads for the design ice. Second, the patch over which this load is applied is determined and idealized. Third, the distribution of load within the patch is modified to account for local loading peaks.

The force that results from a ship striking an ice edge is derived. The mechanics are based on the Popov collision but are modified to include a wedge shaped ice edge and a pressure/area ice indentation model.

The force is found by equating the normal kinetic energy with the ice crushing energy,

$$KE_n = E_{crush} \tag{2.1}$$

The crushing energy is found by integrating the normal force over the penetration depth, δ,

$$E_{crush} = \int_0^{\delta} F_n(\delta) \cdot d\delta \tag{2.2}$$

The normal kinetic energy combines the normal velocity with the effective mass at the collision point,

$$KE_n = \frac{1}{2} M_e \cdot V_n^2 \tag{2.3}$$

Substituting equations (2.2) and (2.3) into equation (2.1);

$$\frac{1}{2} M_e \cdot V_n^2 = \int_0^{\delta m} F_n(\delta) \cdot d\delta \tag{2.4}$$

Where

δ = normal ice penetration,

F_n = normal force

M_e = effective mass (= M_{ship}/Co)

Co= Mass reduction coefficient

V_n = normal velocity (=V_{ship} *l)*

l = direction cosine

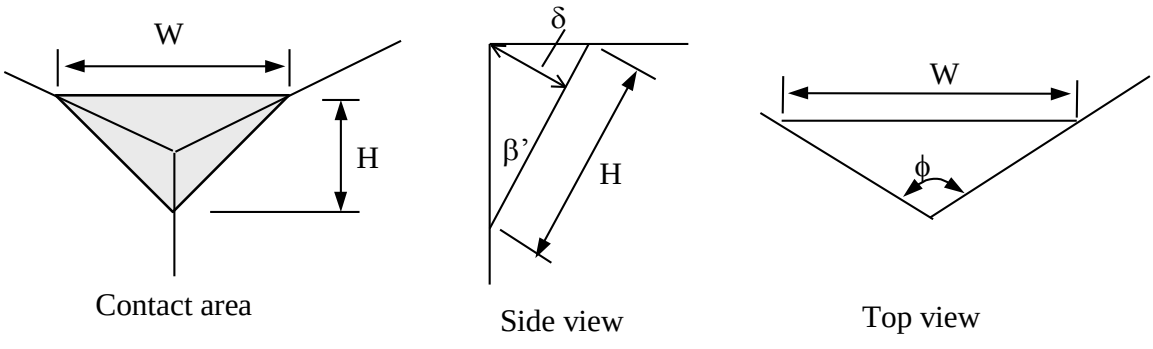

Figure 2 Nominal contact geometry during oblique collision with an ice edge.

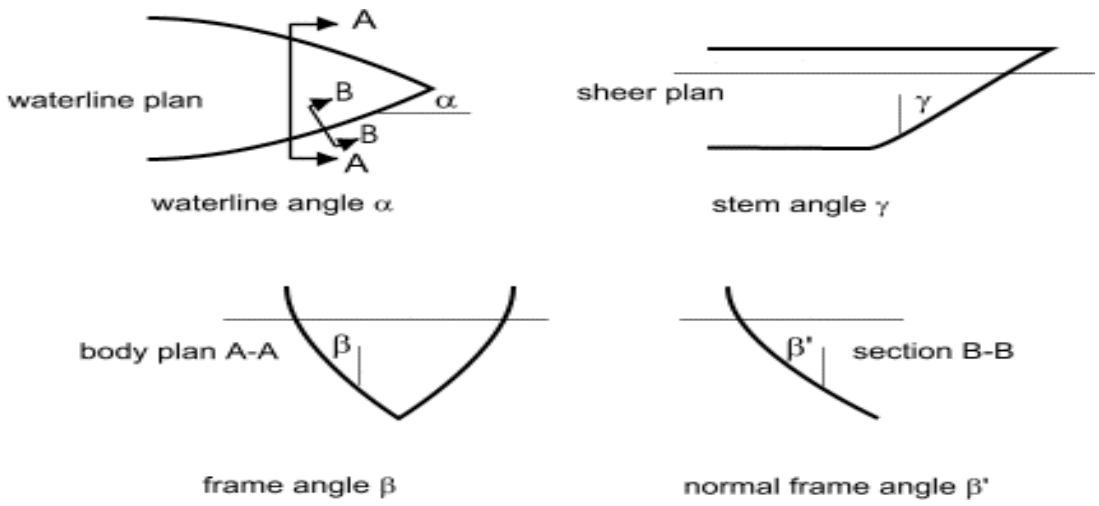

Figure 3 Definition of hull angles, Daley [16]

The nominal contact area is found from figure 2 as follows

$$A = \frac{1}{2}WH \qquad (2.5)$$

Where,

$$W = \frac{2\delta tan\left(\frac{\emptyset}{2}\right)}{\cos(\beta')} \qquad (2.6)$$

$$H = \frac{\delta}{\sin(\beta')\cos(\beta')} \qquad (2.7)$$

Hence the area become

$$A = \frac{\delta^2 tan\left(\frac{\emptyset}{2}\right)}{(\cos(\beta'))^2 \sin(\beta')} \qquad (2.8)$$

The average pressure is found from the pressure-area relationship,

$$P = Po\, A^{ex} \qquad (2.9)$$

Where, $P_0 = class\ dependent\ ice\ Pressure\ at\ 1m^2, [MPa]$

ex = pressure area exponent, assumed -0.1,

The normal force become

$$F_n(\delta) = P\, A = Po\, A^{1+ex} \qquad (2.10)$$

$$F_n(\delta) = Po\, ka^{1+ex}\ \delta^{2+2ex} \qquad (2.11)$$

Where,

$$ka = \frac{\delta^2 tan\left(\frac{\emptyset}{2}\right)}{(\cos(\beta'))^2 \sin(\beta')} \qquad (2.12)$$

Substituting equation (2.11) into equation (2.4) the following expression is found,

$$\frac{1}{2} M_e \cdot V_n^2 = Po \cdot ka^{1+ex} \int_0^{\delta m} \delta^{2+2\cdot ex} \cdot d\delta \qquad (2.13)$$

After some calculation this equation end up as follows

$$F_n = fa \;\; Po^{0.36} \;\; V_{ship}{}^{1.28} \, D_{ship}{}^{0.64} \qquad (2.14)$$

Where, $D_{ship} = Ship\ displacement$

Crushing class factor is defined as;

$$CF_C = \;\; Po^{0.36} \;\; V_{ship}{}^{1.28} \qquad (2.15)$$

So, Equation (2.14) become

$$F_n = f_a . CFc . D_{ship}{}^{0.64} \qquad (2.16)$$

Where,

$$f_a = minimum\ of \begin{cases} (0.097 - 0.68\left(\frac{x}{L} - 0.15\right)^2 \frac{\alpha}{\sqrt{\beta'}} & Crushing\ failure \\ \frac{1.2\ CF_F}{\sin(\beta') . CFc . D_{ship}{}^{0.64}} & flesural\ failure \\ 0.60 & Limiting\ value \end{cases} \qquad (2.17)$$

Where,

$x = distance\ from\ forward\ perpendicular\ to\ the\ satation\ under\ consideration$

Flexural class factor $CF_F = \;\; \sigma_f \;\; h_{ice}{}^2$

The equation (2.16) is presented in the UR IACS [6]

When the load is known, a load patch area, A, over which the load is applied is found from equation (2.10)

$$A = \left(\frac{F_n}{Po}\right)^{\frac{1}{1+ex}} \qquad (2.18)$$

To keep the process manageably simple, the shape of patch load is changed from triangular to rectangular. Assume that the load patch is H_{nom} x W_{nom} , with Area A. The aspect ratio AR (W_{nom}/H_{nom}) is found by using equations (2.6) and (2.7)

$$AR = 2\ \tan(\phi/2)\ \sin(\beta') \\ = 7.46\ \sin(\beta') \quad [\text{ assumes } \phi = 150 \text{ deg}] \tag{2.19}$$

Therefore, A can be written as

$$A = H_{nom}\ \ H_{nom}\, AR \tag{2.20}$$

And using (2.18)

$$H_{nom} = \left(\frac{F_n}{Po \cdot AR^{1+ex}} \right)^{\frac{1}{2+2ex}} \tag{2.21}$$

$$W_{nom} = \left(\frac{F_n}{Po \cdot AR^{1+ex}} \right)^{\frac{1}{2+2ex}} \cdot AR \tag{2.22}$$

A conservative reduction of the load area is further done to account for typical force concentrations that take places as ice edges spall off (see figure 7). The force will remain unchanged, so design pressure rises correspondingly. The design patch load length w is;

$$w = W_{nom}^{\ wex} = W_{nom}^{\ 0.7} = \mathrm{Fn}^{\,0.389}\ \mathrm{Po}^{\,-0.389}\ \mathrm{AR}^{0.35} \tag{2.23}$$

The design load height is

$$b = \frac{w}{AR} \tag{2.24}$$

$$\mathrm{b} = \mathrm{Fn}^{\,0.389}\ \mathrm{Po}^{\,-0.389}\ \mathrm{AR}^{\,-0.65} \tag{2.25}$$

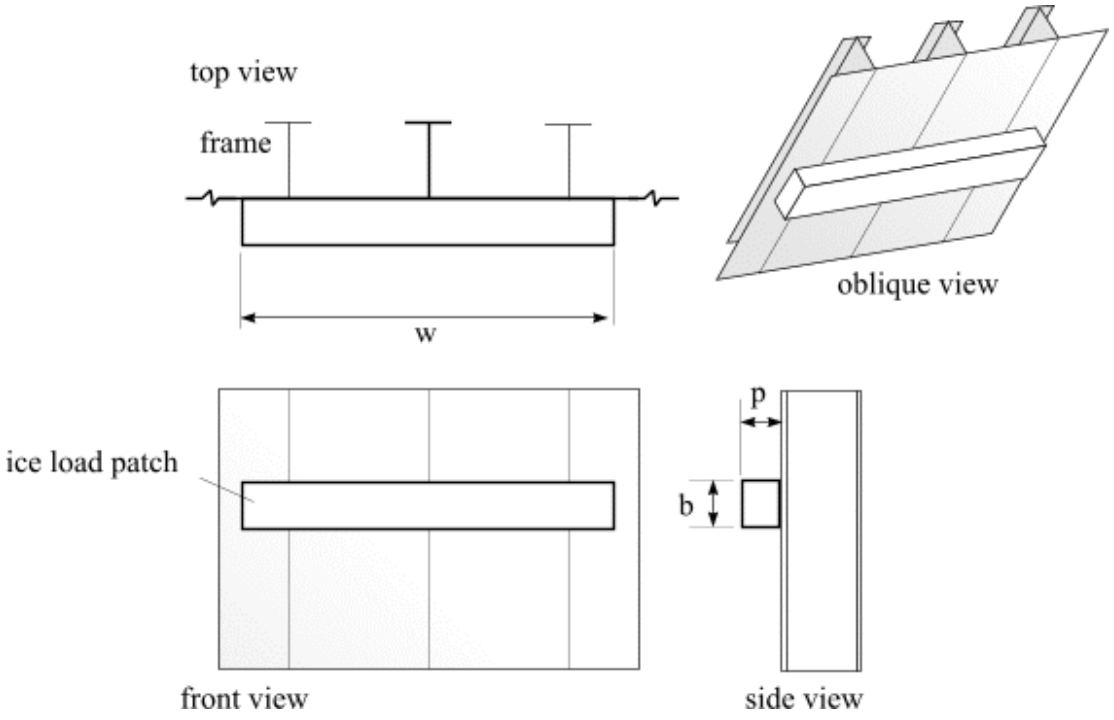

Figure 4 Ice patch load configuration

The line load and pressure are then derived as follows

$$Q = \frac{F_n}{w} \qquad (2.26)$$

$$P = \frac{Q}{b} \qquad (2.27)$$

Which result in the following rule formulas used in IACS [6]

$$Q = \frac{F_n^{0.61} CF_D}{AR^{0.35}} \qquad (2.28)$$

And

$$P = F_n^{0.222}\, CF_D^{\,2}\, AR^{0.3} \qquad (2.29)$$

Where, Patch class factor, $CF_D = Po^{.389}$

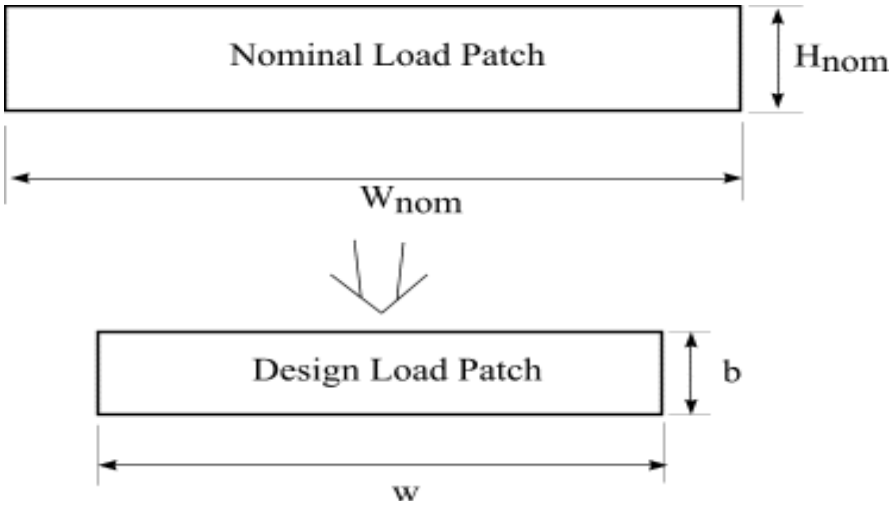

Figure 5 Nominal and design rectangular load patches

Ice load are quite peaked within the load patch. C. Daley [16] stated that a set of peak pressure factors (PPF) is used when using the pressure in design formula to account the effect of peaked load. Figure 6 represents how the pressure in the design formula is magnified.

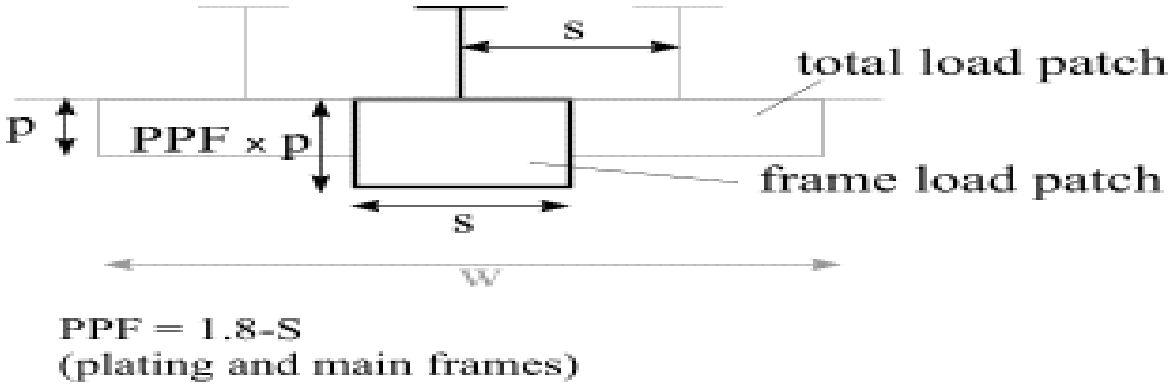

Figure 6 Peak Pressure Factor used to design individual elements.

2.4 Ice Pressure and contact area relationship

How the ice pressure is conceived has varied much and there still is quite large controversy how to treat it. Often ice pressure is described by the average pressure on the area considered. Usually this area is the gauge area but also some geometric considerations may determine the area – if for example the load is observed on a pile of straight face towards level ice, then this area can be assumed to be $D \cdot h_i$ where D is pile diameter and h_i ice thickness. Observations of the ice pressure on smaller areas have suggested that considerable variation in local ice pressure magnitude exists inside the nominal contact area. The nominal contact area is defined by the geometry of the cross section between the ice feature and the structure – like the area $D \cdot h_i$ mentioned above. Several different theories about ice pressure have been suggested.

The highest values of ice pressure are coupled with ice failure by crushing. As ice must be broken along the whole contact surface, it is clear that some flow of crushed ice from the centre of the contact must take place. Russian scientists have analyzed the flow of crushed ice assuming that the crushed ice is viscous fluid. The situation of the flow is depicted in Fig. 7. Based on this assumption and Reynolds thin film fluid flow equations the following form for the pressure have been derived (Kurdjumov & Kheisin 1976, Popov & al. [18])

$$P\alpha\left(\left(\frac{h_c}{2}\right)^2 + x^2\right) \qquad (2.30)$$

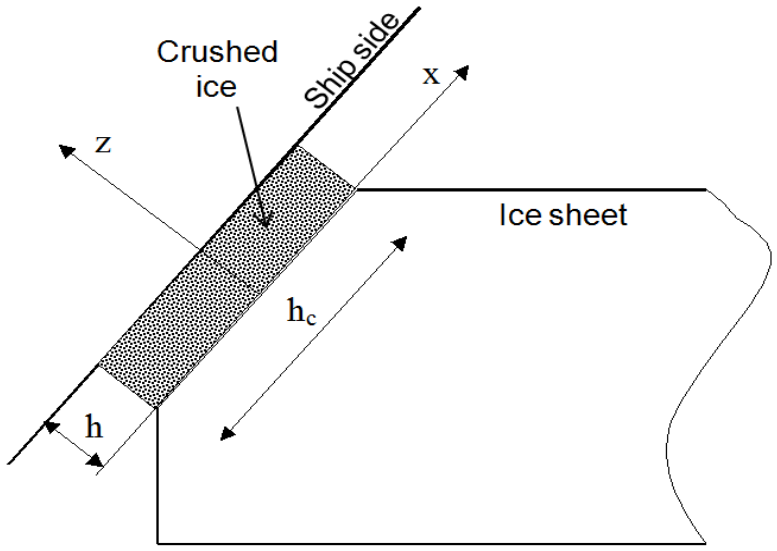

Figure 7 Geometry of the assumed viscous layer of crushed ice.

This form of ice pressure has been used in the development of IACS [6] UR formulation for ice force using energy principles in an impact between an ice feature and a ship (Popov et al. [18]). The drawback of this ice pressure formulation is that many assumptions have been made (viscosity, uniform film thickness, uniform source of crushed ice, constant thickness of the film to mention a few), K. Riksa [17].

The third formulation used for ice pressure is based on observation that the average ice pressure on an area is dependent on the magnitude of the area. Sanderson (1988) has collected many different results and then suggested the upper limit for this pressure-area relationship as

$$P_{avg} = 8.1A^{-0.57} \qquad (2.31)$$

Where p is in units of MPa and A in m^2. The constant and exponent in this pressure-area relationship has been studied for example by Riska (1987) and Frederking (1999) – the presented values for the constant vary between roughly 2 ... 10 and for the exponent between

-0.3 ... -0.6. The drawback of the pressure-area relationship is that it is empirical and little physical basis exists for the area dependence. One possible reason for the pressure-area relationship is based on the observation that within the nominal contact area there is a line-like feature along which the ice pressure is transmitted. The line is produced by a flaking process leaving a line on which a high pressure is acting. The flakes seem to be created so that the line of high pressure is directed towards the corners of the nominal contact area (Riska et al 1990 [19]).

The assumption of the line can also be investigated making a thought experiment where the ice pressure is measured with gauges of different area but symmetrically located, see Fig. 8. The ice pressure is assumed to act on a line of somewhat nonuniform width – here also the pressure-area relationship emerges with the pressure exponent of -0.5.

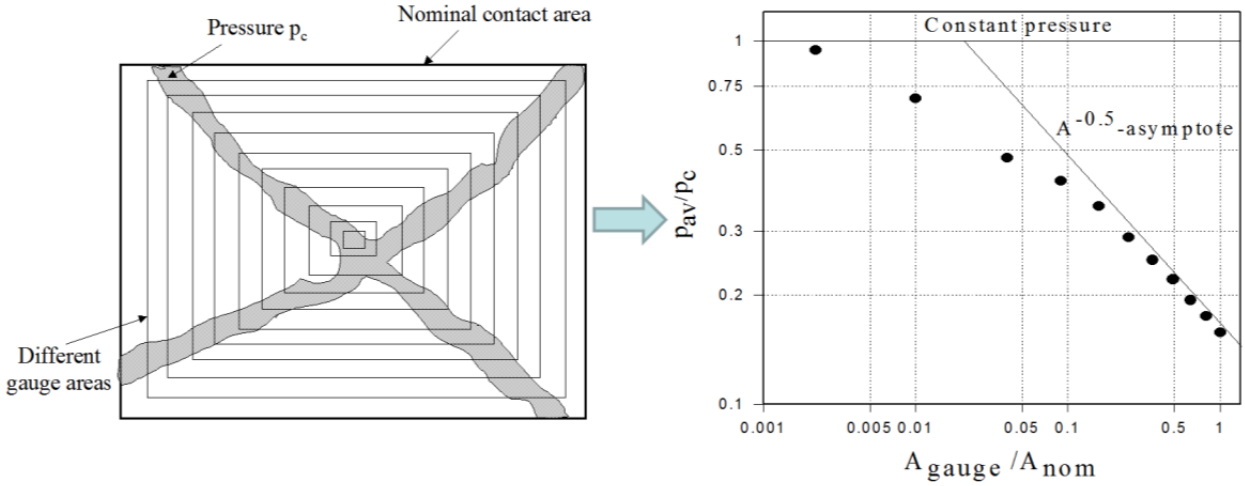

Figure 8 A fictitious experiment of measuring the ice pressure with different gauge areas and the resulting average pressure results. [17]

DNV [12] has used the following pressure area relationship to determine the design ice pressure for Polar class vessels

$$P \propto \begin{cases} A^{-0.5} & for\ A \leq 1.0\ m^2 \\ A^{-0.15} & for\ A > 1.0\ m^2 \end{cases} \qquad (2.32)$$

After carrying out non linear analysis for rectangular plates to patch loading J. Amdahl [13] concluded that the small patches tend to become critical when the pressure is inversely proportional to the square of the patch area while uniform loading over the entire plate is critical when the pressure is proportional to Area-0.15. The first pressure area relationship is often used for small areas (< 1 m2) and the second relationships for larger areas (> 1 m2)

Design pressure is given in Finnish-Swedish ice class rules as follows;

$$p = c_d \cdot c_1 \cdot c_a \cdot p_o [MPa] \qquad (2.33)$$

Finnish-Swedish rules didn't relate the design pressure with contact area. Instead they relate the design pressurec_d, $c_1 and\ c_a$.

Where,
c_d = a factor which takes account of the influence of the size and engine output of the ship.

c_1 = a factor which takes account of the probability that the design ice pressure occurs in a certain region of the hull for the ice class in question.
c_a= a factor which takes account of the probability that the full length of the area under consideration will be under pressure at the same time.

Chapter 3

3 Review of Framing Rule Requirements

3.1 Introduction

Plates, stiffeners and girders are the main basic structural components of ships and other marine structure. The plastic capacity of these structures is determine by postulating simple plastic collapse mechanism. By "simple" it is assumed that the material is perfectly plastic and the collapse mechanism contains pure plastic bending hinge.

3.2 Energy method

In determining plastic capacity of plates and beam by postulating simple plastic collapse mechanism, the energy method is used. Energy methods provide a powerful analytical tool. However, some features of energy methods should be understood by their users.

In order to apply the method, a response mechanism has to be selected. There are many possible mechanisms for any load/structure combination, and it is necessary to find the one that gives the lowest structural capacity, as this will be closest to the capacity that the structure actually provides. Even if the lowest solution has been found, the represents the upper bound to capacity; i.e. the structure can do no better than this, and may well do worse. This statement is true as long as the postulated mechanism is valid for the boundary conditions and if the material is ideally plastic. In the absence of other factors, energy methods produce non-conservative results.

Counterbalancing these potential sources of non-conservatism, energy methods (as normally applied) do not include all components of any response. Typically, they assume elastic/perfectly plastic material response and thus exclude both membrane and strain hardening effects. These are small in the initial stages of response but provide considerable reserves of strength when the structure deflects significantly. In addition, approval procedures for the steels specified for polar ships will ensure that their specified material properties are lower bounds to their actual capacity. Thus, although the mechanisms describing response may appear to permit 'collapse', the actual collapse load will be significantly in excess of the 'mechanism formation' load.

3.3 Collapse mechanisms

The energy method is utilized in deriving the IACS [6] unified requirements take account following possible energy absorbing mechanism:

1. A pure bending hinge;
2. A combined shear and bending hinge;
3. A shear hinge;

3.4 Bending and shear interaction

In most structures, elements support a combination of bending and shear loads and associated stresses. A frame carrying shear load will have less bending capacity than one in pure bending; likewise when bending stresses are present full shear capacity is no longer available.

The current UR proposals treat bending and shear interaction more rigorously than any existing rules or standards, by taking into account actual section shape in the calculation procedure. Daley CG. [10] Presented that this interaction can be represented by equation (3.1) [11], where α is section-dependent, and greater than or equal to one.

$$\left(\frac{M}{M_{ult}}\right)^2 + \left(\frac{T}{\alpha \,.\, T_{ult}}\right)^2 = 1 \qquad \ldots (3.1)$$

Bending moment, M, and Shear, T have actual and ultimate values as indicated.

Reviewing this equation, and the curve that can be used to represent it (figure 9) it is seen that at full shear any section with $\alpha > 1$ will have some reserve bending capacity.

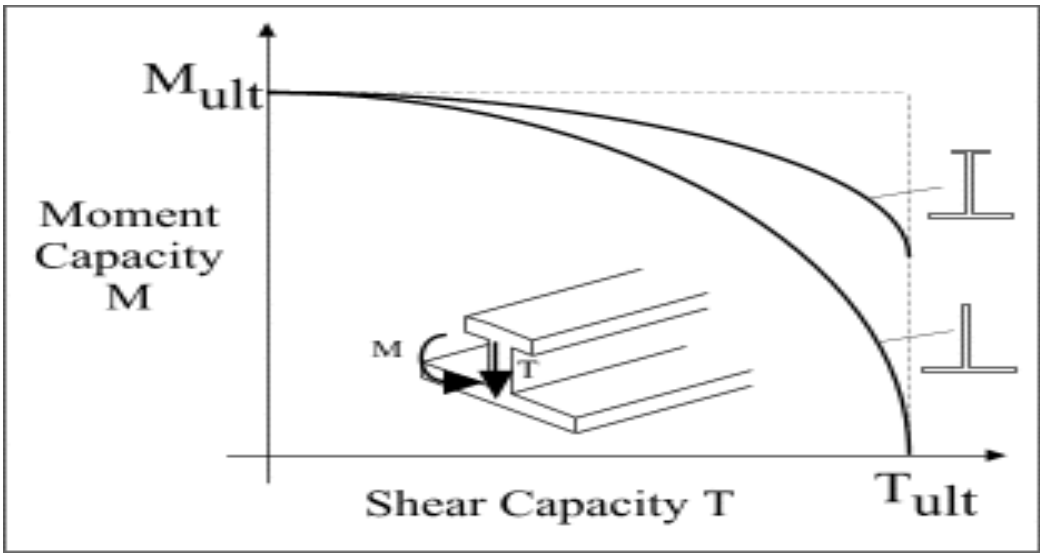

Figure 9 Bending/shear interaction diagram

Only the vertical part of the stiffener is assumed to contribute to shear capacity, but for a variety of reasons the full height is taken as contributing to the shear area, not merely the web as normally defined. In the description that follows, 'web' is taken as referring to this full height or depth. As the shear capacity of the web is used up, the moment capacity of the section reduces until, at the full shear condition, the residual section modulus is defined by the free flange contribution only. Thus, a flat bar has no residual capacity, whereas a stiffener with flange area equal to web area would retain 2/3 of its initial moment capacity. This approach is only applicable up to the point where the web yields fully and forms a shear hinge. Beyond that point, a different approach is needed, as described below.

In a pure bending hinge, the interaction between shear and bending is not an issue, and in a combined hinge it is dealt with as described. The shear hinge has required some additional consideration in order to allow reasonably full treatment of some response mechanisms beyond the full shear condition described above. When a shear hinge is assumed to form by fully yielding the web, the flanges can still provide additional load bearing capacity. In a truly pure shear collapse, the total areas of these flanges would also need to reach yield. However, there will normally be a lower energy collapse path involving localized bending hinges in each of the flanges. These local hinges form part of the assumed response mechanisms for the asymmetrical case described below. In the symmetrical case (centered load) shear hinges are 'designed out', and the local hinges can be omitted.

3.5 Assumption

Several additional assumptions or corrections have been made by both IACS and DNV during the development of their rule requirements.

The first is regarding the position of the plastic neutral axis when calculating the plastic section modulus. Normally the area of the plate flange is greater than that of stiffener. In that case, the position of the plastic neutral axis goes through inside the plate flange resulting unrealistic high strain in the stiffener flange before the cross section is fully yielded. IACS has solved this problem by using a more realistic assumption. They have located the plastic neutral axis at the web-plate intersection. This implies a more conservative approach where the stress in the plate is, on average, less than or equal to yield stress. DNV on the other hand has chosen to neglect the contribution from the plate to the plastic section modulus. However, the assumptions from both DNV and IACS are equivalent and both of them are only valid as long as the cross-sectional area of the attached plate flange exceeds the cross-sectional area of the web and stiffener flange. As a consequence of these assumptions it is possible to split the plastic section modulus into two contributing parts. One is for the web Z_w and the other one is for the flanges Z_f. IACS expressions for the plastic section modulus is given in equation (3.2) and DNV's is given in equation (3.3).

$$Z_{p,IACS} = Z_{f,IACS} + Z_{w,IACS} = A_f\left(\frac{t_f}{2} + h_w + \frac{t_p}{2}\right) + A_w\left(\frac{h_w}{2} + \frac{t_p}{2}\right) \qquad (3.2)$$

$$Z_{p,DNV} = Z_{f,DNV} + Z_{w,DNV} = A_f\left(\frac{t_f}{2} + h_w\right) + \left(\frac{{h_w}^2 t_w}{2}\right) \quad (3.3)$$

In the equations given above t_f is the flange thickness, h_w is the web height, t_w is the web thickness, A_f is the stiffener flange area, t_p is the plate thickness and A_w is the web area.

Another assumption about the boundary conditions is that both IACS and DNV have considered clamped boundary conditions in deriving the requirements for framing design.

3.6 IACS framing requirements

3.6.1 Load case

C. Daley [10] stated that two load cases are considered for framing design in the development of URs as shown in figure 10.

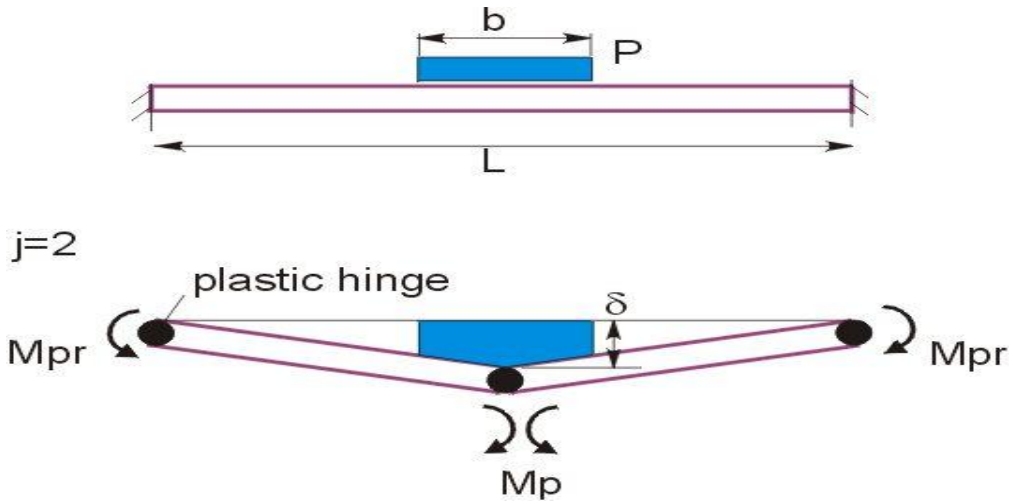

Symmetrical (centered) load

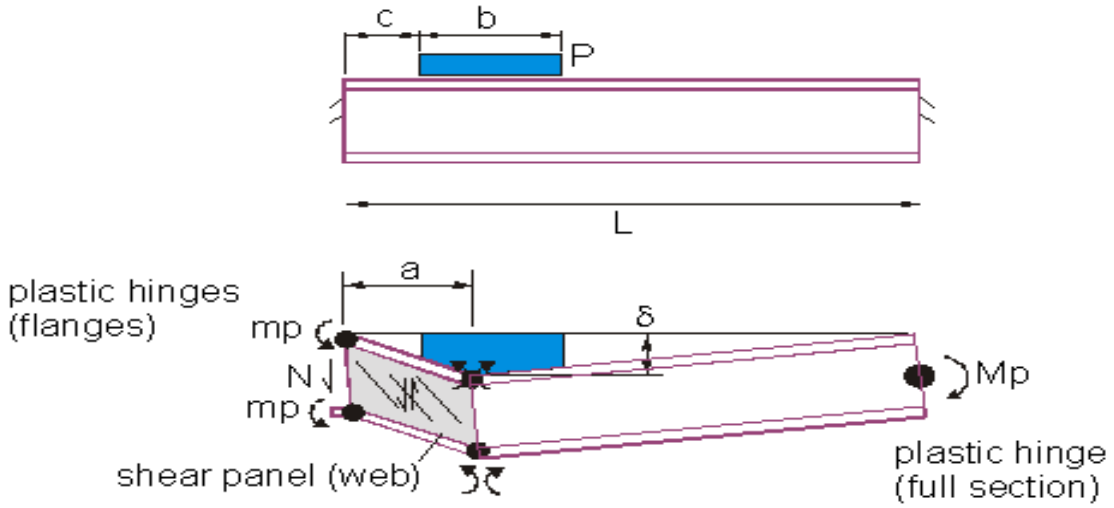

Asymmetrical (end) load

Figure 10 Load cases

3.6.1.1 Symmetry load case

There are several possible response mechanisms occur under the centered load, including:

- 3-hinge bending/shear;
- 4-hinge bending/shear;
- 2 shear hinge;

These are illustrated in figure 11.

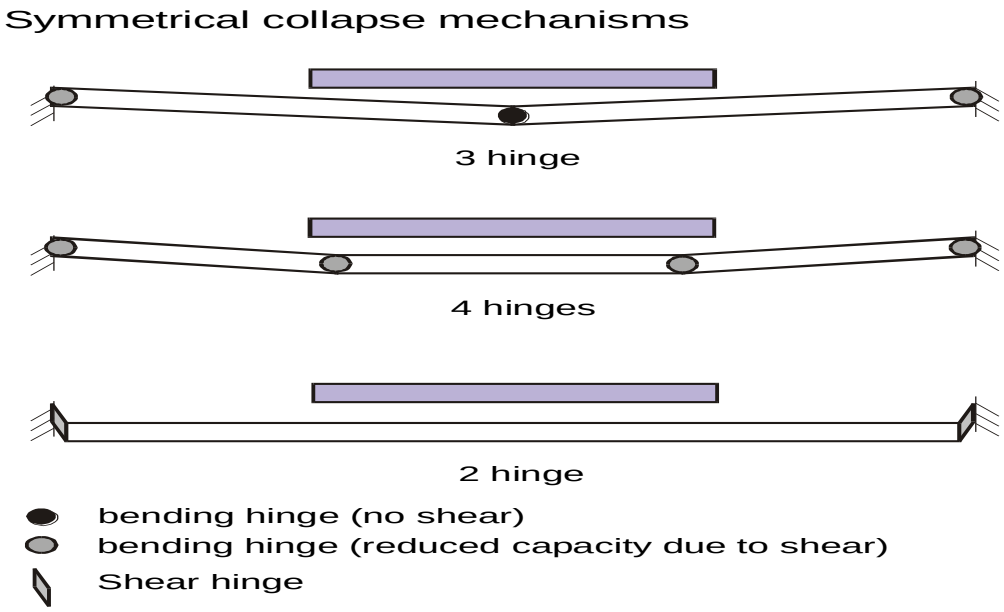

Figure 11 Symmetrical Collapse Mechanisms

The dominant mechanism is the one with lowest load capacity that depends on the section shape, the load length and the load intensity. Although 4-hinged mechanism gives smaller collapse load than that of 3-hinged mechanism, the 3-hinged mechanism normally dominates. Because by large number of finite element analysis C. Daley [10] has proved that the difference of collapse loads between 4-honged and 3-hinged mechanism always seem to be acceptably small. A centered load can also in principle give the 2-hinge mechanism, but by setting the minimum permissible web area (see equation 3.4) at a value corresponding to full shear this will be avoided. The design point can therefore be defined by the 3-hinge mechanism.

The shear area (the minimum web area required to carry the load in pure shear) is found as:

$$A_0 = \frac{1}{2} P.b.S.\frac{\sqrt{3}}{\sigma_y} \qquad (3.4)$$

It is also possible that an ice frame will have only one end fixed and the other (outside the ice belt) simply supported. Under this condition the hinge system has a single bending/shear hinge at the fixed end and the same pure bending hinge at the center [10] (see figure 12). This has been provided for by introducing a frame support coefficient, j, to the IACS URs rule equations (j=1 or 2 fixed ends). In practice it is highly improbable that such a loading would apply, as the ice belt already extends above the water line and the peak loads are unlikely be seen in this area. So only the three hinge mechanism is considered here for the centered load case.

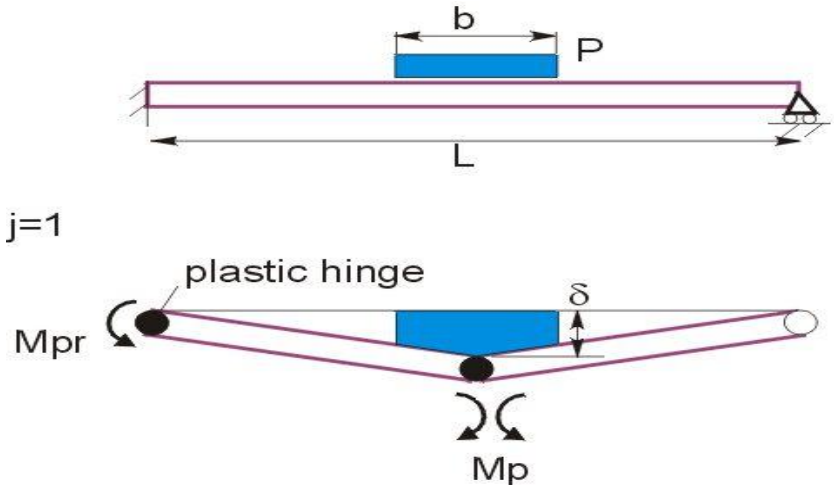

Figure 12 Plastic hinge mechanism for j=1

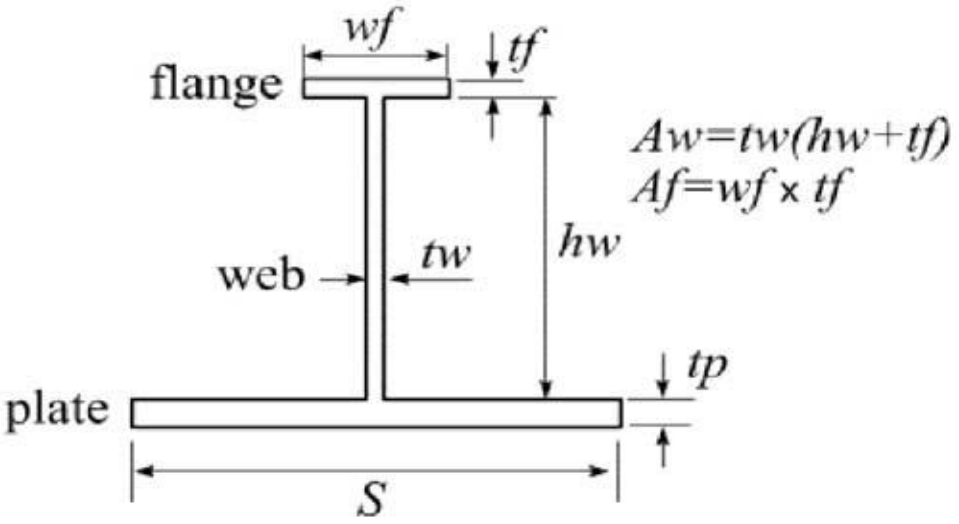

Figure 13 Frame section

By equating internal and external work, taking the reduced end moment capacities due shear into consideration, the collapse pressure for centered load three hinge mechanism is obtained [10]

$$P_{3h} = \frac{(2 - kw) + kw \cdot \sqrt{1 - 48 \cdot Zpns(1 - kw)}}{12 \cdot Zpnskw^2 + 1} \cdot \frac{Zp \cdot \sigma_y \cdot 4}{\left[S \cdot b \cdot L \cdot \left(1 - \frac{b}{2 \cdot L} \right) \right]} \tag{3.5}$$

Where, k_w is the term expressing the relations between web section modulus and frame section modulus;

$$k_w = \frac{Z_w}{Z_p} \tag{3.6}$$

And the term *Zpns* (*Zp*-normalized-squared) is:

$$Zpns = \left[\frac{Zp}{Aw \cdot L \cdot \left(1 - \frac{b}{2 \cdot L} \right)} \right]^2 \tag{3.7}$$

For the term under the root sign of equation (3.5) to stay positive, Zp must be less than Zpmax, where;

$$Zpmax = \sqrt{\frac{1}{48 \cdot (1 - kw)}} \cdot Aw \cdot L \cdot \left(1 - \frac{b}{2 \cdot L}\right) \tag{3.8}$$

Note: in cases in which Zp > Zpmax, the frame will first fail by shear at both supports (central load). In this case the capacity is nominally limited by:

$$Plim = 2 \cdot \frac{Aw \cdot \sigma_y}{\sqrt{3} \cdot S \cdot b} \tag{3.9}$$

The required section modulus is:

$$Zp = \frac{Zo \cdot 2}{\left[2 + kw\left[\sqrt{1 - \left(\frac{1}{An}\right)^2} - 1\right]\right]} \tag{3.10}$$

Rearranging the above equation it can be written

$$Z_n = \frac{Zp}{Zo} = \frac{2}{\left[2 + kw\left[\sqrt{1 - \left(\frac{1}{An}\right)^2} - 1\right]\right]} \tag{3.11}$$

Where,

Zo is minimum modulus (required if web is fully effective) and given as

$$Zo = \frac{P \cdot b \cdot S}{8 \cdot \sigma_y} \cdot \left(1 - \frac{b}{2 \cdot L}\right) \cdot L \tag{3.12}$$

$$An = \frac{Aw}{Ao} \tag{3.13}$$

By substituting equations (3.12) and (3.13) into equation (3.11) the required section modulus can be found as

$$Z_p = \frac{PbSL}{4\sigma_y}\left(1 - \frac{b}{2L}\right) \frac{1}{2 + k_w\left(\sqrt{1 - \left(\frac{A_0}{A_w}\right)^2} - 1\right)} \tag{3.14}$$

Required section modulus stated in IACS [6] URs (UR equation 23) is

$$Z_p = \frac{100^3\left(AF.PPF_t.P_{avg}\right)b.s.l.Y.A_{1A}}{4\sigma_y} \qquad [cm^3] \qquad (3.15)$$

Where,

$$Y = \left(1 - \frac{b}{2L}\right)$$

$$A_{1A} = 2 + k_w\left(\sqrt{1 - \left(\frac{A_0}{A_w}\right)^2} - 1\right) \qquad (3.15a)$$

3.6.1.2 Asymmetric load case

The way in which this mechanism develops, differs considerably from the central case. Figure 14 shows the full collapse mechanism for this case.

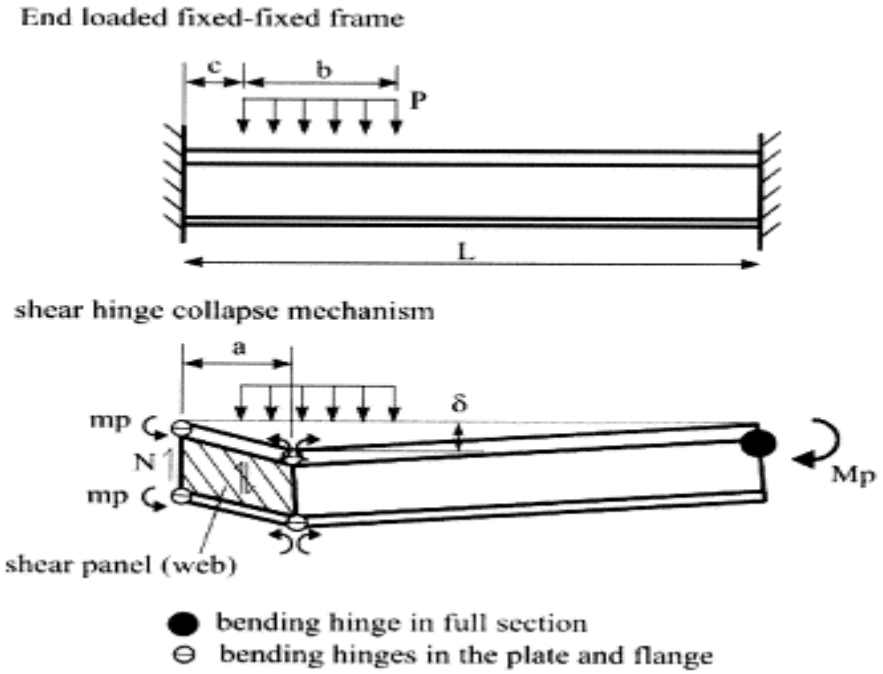

Figure 14 Plastic mechanism for asymmetrical load case

In the central load case, the formation of the hinges is almost simultaneous, leading to rapid loss of stiffness (see figure 15). In the asymmetrical case the shear hinge at closer support develops first at a significantly lower load level than that for the bending hinge in the flanges and at the far end. As a result, the local plastic strain can be much larger than those in the central case (though still normally quite small in absolute terms) (see figure 15).

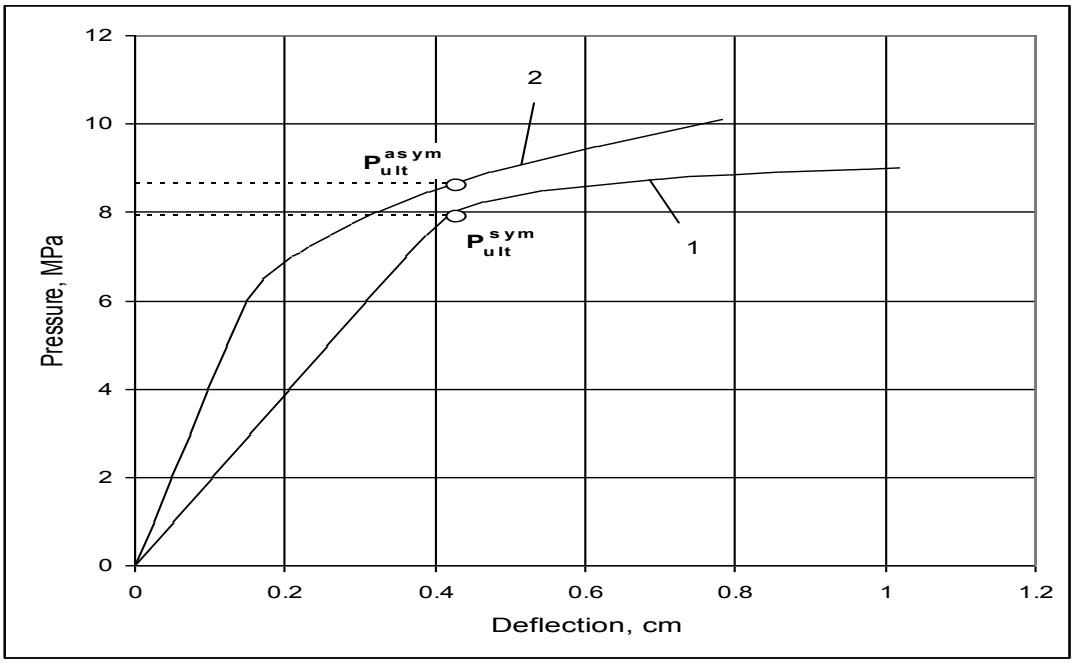

Figure 15 Comparison of response under analytical collapse load, C. Daley [10].

The minimum energy solution for this mechanism has the load located some distance along the frame (see figure 14). The location can be found by maximizing the work done for the location (value of c). The internal work is a sum of the plastic work done by shear panel, the four plastic hinges in the flanges and the hinge at the far end. The value of a can be found by minimizing the internal work done with respect to a.

By energy balance and some simple approximation, the following equation appears for the asymmetrical case:

$$(P.b.s)\left(1-\frac{b}{2L}\right)=\sigma_y\left(\frac{A_w}{\sqrt{3}}+\frac{Z_p}{L}f_z\right) \qquad (3.16)$$

Where $f_z$is approximated as

$$f_z = 1.1 + 5.75{k_z}^{0.7} \qquad (3.17)$$

Where, $k_z$is ration of the combined flange moduli to the total section modulus

$$k_z = \frac{z_p}{Z_p} \qquad (3.18)$$

$$z_p = z_{plate} + z_{flange} = s\frac{{t_p}^2}{4} + w_f\frac{{t_f}^2}{4} \qquad (3.19)$$

So, the equation of plastic capacity for asymmetrical load case become

$$P_{asym} = \frac{\sigma_y}{b.s\left(1-\frac{b}{2L}\right)}\left(\frac{A_w}{\sqrt{3}}+\frac{Z_p}{L}\left(1.1+5.75.{k_z}^{0.7}\right)\right) \qquad (3.20)$$

The rule requirement for section modulus is also found from equation (3.16) as;

$$Z_{p,asym} = \frac{P.b.s.L\left(1-\frac{b}{2L}\right)}{4\sigma_y}\left(\frac{1-\frac{A_w}{2A_0\left(1-\frac{b}{2L}\right)}}{0.275+1.44.{k_z}^{0.7}}\right) \qquad (3.21)$$

Required section modulus stated in IACS [6] URs (equation 23) is

$$Z_{p,asym} = \frac{100^3\left(AF.PPF_t.P_{avg}\right)b.s.l.Y.A_{1B}}{4\sigma_y} \qquad [cm^3] \qquad (3.22)$$

Where,

$$Y = \left(1-\frac{b}{2L}\right)$$

$$A_{1B} = \left(\frac{1-\frac{A_w}{2A_0\left(1-\frac{b}{2L}\right)}}{0.275+1.44.{k_z}^{0.7}}\right) \qquad (3.22a)$$

The governing section modulus requirement comes to be the largest of the equations (3.15) and (3.22), controlled by the factors $A_{1A} and\ A_{1B}$ for the symmetrical and asymmetrical case respectively.

3.7 DNV framing requirements

The framing requirements of DNV are in accordance with IACS focusing on describing the shear and bending response of frames. But in addition to IACS framing requirements the warping effect of frame has been considered in DNV framing requirements, which appears when frames of unsymmetrical cross-sections are subjected to lateral pressure loads. It is obvious that lateral pressure loads applied on frames will develop stresses in the flange of the stiffener. But the stresses in an unsymmetrical stiffener flange will create a second-order bending moment with respect to the web location. The effect may be an unsymmetrical response, which tends to increase the stress in the flange and reduce the effectiveness of the flange as member of the cross-section. This is the warping effect. However, the warping effect will not appear when the constraining capacity of the stiffener web has sufficient strength to counteract the unsymmetrical response of the flange.

3.7.1 Warping effect

It is known that the plastic bending capacity is related to the plastic section modulus. When the attached cross sectional area of the plate flange exceeds the cross sectional area of the stiffener, the plastic section modulus is given in DNV [22] as

$$Z_p = \frac{{h_w}^2 t_w sin\emptyset_w}{2} + A_f\left(h_{fc} sin\emptyset_w - b_w cos\emptyset_w\right) \qquad (3.23)$$

Where,

h_{fc} = Height of the stiffener measured to the center of the flange area.
b_w= Distance from the mid thickness plane of the stiffener web to the flange area.
= 0.0 for T-profiles

$\emptyset_w$ = Angle between shell plate and flange side of stiffener web

This formulation of the plastic section modulus ignores the unsymmetrical response, which is observed in panel stiffener of unsymmetrical cross section subjected to lateral loads. The lateral load will not appear when the constraining capacity of the stiffener web by being rigidly attached to the plate has sufficient bending strength to counteract the unsymmetrical bending stress of the flange.
If an inverted angle panel stiffener subjected to lateral pressure, the stress distribution for the cross section will be as shown in figure 16 (provided that no unsymmetrical response).

For the uniformly stress flange at yield, the flange force exert a bending moment relative to the flange edge as follows

$$M_{pfo} = \frac{{b_f}^2 t_f \sigma_y}{2} \qquad (3.24)$$

When the stiffener web is located a distance, b_e, away from the edge of the flange, the bending moment by the flange with respect to the web location, M_{pf}, is given as.

$$M_{pf} = M_{pfo}\left(1 - \frac{2b_e}{b_f}\right) = \frac{{b_f}^2 t_f \sigma_y \left(1 - \frac{2b_e}{b_f}\right)}{2} \qquad (3.25)$$

This bending moment has to be carried by the web in order to prevent an unsymmetrical response. Whether the web can offer enough constraining to prevent the warping effect, a line load, q_{tr}, is applied along the flange web intersection (see figure 17). The line load is expressed in DNV [22] as

$$q_{tr} = \frac{{t_w}^2 \sigma_y}{5h_{fc}} \qquad (3.26)$$

This line force would give rise to a bending moment at support minus the moment at mid-span in the flange, M_{pw}, equal to:

$$M_{pw} = \frac{q_{tr} l^2}{8} \qquad (3.27)$$

As long as M_{pw} is larger or equal to $2M_{pf}$the web has enough constraining capacity to prevent the unsymmetrical response, then the plastic section modulus will be unaffected by the unsymmetrical shape of the stiffener.

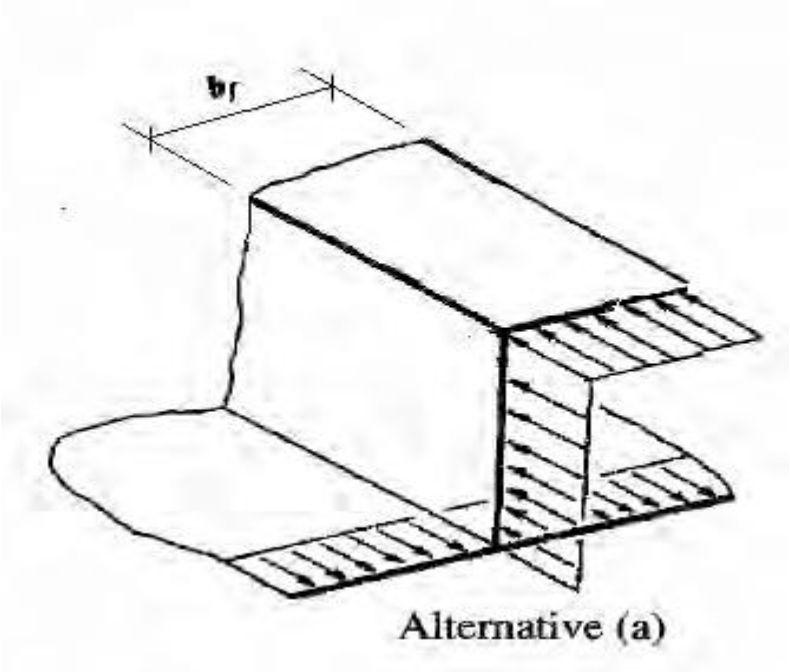

Figure 16 Stress distribution

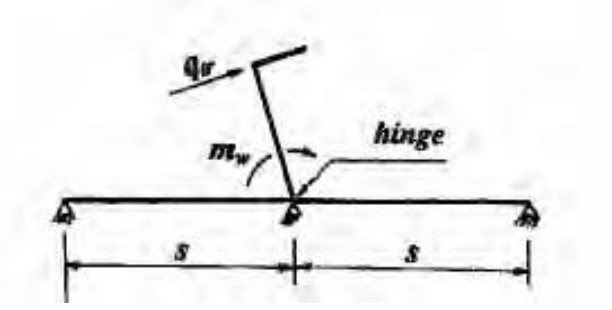

Figure 17 Warping constant exerted by stiffener web

So the requirements read as

$$\frac{{t_w}^2 l^2 \sigma_y}{80 h_{fc}} \geq \frac{{b_f}^2 t_f \sigma_y \left(1 - \frac{2b_e}{b_f}\right)}{2} \qquad (3.28)$$

The above expression may be reformulated as

$$\frac{{t_w}^2 l^2 \sigma_y}{80 h_{fc}} + b_f b_e t_f \sigma_y \geq 0.5 {b_f}^2 t_f \sigma_y \qquad (3.29)$$

For the general case the stiffener cross section may not comply with the above expression, in that case the expression may be written as:

$$\frac{{t_w}^2 l^2 \sigma_y}{80 h_{fc}} + b_f b_e t_f \sigma_y \geq \beta {b_f}^2 t_f \sigma_y \qquad (3.30)$$

Where, $\beta {b_f}^2 t_f \sigma_y$ represents the bending moment of the flange with respect to flange edge closest to the stiffener web. From the equation (3.30), the following expression can be written

$$\beta = \frac{{t_w}^2 l^2}{80 h_{fc} {b_f}^2 t_f} + \frac{b_e}{b_f} \qquad (3.31)$$

When $\geq \frac{1}{2}$, the stress distribution in the flange at support and midspan will be uniform. Consequently there will be no warping effect. When $< \frac{1}{2}$, the effective section modulus of the stiffener will be reduced due to the warping effect.

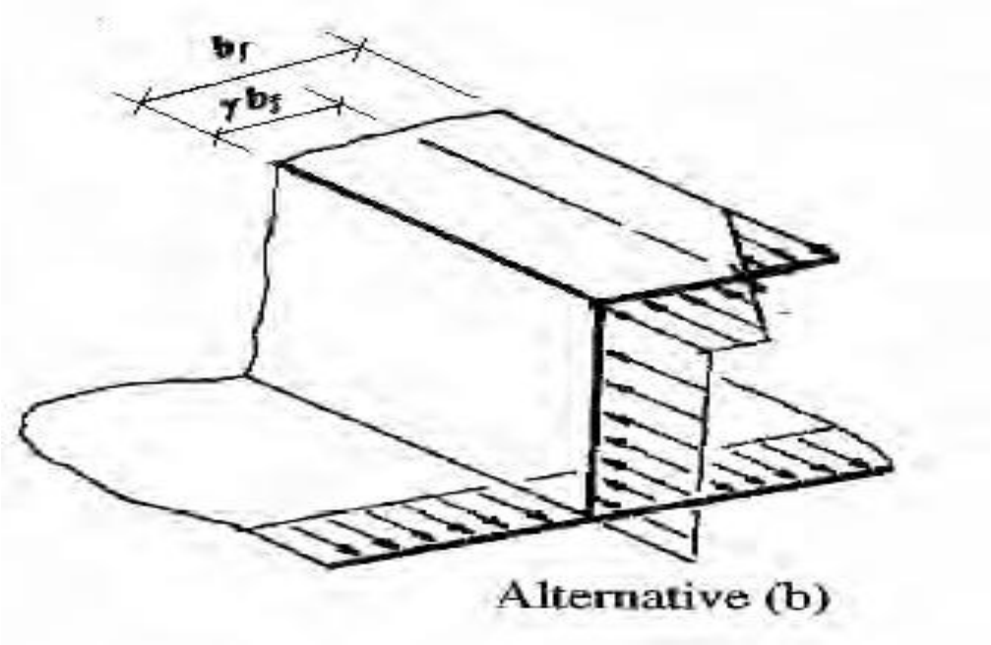

Figure 18 Stress distribution when the web is unconstrained

The effective plastic section modulus of a tilted stiffener including the effect of warping, Z_{wp}, related to the mean stress of the flange may be expressed as:

$$Z_{pw} = \frac{{h_w}^2 t_w sin\emptyset_w}{2} + (2\gamma - 1)A_f\left(h_{fc} sin\emptyset_w - b_w cos\emptyset_w\right) \qquad (3.32)$$

Where, $\gamma (see\ figure\ 18)$ can be read as follows

$$\gamma = 0.25\left(1 + \sqrt{3 + 12\beta}\right) = minimum\ 0.683\ and\ maximum\ 1.0\ for\ angle\ stiffener$$

3.7.2 Symmetric load case

Like IACS, DNV considered the reduction of plastic section modulus at the support due to shear stress effect at the support.

For the panel stiffeners which are laterally loaded at midspan to their plastic bending capacity at support and at midspan, the mean web shear stress outside of the load patch, τ_w, is related to effective plastic section modulus, Z_{pe}, as follows . [22]

$$\tau_w = \frac{4\, Z_{pe}\sigma_y}{l\left(1 - \frac{b}{2l}\right) h\, t_w} \qquad (3.33)$$

Where, h= stiffener height and b= the length of the lateral patch load.

The fraction reduction in the normal stress component of the stiffener which in combination with the shear stress components equals yield, f_w, is given as:

$$f_w = \sqrt{\frac{{\sigma_y}^2 - 3{\tau_w}^2}{{\sigma_y}^2}} \qquad (3.34)$$

The overall effective plastic section modulus of the stiffener, Z_{pe}, considering the effects of warping deformation and shear stress, and assuming bending failure at midspan and at support is given as.

$$Z_{pe} = \frac{{h_w}^2 t_w sin\emptyset_w (1 + f_w)}{4} + (2\gamma - 1)A_f\left(h_{fc} sin\emptyset_w - b_w cos\emptyset_w\right) \qquad (3.35)$$

Consequently the design pressure that complies with the effective section modulus is given as:

$$P_{symm} = \frac{8\eta_b Z_{pe}\sigma_y}{b.l.s\left(1 - \frac{b}{2l}\right)} \qquad (3.36)$$

Where, η_b= Usage factor with respect to development of plastic bending failure in the stiffener

η_b= 0.8

3.7.3 Asymmetrical Load case

DNV collapse mechanism for the asymmetrical case considerably differs from the IACS. In the development of the collapse mechanism, DNV also considered the warping effect. The contribution of the flange to the plastic section modulus of the stiffener reduces due to the reduce distance from the load patch area to the nearby support [22]. As the distance from the support to the load patch is reduced, the warping response of the flange is increased, and the contribution of the flange to the effective plastic section modulus of the cross section is reduced.

The hinge location parameter, l_r, (see figure 19) can be expressed as follows

$$l_r = c + b - \frac{cb}{l - b} \qquad (3.37)$$

Where, c = distance from the support to nearby patch area = 0.75.s

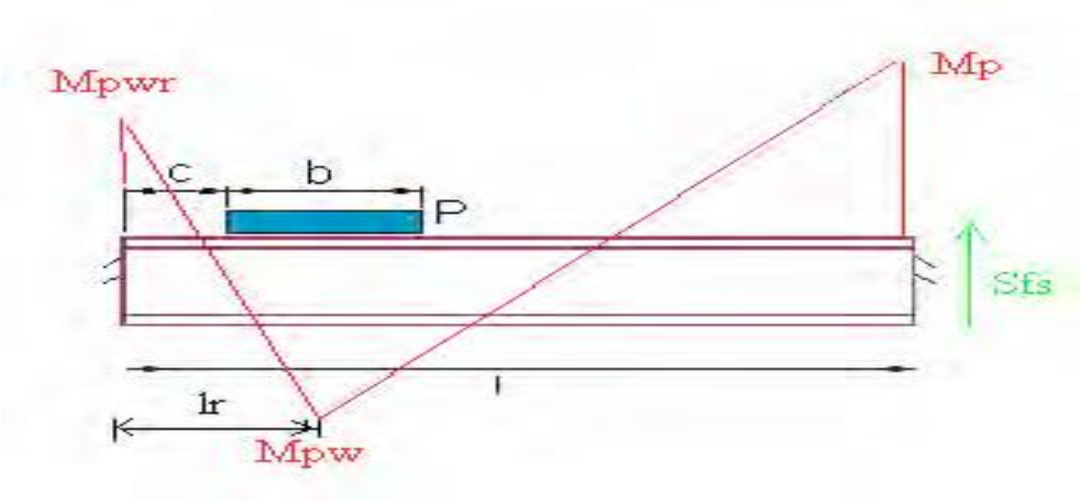

Figure 19 Collapse mechanism for asymmetric load case with bending moment diagram, DNV [22].

At the far away support the effective plastic section modulus of the stiffener is assumed to be unaffected by the web shear stress as well as by warping effect of the flange.

Consequently the maximum limit to the web shear force at the far away support may be expressed as:

$$S_{fs} = \frac{(Z_p + Z_{pw})\sigma_y}{l - l_r} \qquad (3.38)$$

Hence, the force equilibrium in the vertical direction is used to find the shear force at the nearby support, equal to:

$$S_{ns} = P.s.b - S_{fs} \qquad (3.39)$$

Accordingly the design pressure for shear collapse at the nearby support is given as:

$$P_{asym,shear} = \frac{A_w sin\phi_w \frac{\sigma_y}{\sqrt{3}} + S_{fs}}{b.s} \qquad (3.40)$$

Assuming plastic hinges to be generated at the nearby support and in way of the patch load area, the design pressure for a given stiffener may be expressed as [22]

$$P_{asym} = \frac{4\eta_b Z_{pe} \frac{\sigma_y}{l_r + c} + S_{fs}}{b.s} \qquad (3.41)$$

Chapter 4

4 Review of theory behind Nonlinear Finite Element Analysis

4.1 Introduction

Finite element analysis is based on the following principles.

1. Equilibrium (expressed by stresses).
2. Kinematic compatibility (expressed by strains).
3. Stress strain relationship.

Nonlinearity associate with;

A. Geometry
B. Material
C. Boundary

When the displacements are small, the equilibrium equations can be established with reference to the initial configuration. Moreover, this implies that the strains are linear functions of displacement gradients. When the ultimate strength of structures that buckle and collapse is to be calculated, the assumption about small displacements and linear material need to be modified. If the change of geometry is accounted for, when establishing the equilibrium equations and calculating the strains from displacements, a geometrical nonlinear behavior is accounted for (see figure 20).

Material nonlinear behavior associated with nonlinear stress strain. Material tests with metal show that the linearity between stress and strain does not apply when the stress exceeds a level, σ_p proportionality limit. Above this limit a nonlinear elasto-plastic condition prevails (see figure 21).

Finally, nonlinearity associated with the boundary condition, i.e. when a large displacement leads to contact. Boundary nonlinearity occurs in most contact problems, in which two surface come into or out of contact. The displacements and stresses of the contacting bodies are usually not linearly dependent on the applied loads.

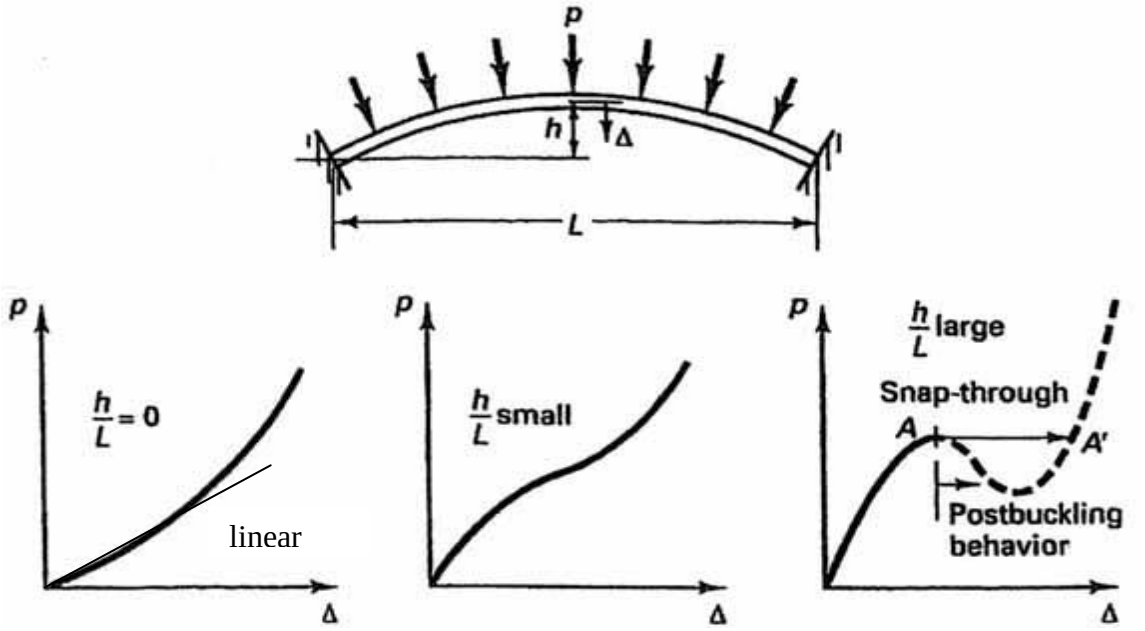

Figure 20 Nonlinear geometrically behavior (response of a thin plate and shell)

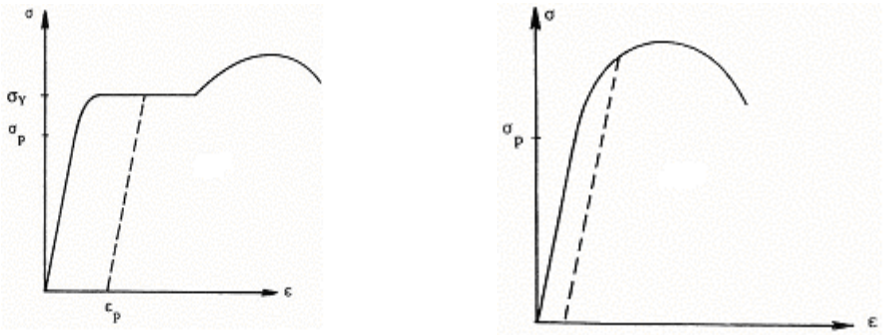

a) Mild steel b) High strength steel

Figure 21 Stress strain curve for metal

4.2 Non linear Geometry

In linear analysis following equation is solved in order to get the load displacement relationship:

$$R = Kr \qquad (4.1)$$

Where, R= external load

K= stiffness matrix found from the linear strain stress relationship and is constant throughout the analysis

r= displacement

When geometrical nonlinearity is accounted for, the equation 4.1 is modified as:

$$R = K(r).r \qquad (4.2)$$

Where, stiffness K(r) is not a constant rather depends on the displacement.

In general the equation 4.2 is not possible to solve analytically. Normally incremental or iterative method is used.

Then the equation 4.2 is expressed as:

$$\mathrm{d}R = K_I(r).dr \qquad (4.3)$$

Where,

$$K_I(r) = \frac{dR}{dr} = tangent\ stiffness\ or\ incremental\ stiffness \qquad (4.4)$$

The differential formulation (4.3) may be written on a finite incremental form

$$\Delta R = K_I(r).\Delta r \qquad (4.5)$$

Implying $\Delta r = {K_I}^{-1}.\Delta R$ (4.6)

Where $\Delta R$and Δr are corresponding increments in load and displacements, respectively.

With a given condition (r, R), K_I can be calculated and the displacement increment Δr due to load increment, ΔR can be calculated by equation (4.6).

4.3 Non linear material

For one dimensional plasticity, when non linear stress strain relationship of a material is accounted for as shown in figure 22, the stress in point A may be expressed as:

$$\sigma = E_s\varepsilon \qquad (4.7)$$

Where E_s is the secant modulus, which depends upon the stress (strain) level.

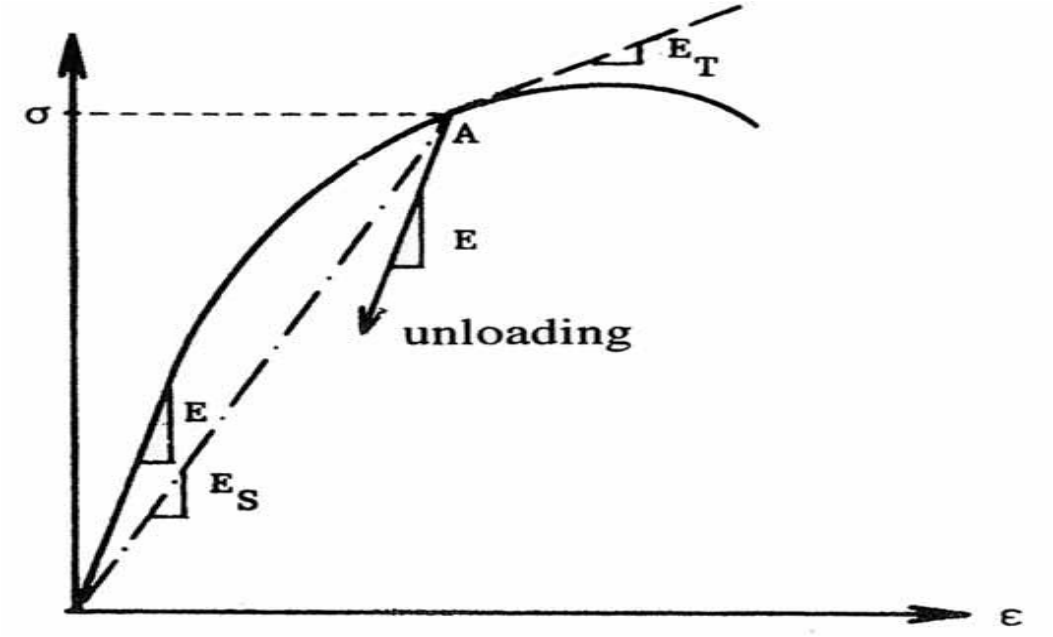

Figure 22 Definition of material properties

When loading is introduced at A, the change of stress, $\Delta\sigma$ can be obtained from

$$\Delta\sigma = \Delta\varepsilon E_T \qquad (4.8)$$

By unloading hook's law applies

$$\Delta\sigma = \Delta\varepsilon E \qquad (4.9)$$

In the same manner as for one-dimensional case elasto-plastic behavior of metals in multidimensional stress state is characterized by [20]

- An initial yield condition for which plastic deformation first occurs.
- A hardening rule which describes the modification of the yield condition due to strain hardening during plastic flow.
- A flow rule which allows the determination of plastic strain increments at each point in the load history.

It is assumed that the material is isotropic, which implied that the stiffness properties are independent of orientation at a point.

It is shown in [20] that the relationship between stress and strain increments may be written as:

$$d\sigma_{ij} = D_{ijkl}{}^{ep} d\varepsilon_{ij} \qquad (4.10)$$

Where,

$$D_{ijkl} = E_{ijkl} - \beta s_{ij} s_{kl} \qquad (4.11)$$

$$\beta = \frac{9G^2}{\bar{\sigma}^2 (H' + 3G)} \qquad (4.12)$$

$$\bar{\sigma} = \sqrt{\frac{3}{2} s_{ij} s_{ij}} = \sqrt{\frac{3}{2} \sigma_{ij} \sigma_{ij} - \frac{1}{2} (\sigma_{kk}{}^2)} \qquad (4.13)$$

4.4 Formulation of nonlinear structural analysis

The most common modes of describing the deformation of solids is Lagrangian approach:

Lagrangian description of motion refers to what happens at a material particle.

Lagrangian approach is divided into two approaches as

1. Total Lagrange (TL)
2. Updated Lagrange (UL)

In TL the Green strain in combination with 2nd Piola Krichoff stress is applied, always referring back to the initial unreformed configuration. All quantities are developed from the initial global reference and using full expression for the quadratic term in the Green strain tensor.

In UL, the natural strain and Cauchy stress are used and referring back to the last obtained equilibrium state and deformed volume.

4.5 Solution Techniques

The basic principle of static structural analysis is to ensure equilibrium between external and internal forces. It can be written as

$$g(R_{ext}, r) = R_{ext} - R_{int} = \lambda R_{ref} - R_{int} = 0 \qquad (4.14)$$

$$R_{ext} = R_{int} = K(r).r \qquad (4.15)$$

$$\Delta R_{ext} = K_I(r).\Delta r \qquad (4.16)$$

Where R_{int} is the vector of internal element reaction forces which is a function of the displacement r and stiffness. R_{ext} represents the external load vector often represented by a reference vector R_{ref} and a scaling factor λ (saclar).

There are several ways of solving the equations including standard load incrementation methods and advanced automatic or semi-automatic methods.

The standard load increment method includes:

1. Euler-Cauchy incrimination without equilibrium iterations
2. Incrementation with Newton-Rapshon iteration
3. Incrementation with modified Newton-Rapshon iteration

In Euler-Cauchy incrementation (see figure 23), the load is incremented in steps and the stiffness matrix is updated at the end of each step. Since the displacement increment is a result of the stiffness at the start of the increment, there will be a deviation between the external and the internal element forces due to change of stiffness within the increment. This deviation tends to increase when applying more increments, i.e. by moving along the force displacement curve.

The only way of reducing the deviation by applying this procedure would be by reducing the increment size. A more accurate method would, however, be by performing iteration at each load step. One way of doing this is by performing a Newton-Rapshon iterative procedure at each load step. The Newton-Rapshon method is based on utilizing tangent to the function g as shown in figure 24.

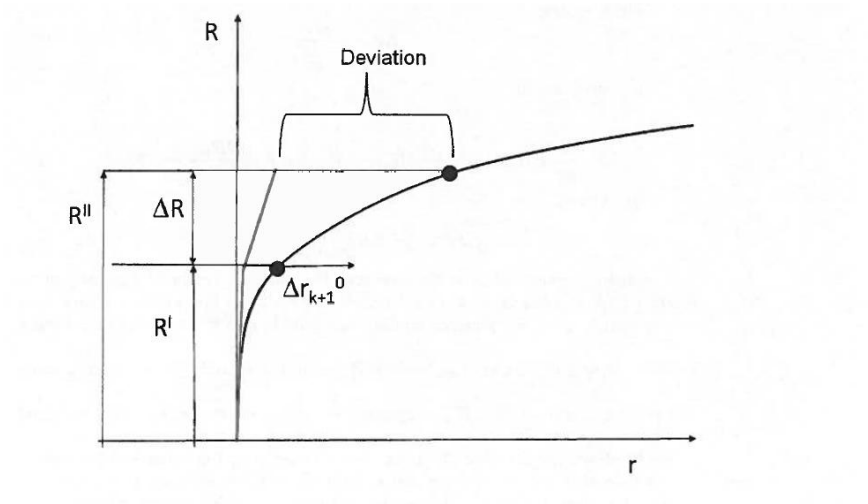

Figure 23 Pure incrementation (Eular-Cachy) method

Applying Newton-Rapshon method it can be written as

$$r^{i+1} = r^i - \frac{g}{\frac{\partial g}{\partial r}} \qquad (4.17)$$

$$\Delta r = -\frac{g}{\frac{\partial g}{\partial r}} \qquad (4.18)$$

From equation (4.14):

$$\frac{\partial g(R_{ext}, r)}{\partial r} = \frac{\partial}{\partial r}(R_{ext} - R_{int}) = 0 - \frac{\partial R_{int}}{\partial r} = -K_I \qquad (4.19)$$

Hence

$$\Delta r^{i+1} = {K_I}^{-1,i}.\left(R_{int,k+1} - {R_{int,k}}^{i}\right) \qquad (4.20)$$

Where, k means load step. During full Newton-Rapshon K_I is updated for each iteration. In modified Newton-Rapshon method the tangential stiffness is updated at each load step only.

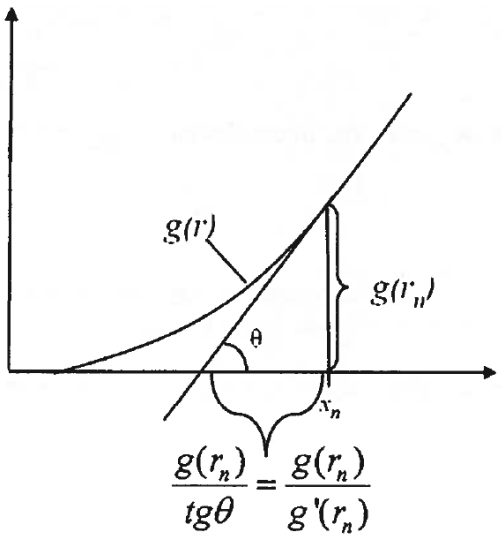

Figure 24 Illustration of the Newton –Rapshon procedure

Advance solution procedure:

It is often necessary to obtain nonlinear static equilibrium solutions for unstable problems, where the load-displacement response can exhibit the type of behavior sketched in Figure 25 that is, during periods of the response, the load and/or the displacement may decrease as the solution evolves. In that case arc-length method is used.

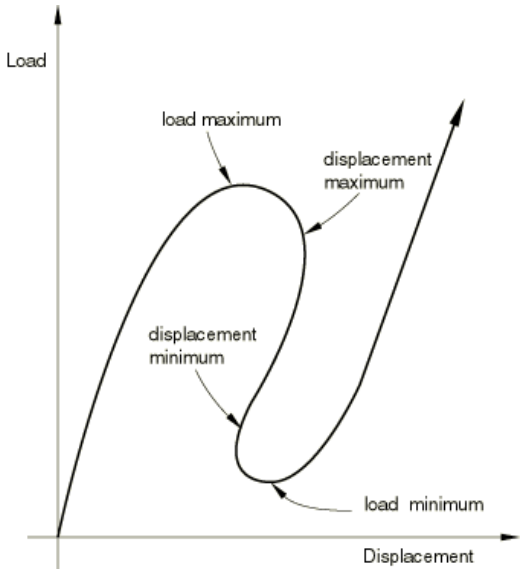

Figure 25 Load deflection

In order to enable a structural analysis to be successfully completed throughout the response space for the above problem, where the structural capacity reduces as the deformation increases, requires the external load to be automatically adjusted to the internal reaction forces of the structures. This requires standard algorithms of which arc-length methods have becomes standard in most computer codes. In figure 26 one of the arc-length method is shown

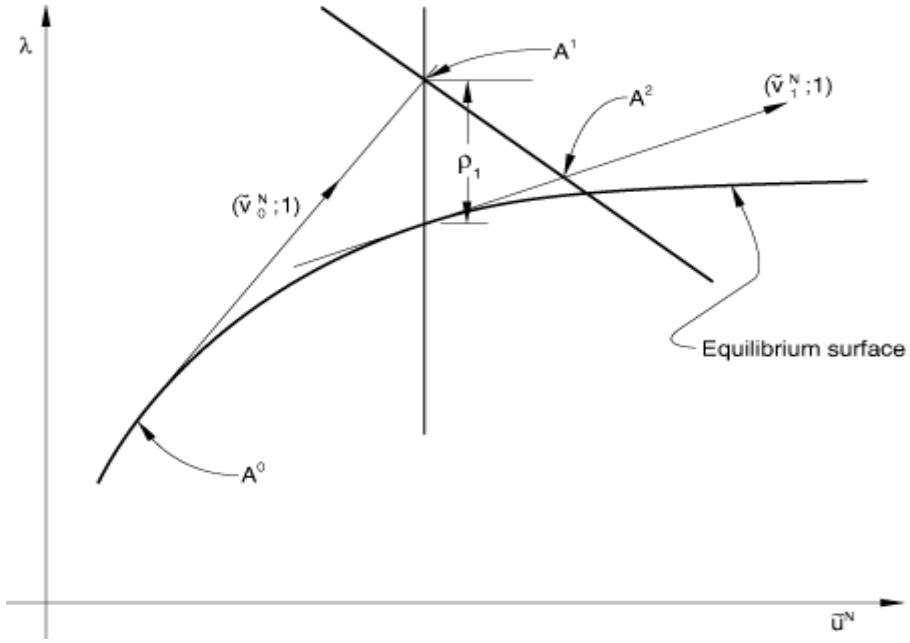

Figure 26 Modified Riks method

Chapter 5

5 Review of ABAQUS Non-linear Finite Element Analysis

5.1 Introduction

ABAQUS is one of the leading finite element programs used by industry and research organizations. Abaqus is a suite of powerful engineering simulation programs, based on the finite element method that can solve problems ranging from relatively simple linear analysis to the most challenging nonlinear simulations. Abaqus contains an extensive library of elements that can model virtually any geometry. It has an equally extensive list of material models that can simulate the behavior of most typical engineering materials including metals, rubber, polymers, composites, reinforced concrete, crushable and resilient foams, and geotechnical materials such as soils and rock. Designed as a general-purpose simulation tool, Abaqus can be used to study more than just structural (stress/displacement) problems. It can simulate problems in such diverse areas as heat transfer, mass diffusion, thermal management of electrical components (coupled thermal-electrical analyses), acoustics, soil mechanics (coupled pore fluid-stress analyses), piezoelectric analysis, and fluid dynamics.

Abaqus offers a wide range of capabilities for simulation of linear and nonlinear applications. Problems with multiple components are modeled by associating the geometry defining each component with the appropriate material models and specifying component interactions. In a nonlinear analysis Abaqus automatically chooses appropriate load increments and convergence tolerances and continually adjusts them during the analysis to ensure that an accurate solution is obtained efficiently.

The basic steps involved in a non-linear finite element analysis using ABAQUS are presented in Figure 27.

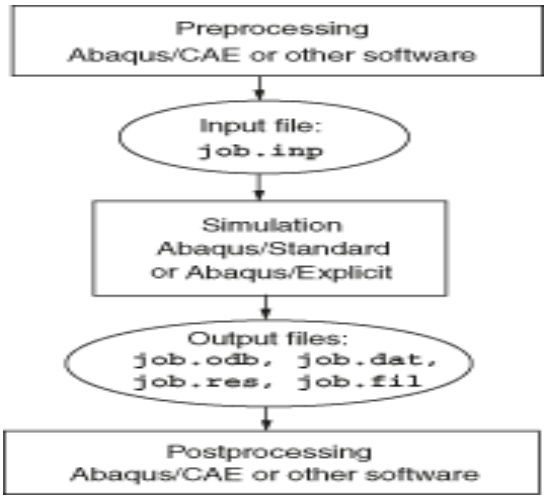

Figure 27 Basic steps involved in a non linear finite element analysis using Abaqus

It is been described in previous chapter that there are different kinds of non-linearities in structural non-linear finite element analysis. And all of these structural non-linearities are supported by Abaqus.

For geometrically nonlinear analysis, small-strain shell elements in Abaqus/Standard (S4R5, S8R, S8R5, S8RT, S9R5, STRI3, and STRI65) use a total Lagrangian strain, and the stress and strain components are given relative to material directions in the reference configuration.

For finite-membrane-strain elements (all membrane elements, S3/S3R, S4, S4R, SAX, and SAXA elements) and for small-strain shell elements in Abaqus/Explicit, the material directions rotate with the average rigid body motion of the surface to form the material directions in the current configuration. Stress and strain components in these elements are given relative to these material directions in the current configuration.

5.2 Finite Element modeling

Abaqus has an extensive element library to provide a powerful set of tools for solving many different problems.

5.2.1 Characterizing elements

Five aspects of an element characterize its behavior:

- Family
- Degrees of freedom (directly related to the element family)
- Number of nodes
- Formulation
- Integration

Each element in Abaqus has a unique name, such as T2D2, S4R, C3D8I, or C3D8R. The element name identifies each of the five aspects of an element.

5.2.1.1 Family

Figure 28 shows the element families that are used most commonly in a stress analysis. One of the major distinctions between different element families is the geometry type that each family assumes.

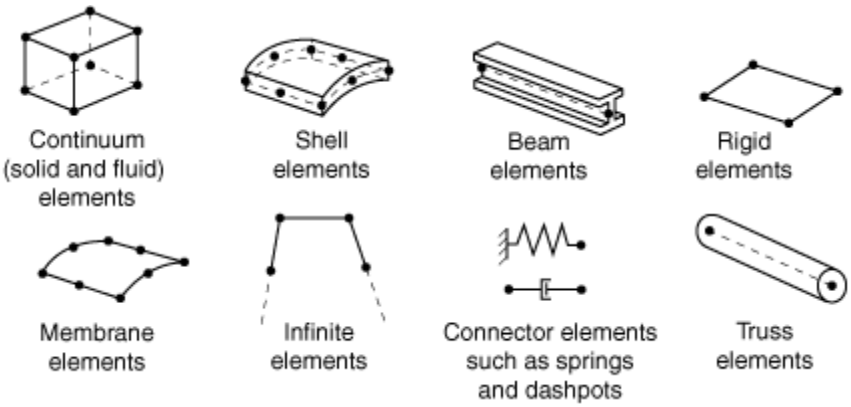

Figure 28 commonly used element families.

The first letter or letters of an element's name indicate to which family the element belongs. For example, S4R is a shell element, CINPE4 is an infinite element, and C3D8I is a continuum element.

5.2.1.2 Degrees of freedom

The degrees of freedom are the fundamental variables calculated during the analysis. For a stress/displacement simulation the degrees of freedom are the translations and, for shell, pipe, and beam elements, the rotations at each node.

5.2.1.3 Number of nodes and order of interpolation

Displacements or other degrees of freedom are calculated at the nodes of the element. At any other point in the element, the displacements are obtained by interpolating from the nodal displacements. Usually the interpolation order is determined by the number of nodes used in the element.

Typically, the number of nodes in an element is clearly identified in its name. The 8-node brick element is called C3D8, and the 4-node shell element is called S4R.

5.2.1.4 Formulation

An element's formulation refers to the mathematical theory used to define the element's behavior. In the Lagrangian, or material, description of behavior the element deforms with the material. In the alternative Eulerian, or spatial, description elements are fixed in space as the material flows through them. Eulerian methods are used commonly in fluid mechanics simulations. Stress/displacement elements in Abaqus are based on the Lagrangian formulation.

To accommodate different types of behavior, some element families in Abaqus include elements with several different formulations. For example, the conventional shell element family has three classes: one suitable for general-purpose shell analysis, another for thin

shells, and yet another for thick shells. In addition, Abaqus also offers continuum shell elements, which have nodal connectivities like continuum elements but are formulated to model shell behavior with as few as one element through the shell thickness.

Abaqus/Standard uses the lumped mass formulation for low-order elements; Abaqus/Explicit uses the lumped mass formulation for all elements. As a consequence, the second mass moments of inertia can deviate from the theoretical values, especially for coarse meshes.

5.2.1.5 Integration

Abaqus uses numerical techniques to integrate various quantities over the volume of each element, thus allowing complete generality in material behavior. Using Gaussian quadrature for most elements, Abaqus evaluates the material response at each integration point in each element. Some continuum elements in Abaqus can use full or reduced integration, a choice that can have a significant effect on the accuracy of the element for a given problem.

Abaqus uses the letter R at the end of the element name to label reduced-integration elements. For example, CAX4R is the 4-node, reduced-integration, axisymmetric, solid element.

Shell, pipe, and beam element properties can be defined as general section behaviors; or each cross-section of the element can be integrated numerically, so that nonlinear response associated with nonlinear material behavior can be tracked accurately when needed. In addition, a composite layered section can be specified for shells and, in Abaqus/Standard, three-dimensional bricks, with different materials for each layer through the section.

5.2.2 Shell element Overview

Abaqus offers a wide variety of shell modeling options.

Shell modeling consists of:

- Choosing the appropriate shell element type.
- Defining the initial geometry of the surface.
- determining whether or not numerical integration is needed to define the shell section behavior and
- Defining the shell section behavior.

5.2.2.1 Conventional vs continuum shell element

Shell elements are used to model structures in which one dimension, the thickness, is significantly smaller than the other dimensions. Conventional shell elements use this condition to discretize a body by defining the geometry at a reference surface. In this case the thickness is defined through the section property definition. Conventional shell elements have displacement and rotational degrees of freedom.

In contrast, continuum shell elements discretize an entire three-dimensional body. The thickness is determined from the element nodal geometry. Continuum shell elements have

only displacement degrees of freedom. From a modeling point of view continuum shell elements look like three-dimensional continuum solids, but their kinematic and constitutive behavior is similar to conventional shell elements.

Figure 29 illustrates the differences between a conventional shell and a continuum shell element.

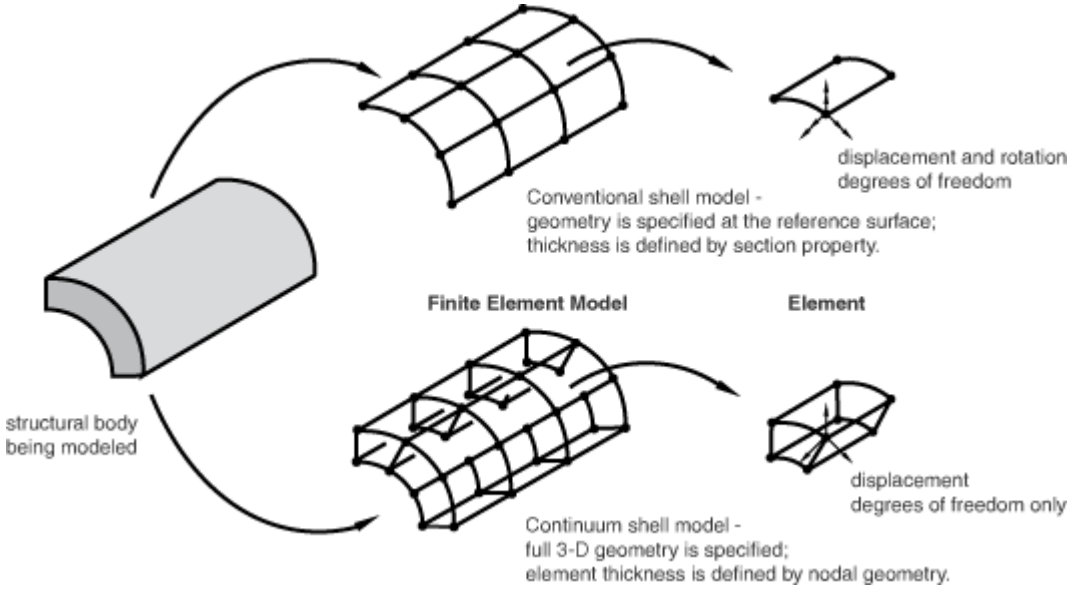

Figure 29 difference between conventional and continuum shell element

5.2.2.2 Choosing the appropriate shell element type

Abaqus includes general-purpose conventional shell elements as well as conventional shell elements that are valid for thick and thin shell problems.

The general-purpose, conventional shell elements provide robust and accurate solutions to most applications and will be used for most applications. However, in certain cases, for specific applications in Abaqus/Standard, enhanced performance may be obtained with the thin or thick conventional shell elements; for example, if only small strains occur and five degrees of freedom per node are desired.

The continuum shell elements can be used for any thickness; however, thin continuum shell elements may result in a small stable time increment in Abaqus/Explicit.

5.2.2.3 General-purpose conventional shell elements

These elements allow transverse shear deformation. They use thick shell theory as the shell thickness increases and become discrete Kirchhoff thin shell elements as the thickness decreases; the transverse shear deformation becomes very small as the shell thickness decreases.

Element types S3/S3R, S3RS, S4, S4R, S4RS, S4RSW, SAX1, SAX2, SAX2T, SC6R, and SC8R are general-purpose shells.

5.2.2.4 Thick conventional shell elements

In Abaqus/Standard thick shells are needed in cases where transverse shear flexibility is important and second-order interpolation is desired. When a shell is made of the same material throughout its thickness, this occurs when the thickness is more than about 1/15 of a characteristic length on the surface of the shell, such as the distance between supports for a static case or the wavelength of a significant natural mode in dynamic analysis.

Abaqus/Standard provides element types S8R and S8RT for use only in thick shell problems.

5.2.2.5 Thin conventional shell elements

In Abaqus/Standard thin shells are needed in cases where transverse shear flexibility is negligible and the Kirchhoff constraint must be satisfied accurately (i.e., the shell normal remains orthogonal to the shell reference surface). For homogeneous shells this occurs when the thickness is less than about 1/15 of a characteristic length on the surface of the shell, such as the distance between supports or the wave length of a significant eigenmode. However, the thickness may be larger than 1/15 of the element length.

Abaqus/Standard has two types of thin shell elements: those that solve thin shell theory (the Kirchhoff constraint is satisfied analytically) and those that converge to thin shell theory as the thickness decreases (the Kirchhoff constraint is satisfied numerically).

- The element that solves thin shell theory is STRI3. STRI3 has six degrees of freedom at the nodes and is a flat, faceted element (initial curvature is ignored). If STRI3 is used to model a thick shell problem, the element will always predict a thin shell solution.
- The elements that impose the Kirchhoff constraint numerically are S4R5, STRI65, S8R5, S9R5, SAXA1*n*, and SAXA2*n*. These elements should not be used for applications in which transverse shear deformation is important. If these elements are used to model a thick shell problem, the elements may predict inaccurate results.

5.2.3 Meshing Technique

The structured meshing technique generates structured meshes using simple predefined mesh topologies. Abaqus/CAE transforms the mesh of a regularly shaped region, such as a square or a cube, onto the geometry of the region one want to mesh. For example, Figure- 30 illustrates how simple mesh patterns for triangles, squares, and pentagons are applied to more complex shapes.

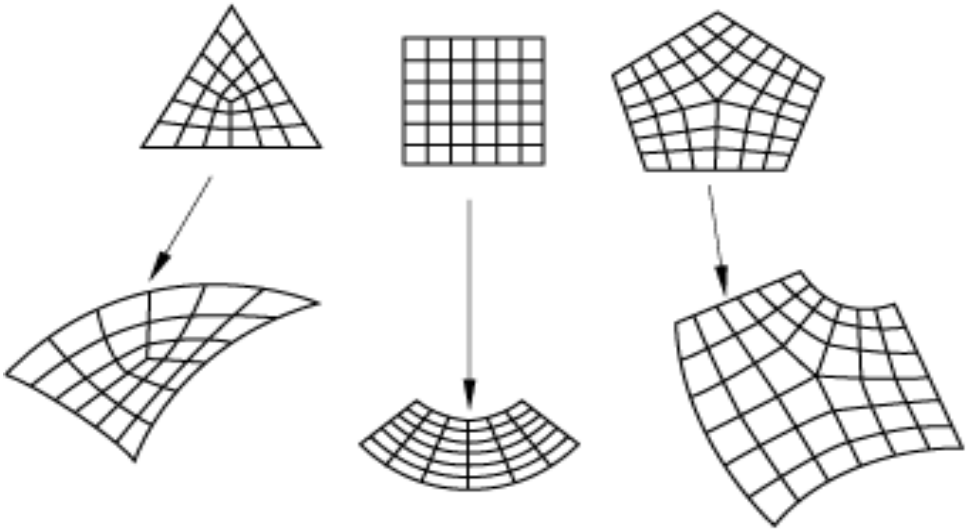

Figure 30 Two dimensional structured mesh patterns

One can apply the structured meshing technique to simple two-dimensional regions (planar or curved) or to simple three-dimensional regions that have been assigned theHex or Hex-dominated element shape option.

Chapter 6

6 Modeling of Ship Side Frames and Panels in Abaqus

6.1 Introduction

Ship hull structure primarily consists of plate stiffened either longitudinally or transversely or a combination of both. In the case of longitudinal framing, the primary stiffeners run in the longitudinal direction and the longitudinals are supported by heavy transverse girders running in the other direction. In case of transverse framing, the primary stiffeners run in the transverse direction and the transverse frames are supported by heavy longitudinal girders running in the other direction. The stiffeners commonly used are flat bars, bulbs, angles and tees. In this chapter modeling of frames, ½+1+½ frames and grillage structure has been described briefly.

The study also verifies the accuracy of boundary conditions assumed in the cases of single frame and grillage. In a single frame, the symmetric boundary condition takes care of the support provided by adjacent side structure. In a grillage, both longitudinal and transverse boundary conditions are incorporated by modeling the longitudinal and transverse continuity in structure.

6.2 Finite element model

J. Abraham [24] has concluded on his FE validation study that both shell and solid elements are suitable in estimating capacity of a frame. And he has also found that for a given set of material properties, capacity estimate using solid element is higher than that using shell element, so that shell elements give conservative results for design.

So in this study, to model the structure shell element is chosen. The general purpose conventional shell S4R element is used due to its capability to model thin to thick shell structures. Also this element provides robust and accurate solutions to most applications. The 4-node element has six degrees of freedom at each node- translation in the x, y and z directions, and rotations about x, y and z-axes. The element uses reduced integration with hourglass control and is well suited for finite membrane strain nonlinear applications.

6.3 Material property model

Non linear model is considered for the analysis. The non-linear material is idealized as shown in figure-31 with an initial slope of Young's Modulus up to yielding and hardening up to about 30% of yield stress.

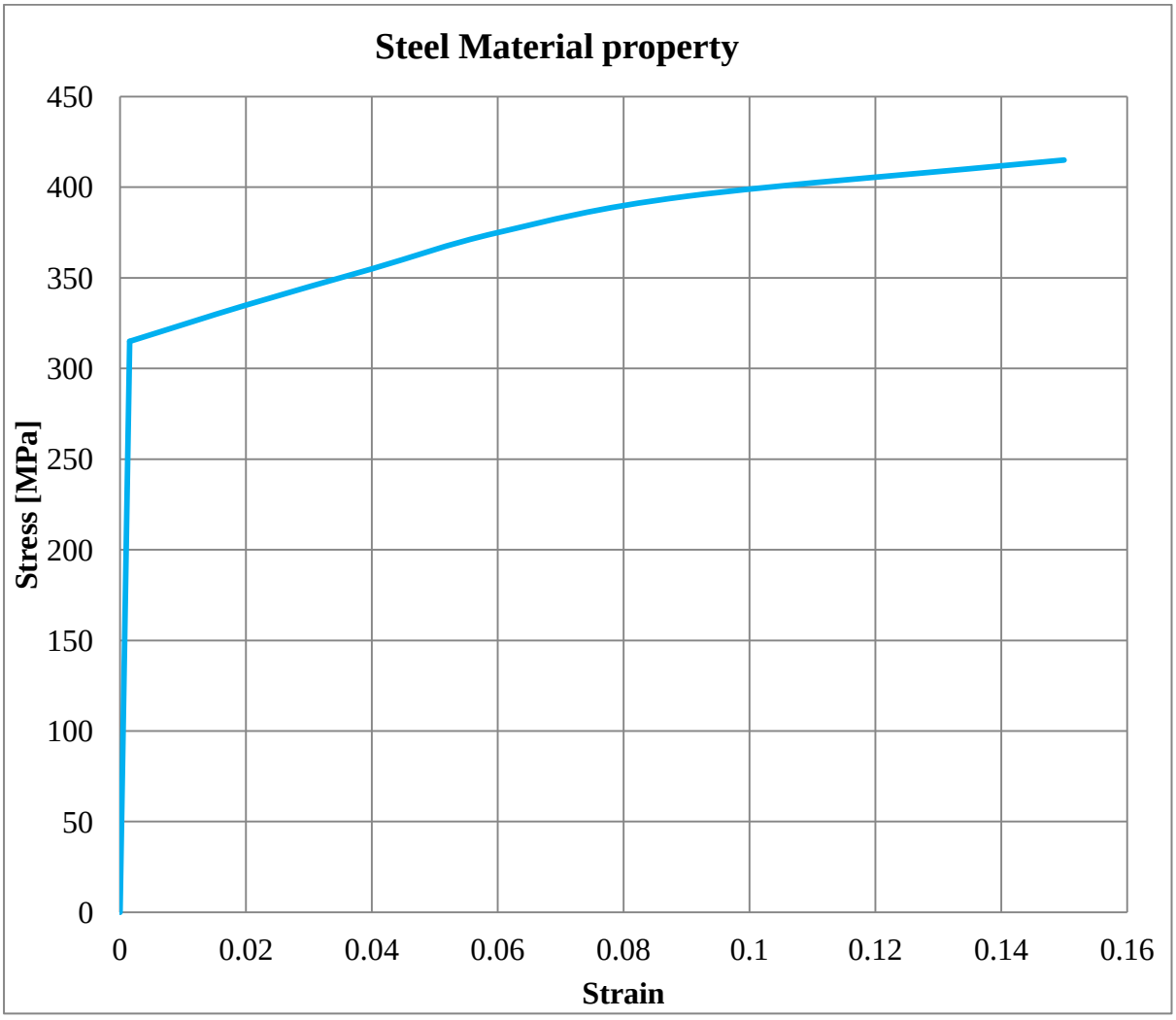

Figure 31 Material property

6.4 Modeling of Single frame

A single frame considers a stiffener with the attached shell plating as a representative model of the entire stiffened panel. The web and flange of a stiffener are free to move both vertically and horizontally whereas the shell plate is restricted to move sideways due to the presence of adjacent structure. The symmetric boundary condition simulates the support condition provided by adjacent side structure. The single frame idealizes the structure considered in design rules.

6.4.1 Boundary conditions

Symmetric boundary conditions are applied at two long edges of the plate to simulate the support provided by the adjacent structure. The two longitudinal ends are fixed to simulate the support provided by the transverse girder.

6.4.2 Steps involved in the modeling of a single frame

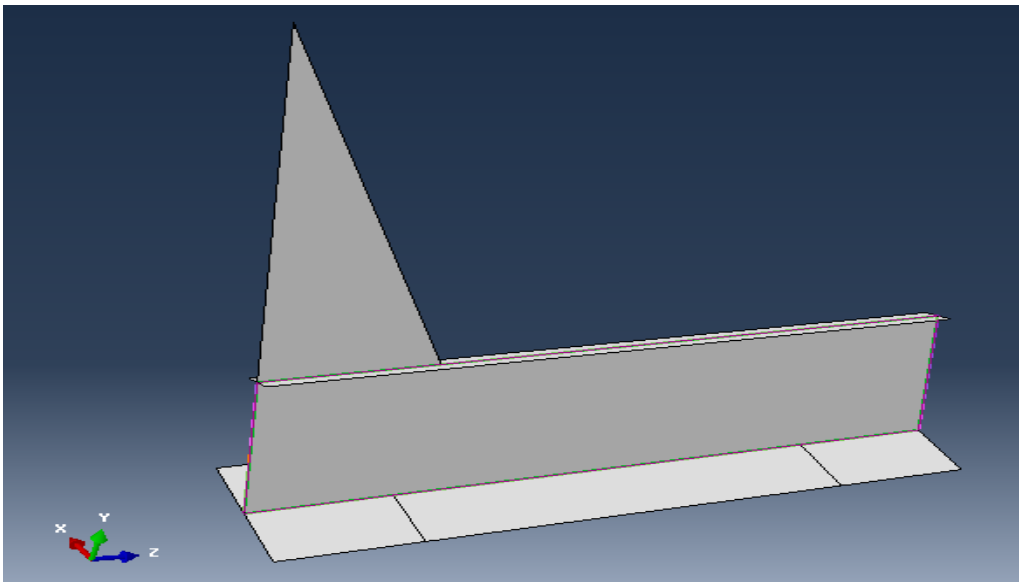

Figure 32 Step 1: 3D modeling of stiffener

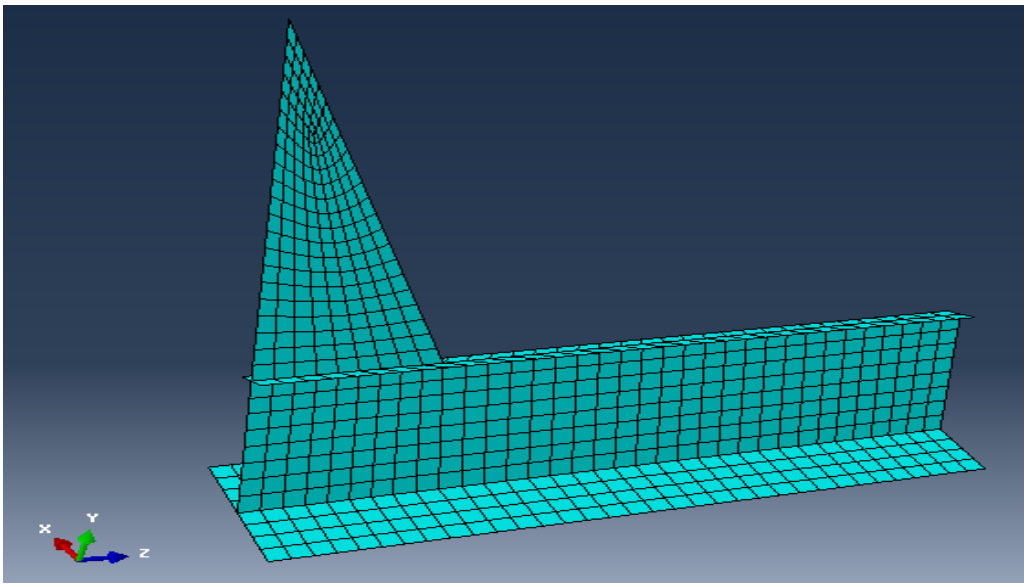

Figure 33 Step 2: Geometry discretized into finite elements

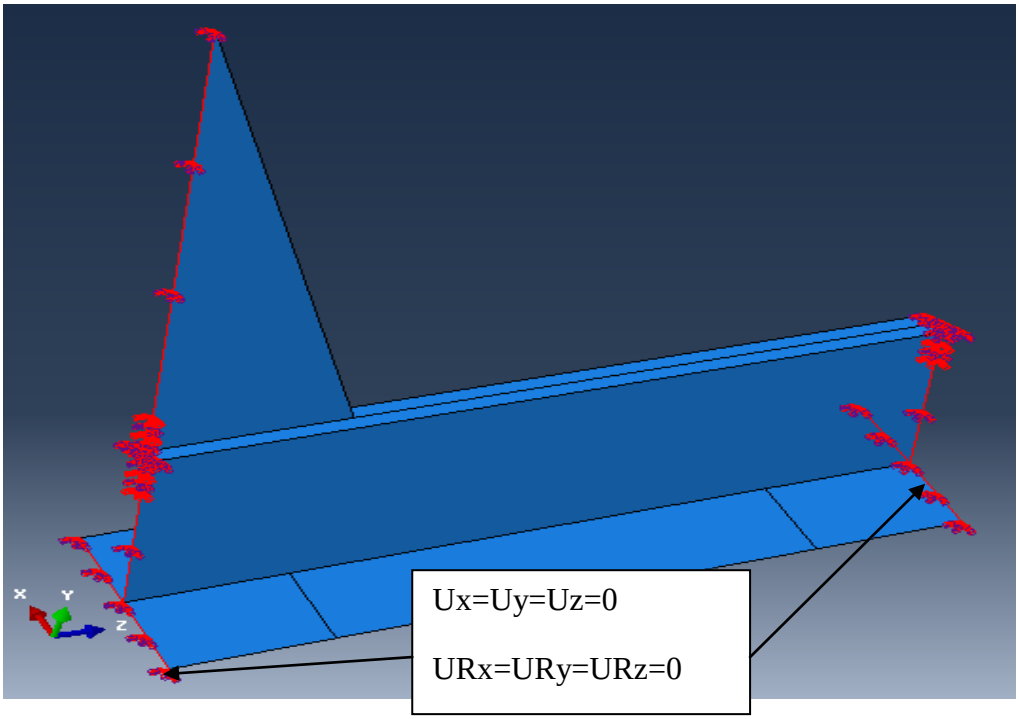

Figure 34 Step 3: Apply fixed boundary condition at longitudinal edges

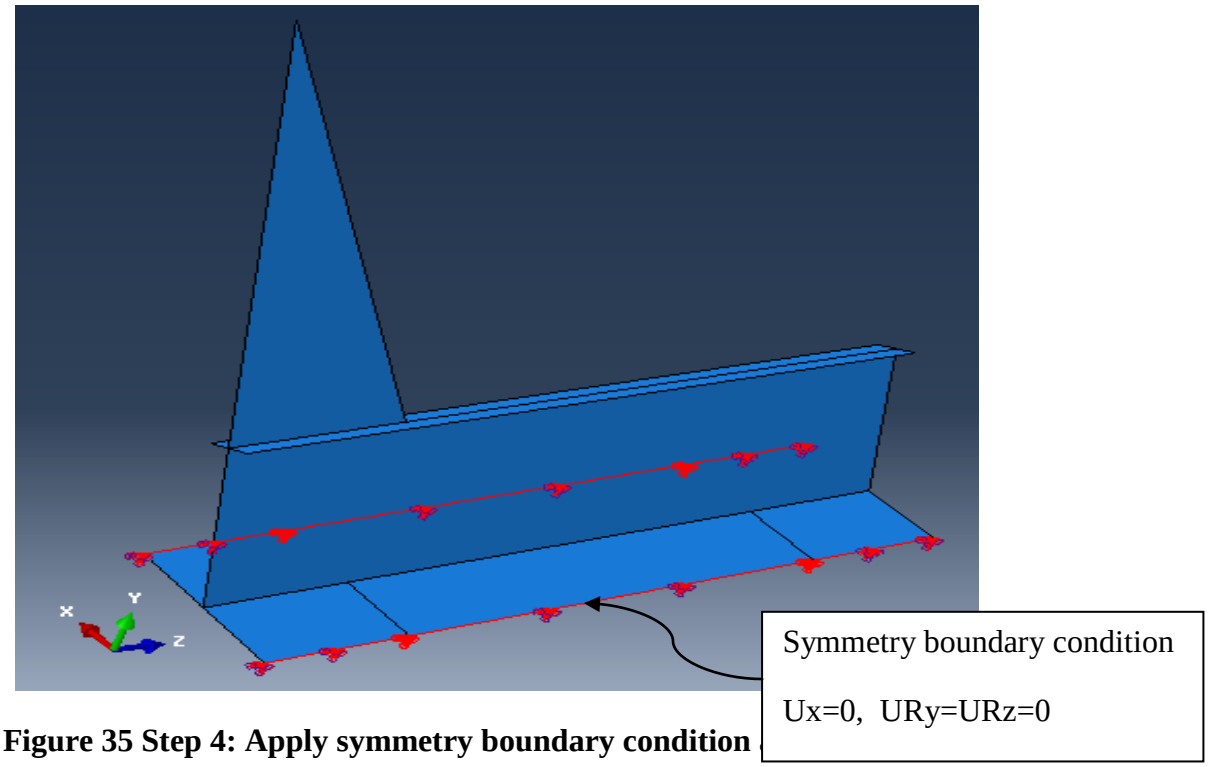

Figure 35 Step 4: Apply symmetry boundary condition

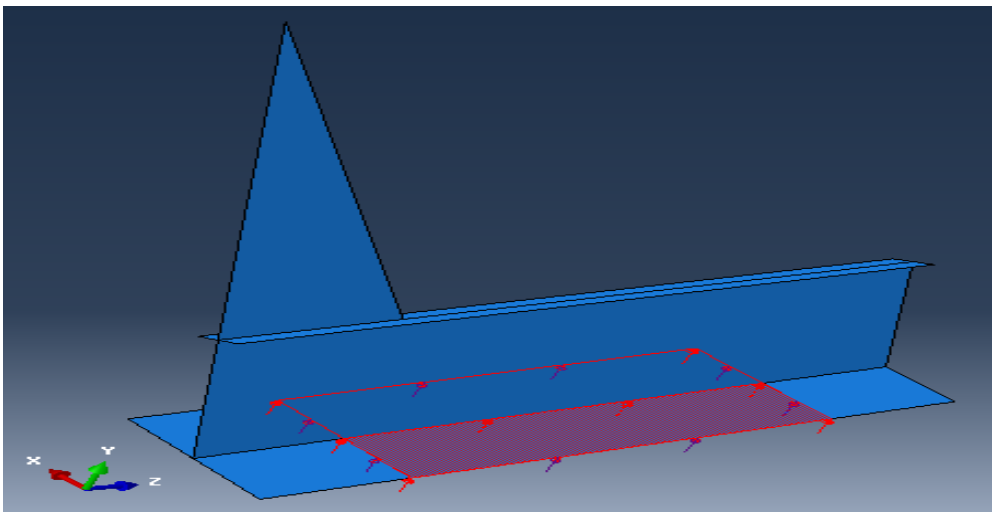

Figure 36 Step 2: Apply Loading

6.5 Modeling of ½+ 1+½ Frames

In order to simulate the boundary condition at longitudinal edges more precisely $^1/_2 + 1 + {}^1/_2$ frames are considered. At the span ends heavy transverse frame is provided which gives the necessary support at that location.

6.5.1 Step involved in the modeling of ½+ 1+½ frames

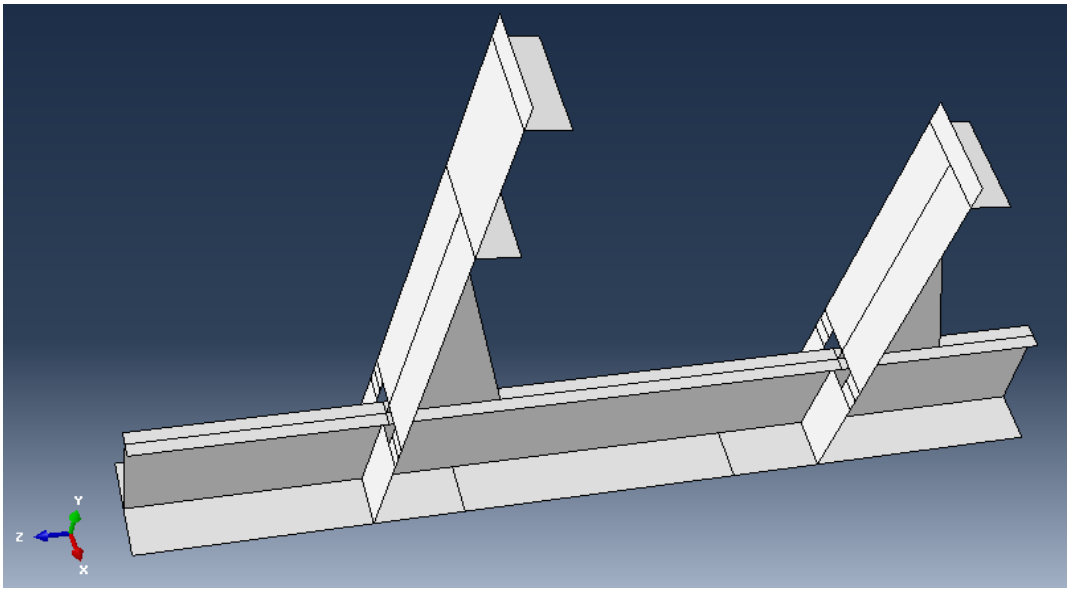

Figure 37 Step 1: 3D modeling of stiffeners

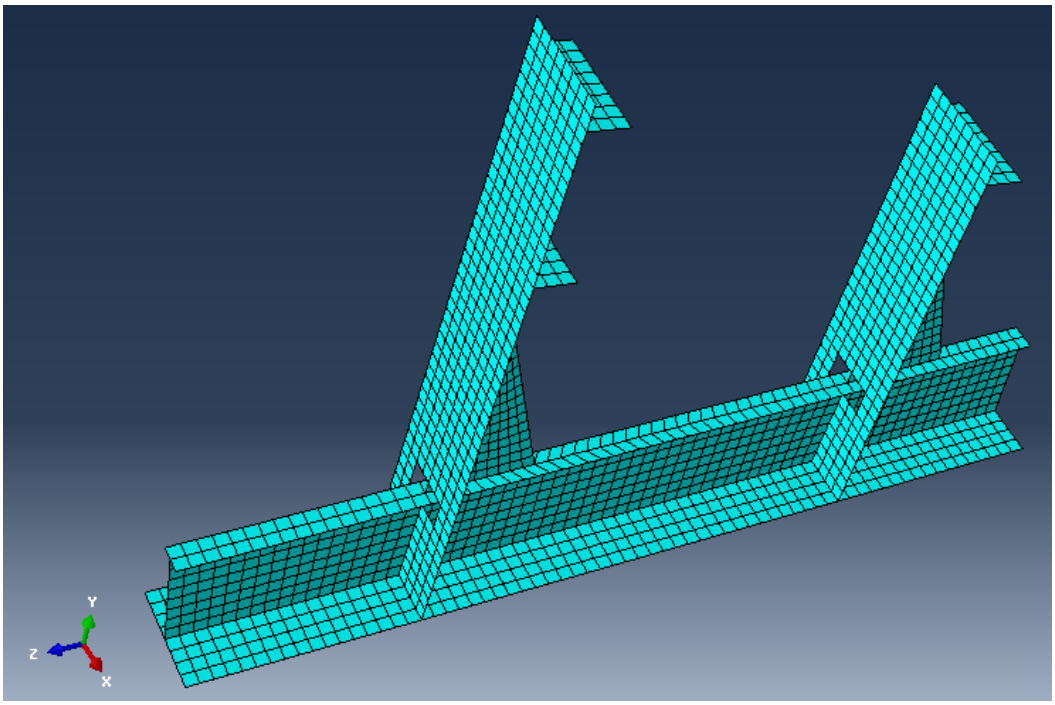

Figure 38 Step 2: Geometry discretized into finite elements

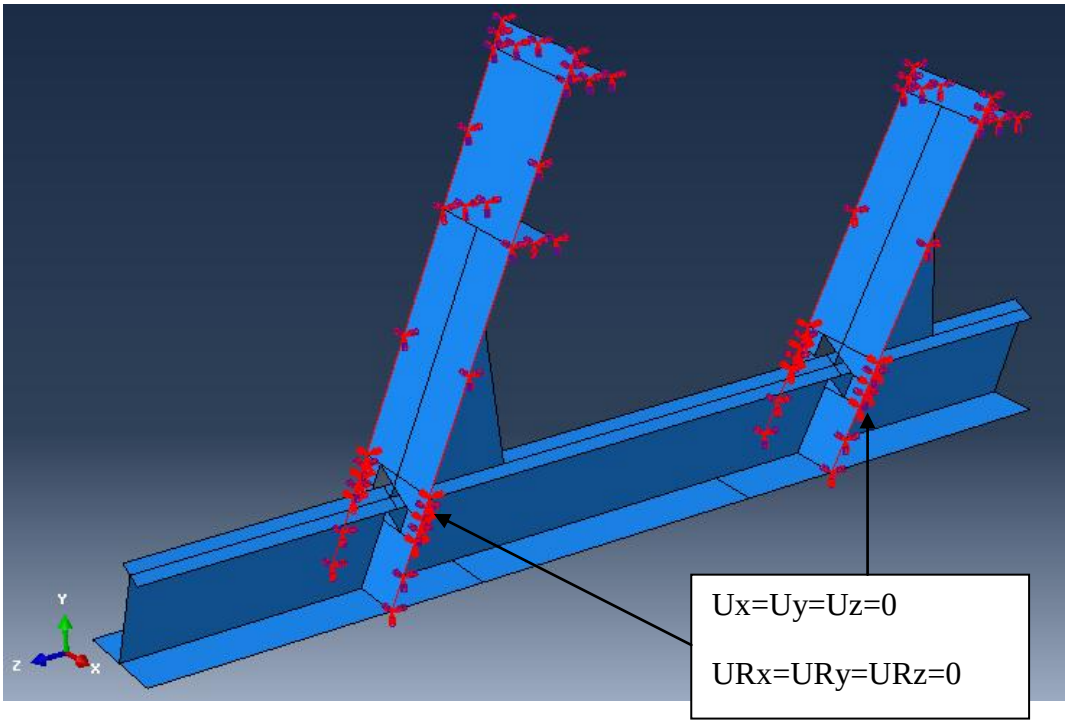

Figure 39 Step 3: Apply fixed boundary condition

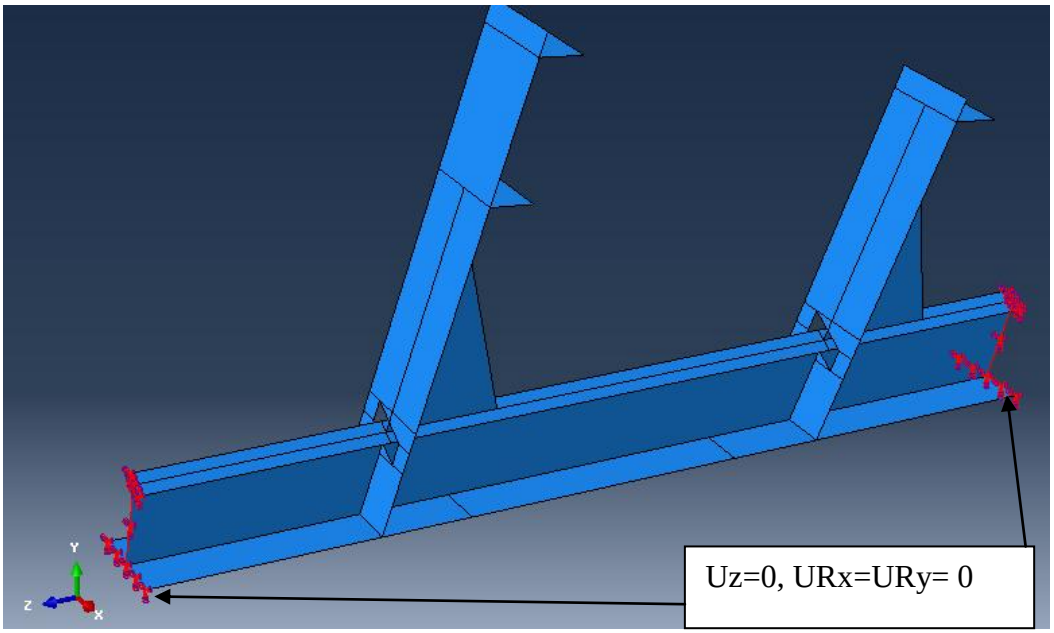

Figure 40 Step 4: Apply XY symmetric boundary condition

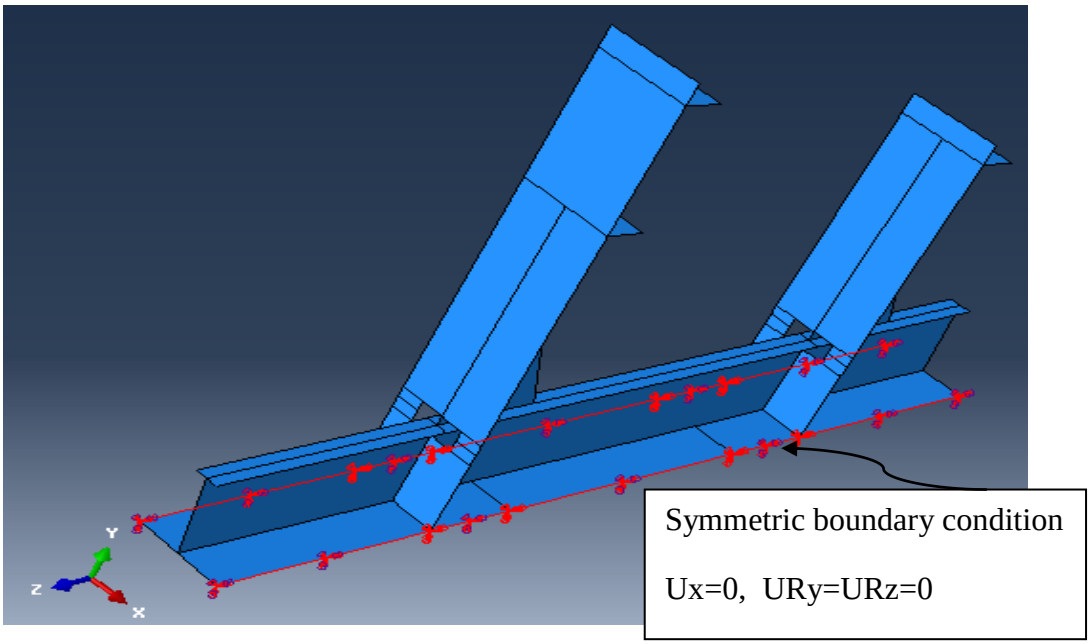

Figure 41 Step 5: Apply YZ symmetric boundary condition at long sides

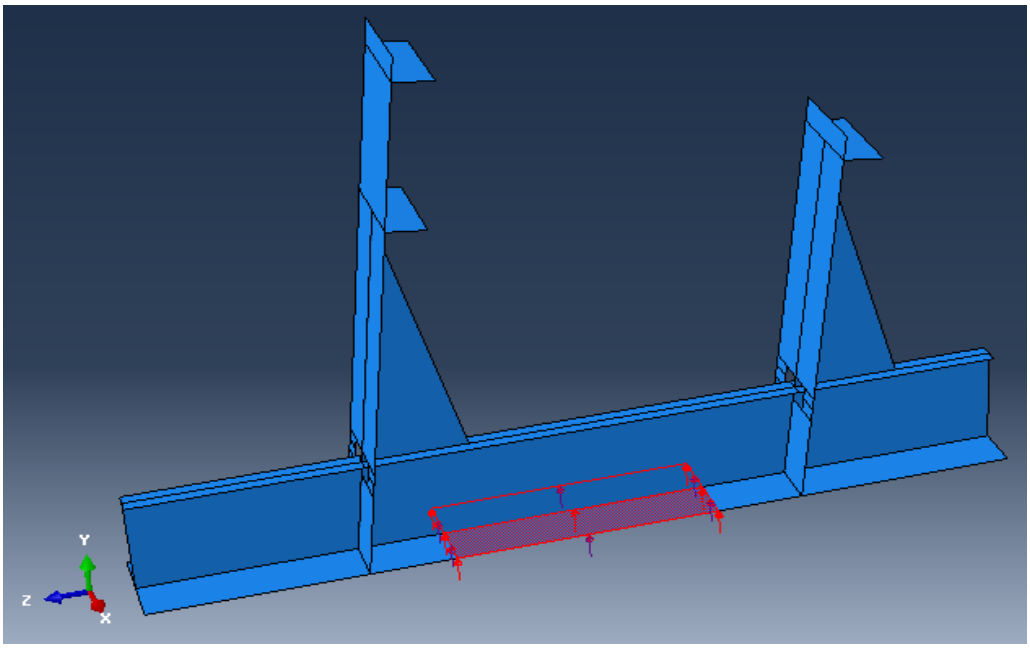

Figure 42 Step 6: Apply Loading

6.6 Modeling of Grillage

A grillage of $^1/_2 + 1 + {}^1/_2$frame spans in the transverse direction is considered. At the each span heavy longitudinal frame is provided which gives the necessary support at that location. Fixed boundary condition is applied at the longitudinal sides of the grillage. Symmetry boundary condition is applied at the transverse ends of the grillage to impose the support provided by the adjacent structure. Since the boundaries are far away from the point of application of load, it is considered that the boundary conditions have no significant effect on response of the frame. Thus in this grillage configuration both sides and longitudinal boundary conditions are considered to be accurate representation as in a real structure.

6.6.1 Loading

The pressure distribution during an ice structure interaction is considered for the analysis. The ice loading is idealized as a distributed pressure load with a center peak.

The ice load during a collision is approximated as patch load with a center peak and low pressure in nearby region. The length of the center peak is approximated as one frame spacing.

Table 2 represents the simplified ice load model considered for this study in consultation with supervisor (see figure 43).

Table 2 Load cases for grillage structure

Grillage case	Pick load on Zone 1-1 or Zone 2-1	Load on Zone 1-2	Load on 2-2	Load on 2-3
1	1	0		
2	1		0.5	0.25
3	5.82	1		

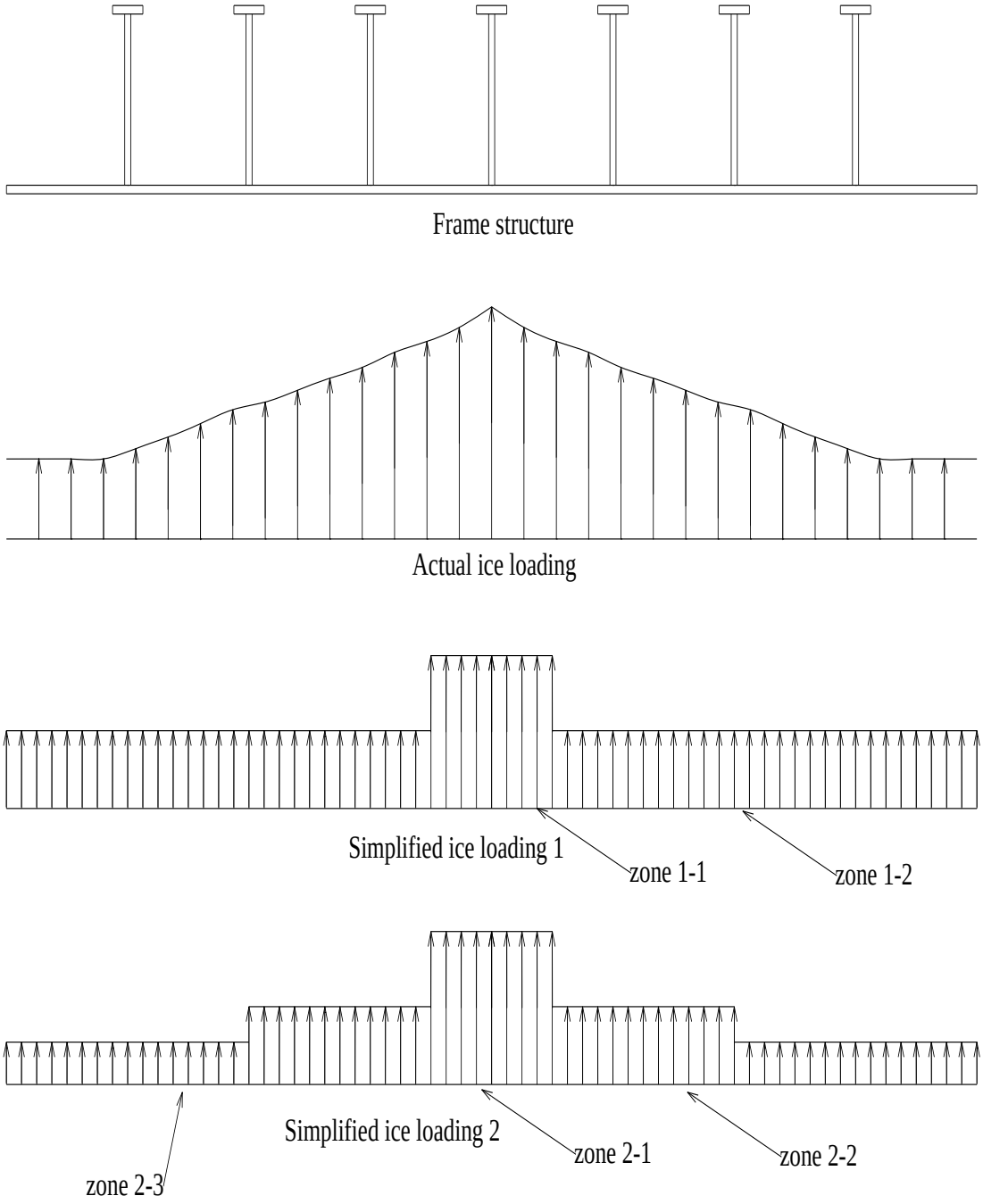

Figure 43 Simplified ice load to grillage structure

6.6.2 Steps involved in the modeling of grillage

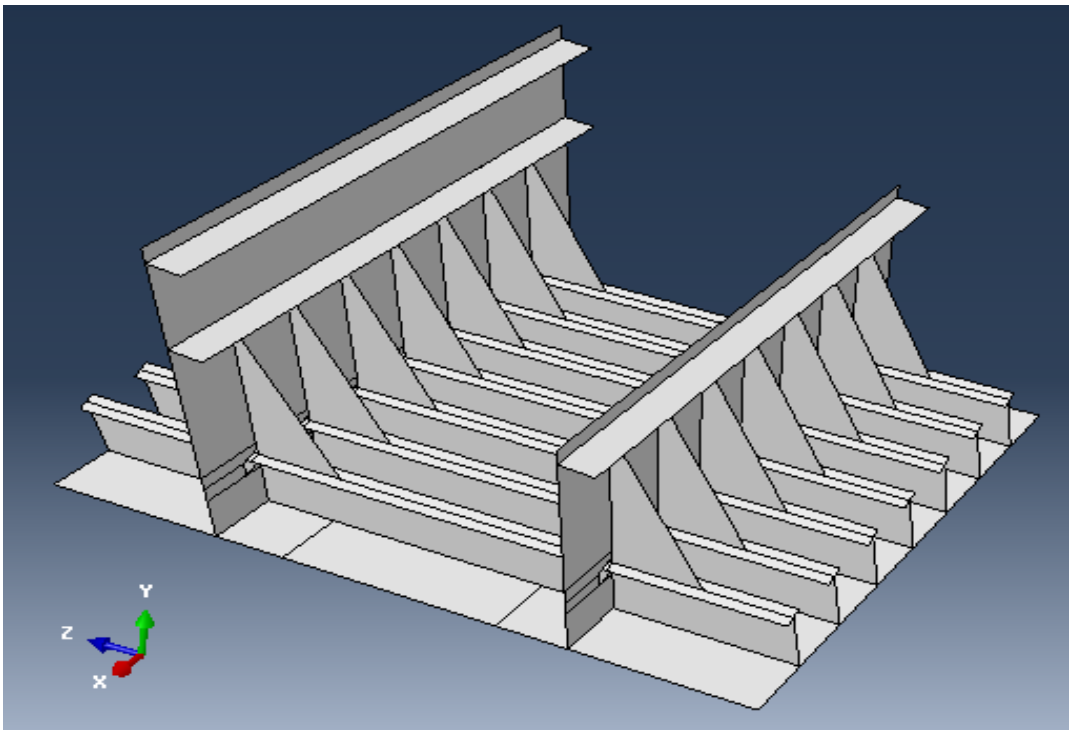

Figure 44 Step 1: 3D modeling of grillage

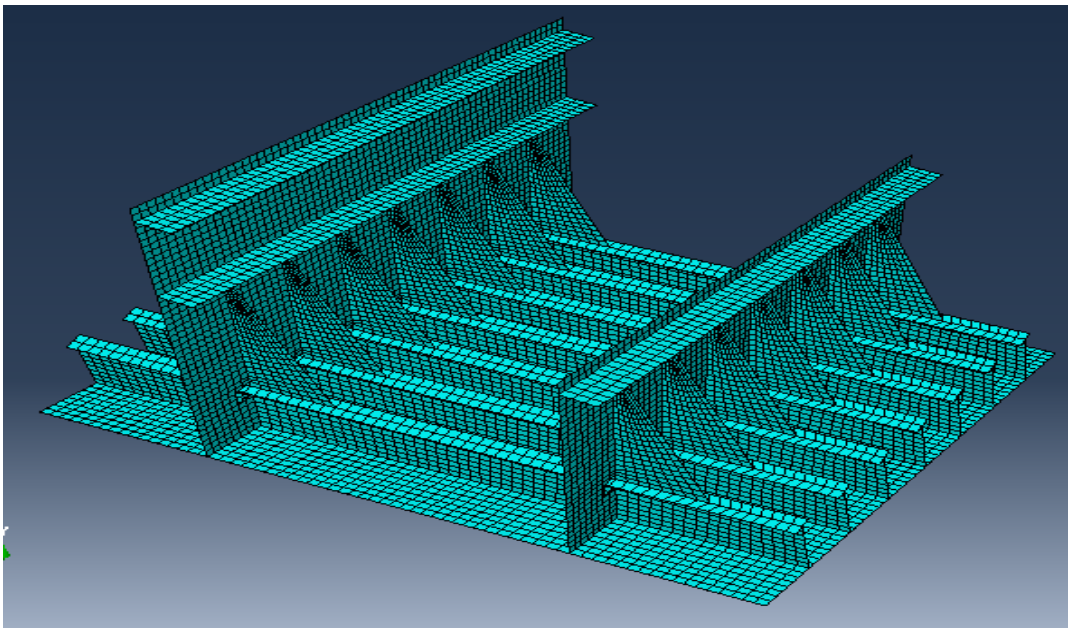

Figure 45 Step 2: Geometry discretized into finite elements

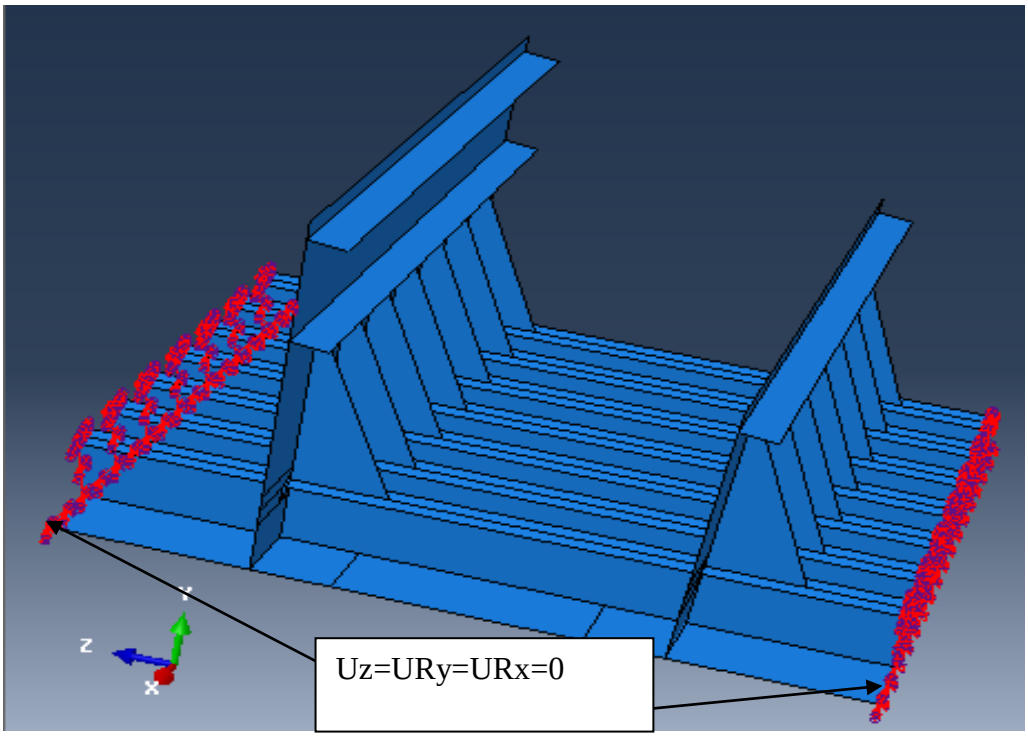

Figure 46 Step 3: Apply XY symmetric boundary condition

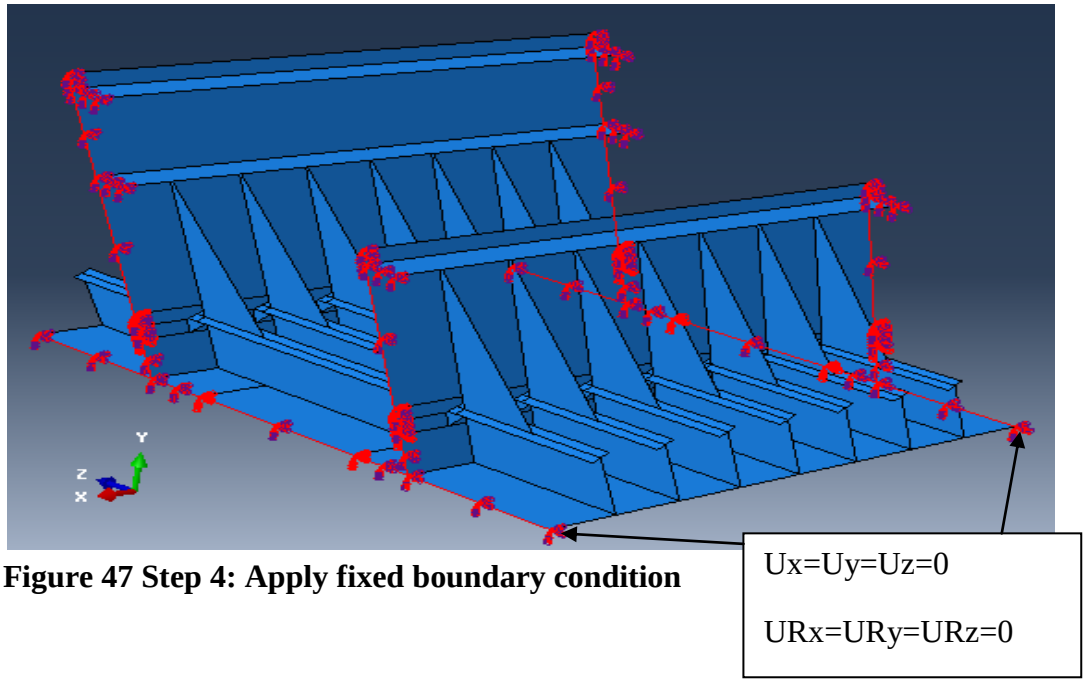

Figure 47 Step 4: Apply fixed boundary condition

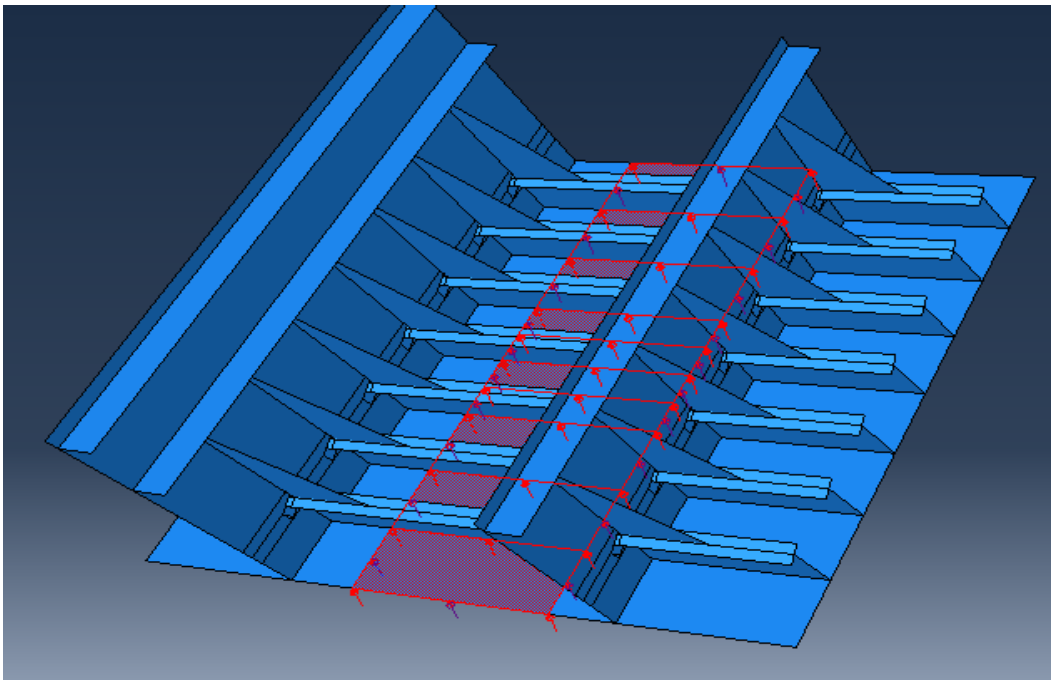

Figure 48 Step 5: Apply Loading

Chapter 7

7 Simulation and Analysis of ships' side frames and panels in Abaqus

7.1 Introduction

Ship hull structure primarily consists of plate stiffened either longitudinally or transversely or a combination of both. In case of longitudinal framing, the primary stiffeners run in the longitudinal direction. The longitudinals are supported by heavy transverse frames running in the other direction. And in the case of transverse framing, the primary stiffeners run in the transverse direction and supported by heavy longitudinal frames running in the other directions. In both framing, the stiffeners commonly used are tees, angles (L), bulb and flat bars. So, to understand the behavior of ships' side structure subjected to ice loads both longitudinal and transverse frames were simulated and analyzed in Abaqus. In order to simulate the effect of adjacent structure on the frame, ½+1+½ frames and stiffened panel were also simulated and analyzed. The outcome of all these analyses has been described here.

7.2 Analysis of Longitudinal frame

As longitudinal frame run in the longitudinal direction, the whole frame span in a region of ice affected zone will be in touch with ice meaning the ice load act over the whole span length of the frame. So, the longitudinal frames shown in Table 3 were all analyzed with a uniform load over the entire span. The main variants were section type, web thickness, frame length and the presence or absence of brackets.

σ_y = yield stress = 315 MPa

Table 3 Longitudinal Frames

Case no.	Section type	Plate thick [mm]	Web height [mm]	Web thick [mm]	Flange width [mm]	Flange thick, [mm]	Frame length [mm]	End bracket [mm]	Capacity by IACS UR formula P_{3h} [MPa]
1	L	20	308	11	95	16	2400	300x300x 15	1.39
2	L	20	308	11	95	16	1800	No brackets	1.62
3	L	20	308	11	95	16	3600	300x300x 15	0.93
4	L	20	308	11	95	16	3000	No brackets	1.01
5	L	20	308	9	95	16	2400	300x300x 15	1.15
6	L	20	308	7	95	16	2400	300x300x 15	0.91
7	L	20	308	8	95	16	2400	No brackets	0.9
8	T	20	308	11	95	16	2400	300x300x 15	1.39
9	T	20	308	11	95	16	1800	No brackets	1.62
10	T	20	308	11	95	16	3600	300x300x 15	0.93
11	T	20	308	11	95	16	3000	No brackets	1.01

7.2.1 Discussion of FE analysis results

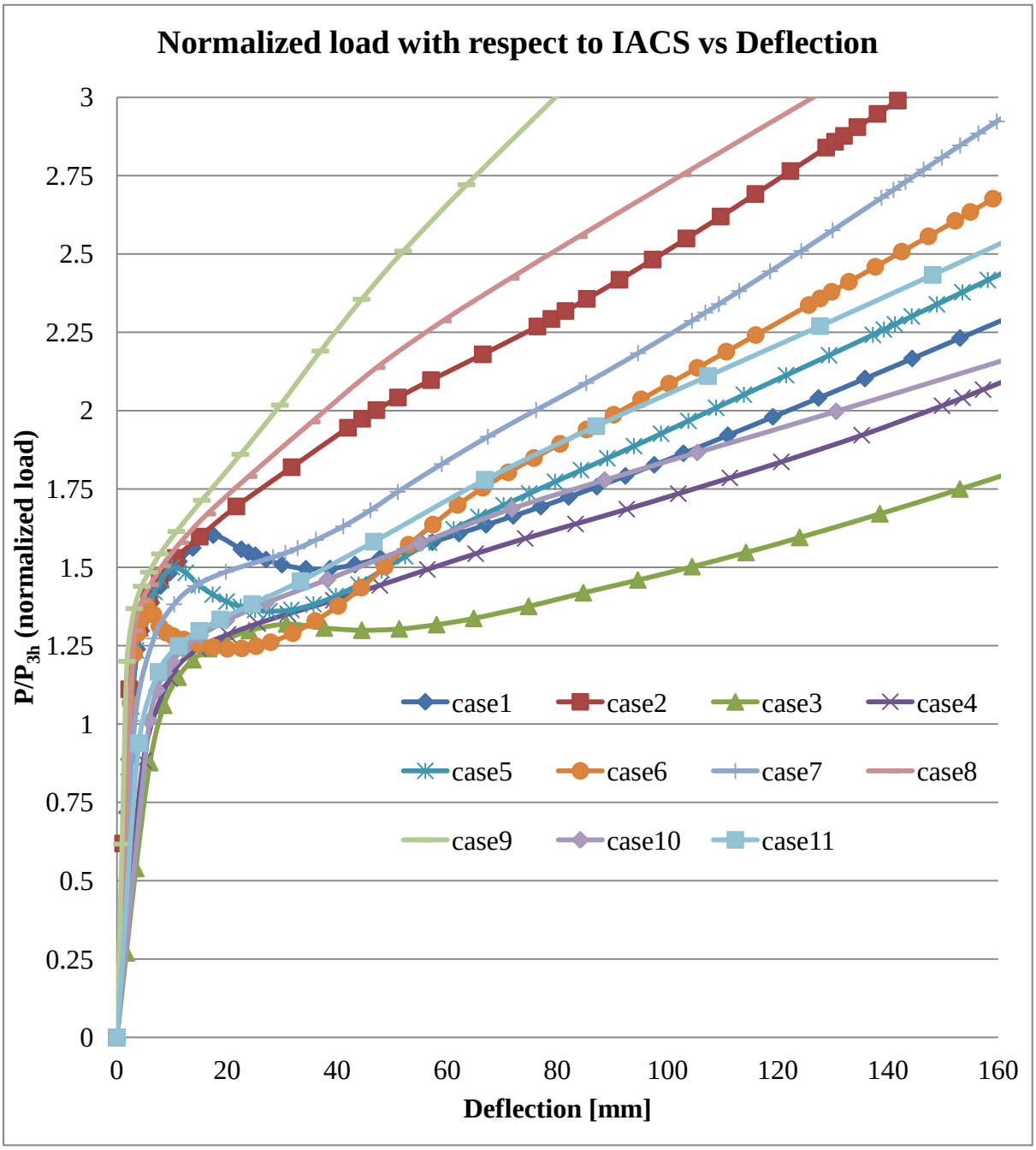

Figure 49 Normalized load (with respect to IACS)-deflection curves for different longitudinal frames

It is observed from the longitudinal frame analysis that all the frames in Table 3 (see Figure 49) have enough capacity to sustain IACS UR formulae design load, and maintain this capacity even at large deformations. The local deformation of the stiffener web under the bracket toe (e.g Figure 50) has no crucial influence on the global stiffener capacity. The small loss of the capacity manifested as slump on the load deflection curves, caused by local web buckling, still leaves a substantial capacity reserve to the stiffener. Those localized deformations seem to be the result of web overloading in shear, causing the web to buckle. Short stiffeners with end bracket fitted are particularly susceptible to this behavior.

The figure 50 represents the load deflection curves for different L frames with and without end brackets. It seems from the figure that the capacity of frame improve in elastic region and onset of plastic deformation due to end brackets but no significant improvement is found at moderate and large deformation.

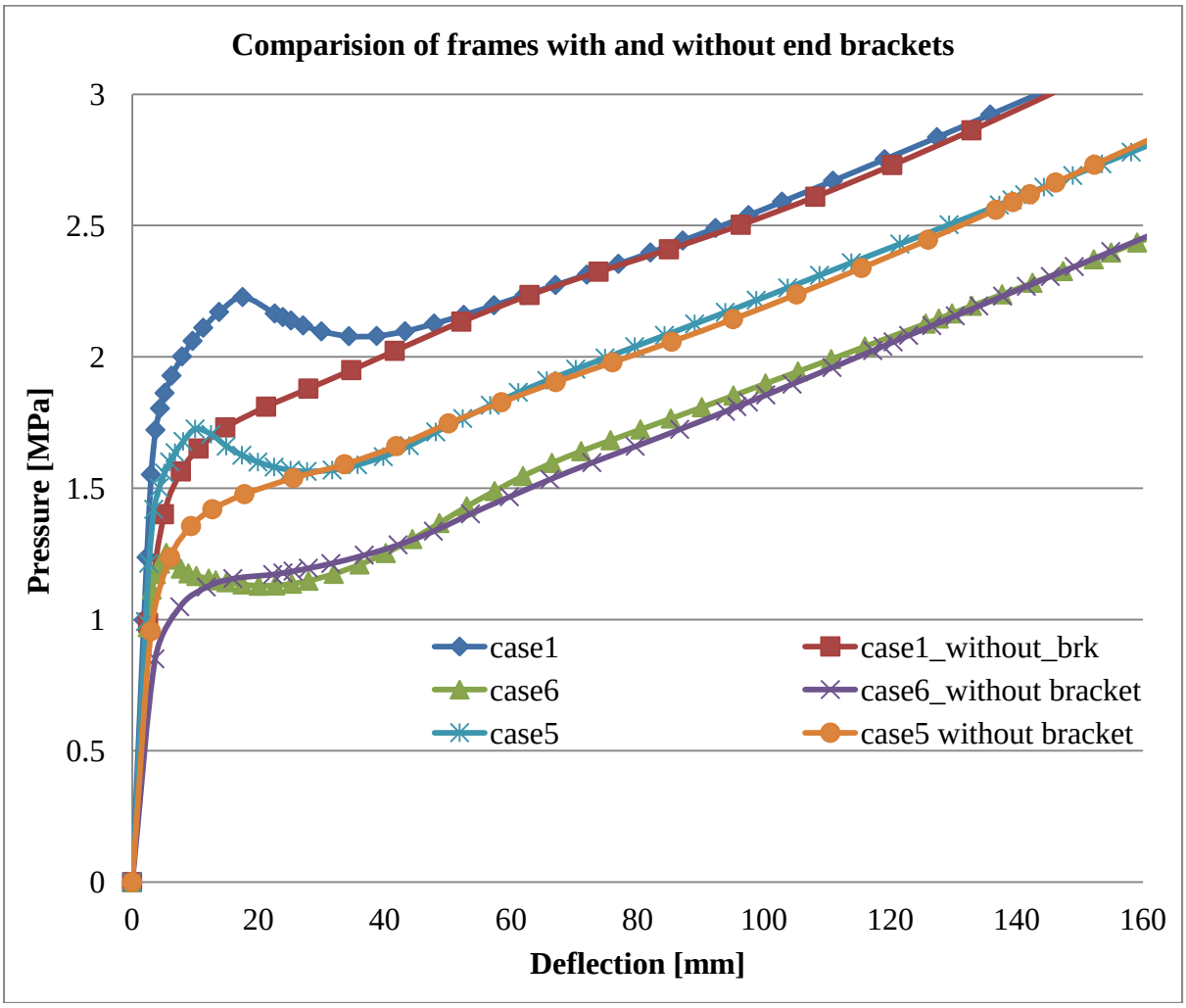

Figure 50 Load deflection curves - Frames with and without end brackets.

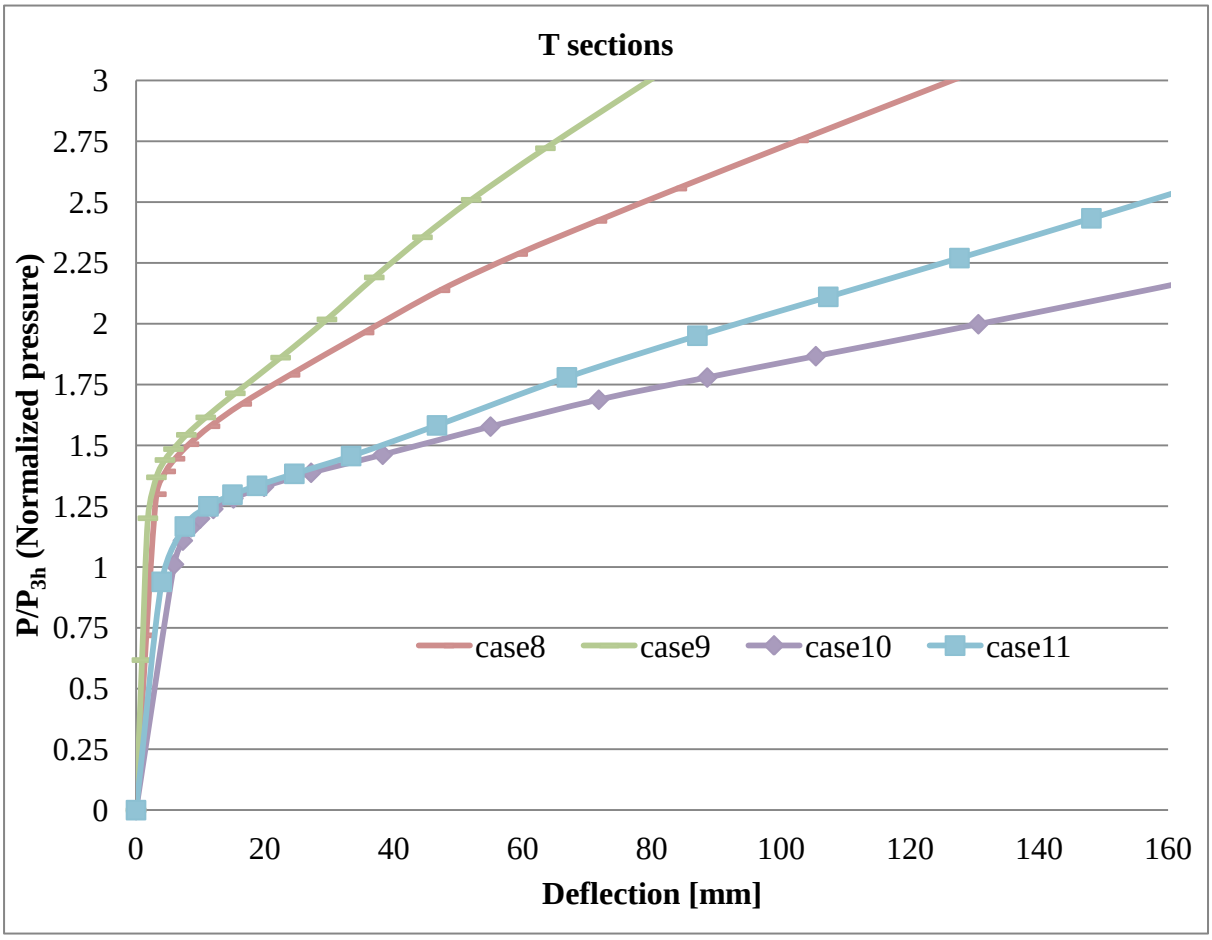

Figure 51 Normalized load-deflection curves for different T sections

Figure 51 shows just the T profiles with and without end brackets. Shorter T frames (case 8&9) result in higher capacity, though the results do not seem to be smoothly dependant on length. It seems that above a certain length, the capacity falls. This may indicate that a certain behavior occurs in frames longer than a critical value.

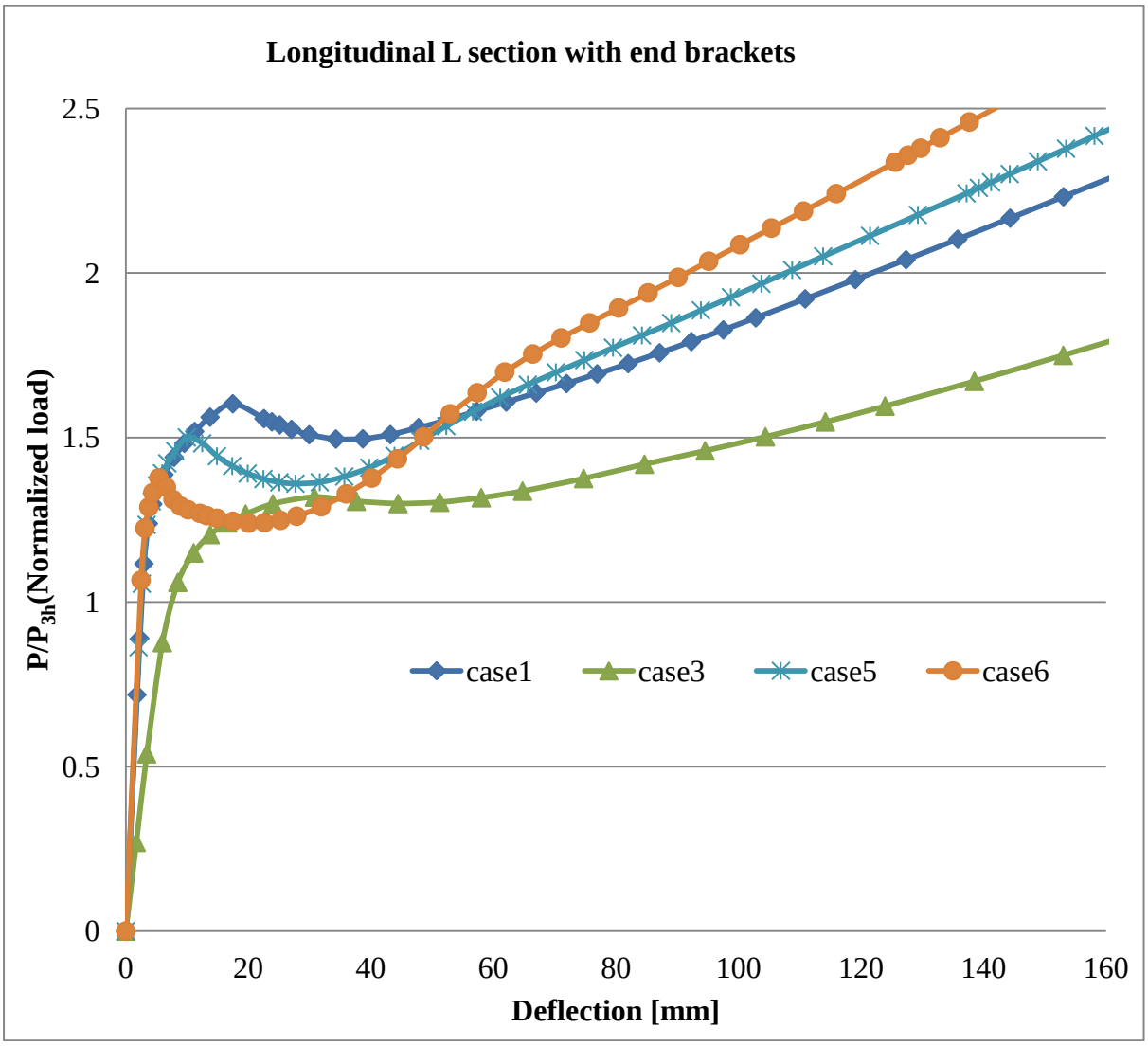

Figure 52 Normalized load-deflection curves for different L sections with end brackets

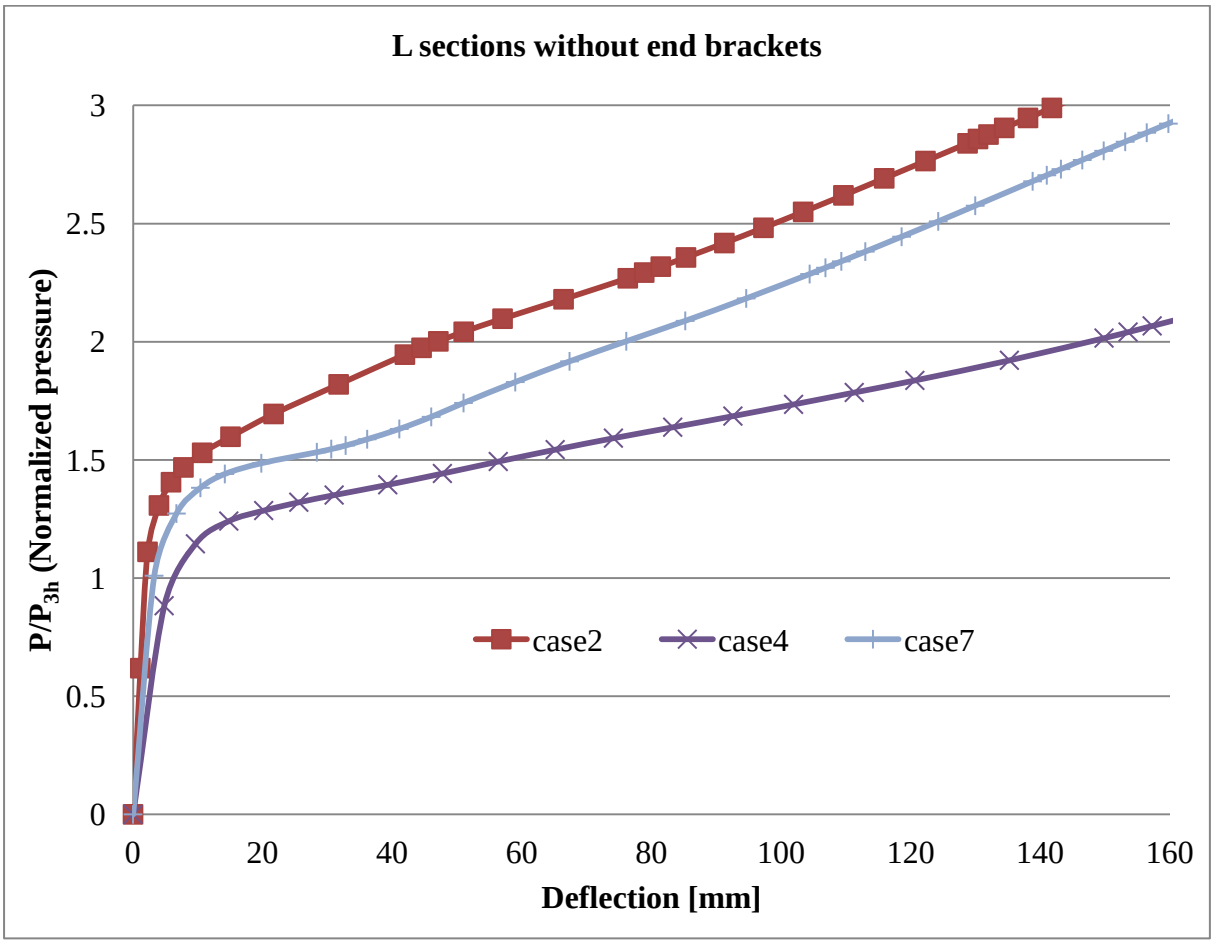

Figure 53 Normalized load-deflection curves for different L sections without end brackets

Figure 53 shows L frames without brackets. Similar to T frames, the shorter frames exhibit greater capacity. Asymmetry causes earlier web overloading problems with L sections. In both L and T sections the membrane effects eventually become effective, though only after large localized web deformations.

Figure 52 shows L frames with brackets. Sudden drop of the capacity is observed in most cases. The frames with thinner webs exhibit a more sudden drop in capacity. The longer frames appear to have a lower design capacity, yet tend not to show any sudden drops in capacity.

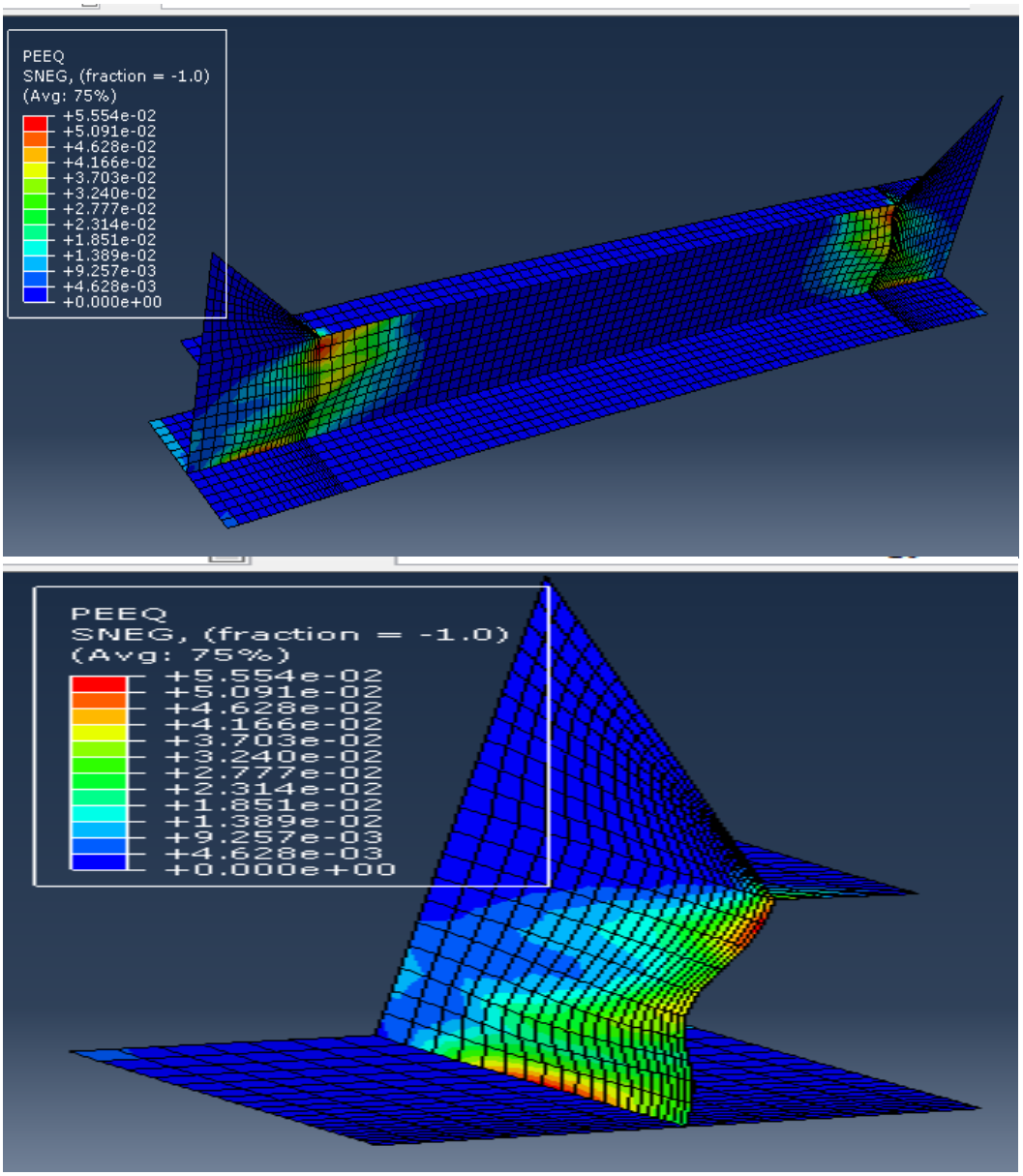

Figure 54 Plot of deformation (with equivalent plastic strain contour) at normalized pressure 1.239868 for L frame case 6.

7.3 Analysis of transverse stiffener

7.3.1 Upright stiffener and warping effect

As transverse stiffeners run in the transverse direction, the portion of the frame in touch with ice will be maximum ice thickness. So, transverse frames shown in Table 4 were all analyzed with a patch load length 400mm and breadth equal to stiffener spacing. The main variants were section type, web thickness, frame length and the presence or absence of end brackets and tripping bracket at mid-span.

Table 4 Transverse frames

Case no.	Section type	Plate thick [mm]	Web height [mm]	Web thick [mm]	Flange width [mm]	Flange thick, [mm]	Frame length [mm]	End bracket [mm]	Capacity by IACS UR formula P_{3h} [MPa]
1	L T	20	308	11	95	16	2400	300x300 x15	7.21
2	L T	20	308	9	95	16	2400	300x300 x15	6.24
3	L T	20	308	8	95	16	2400	300x300 x15	5.55
4	L T	20	308	13	95	16	2400	300x300 x15	8.07
5	L T	20	308	11	95	16	2400	No brackets	6.57
6	L T	20	308	11	95	16	2100	No brackets	7.22
7	L T	20	308	16	95	16	2400	No brackets	8.37
8	L T	20	308	16	95	16	3600	No brackets	5.7722

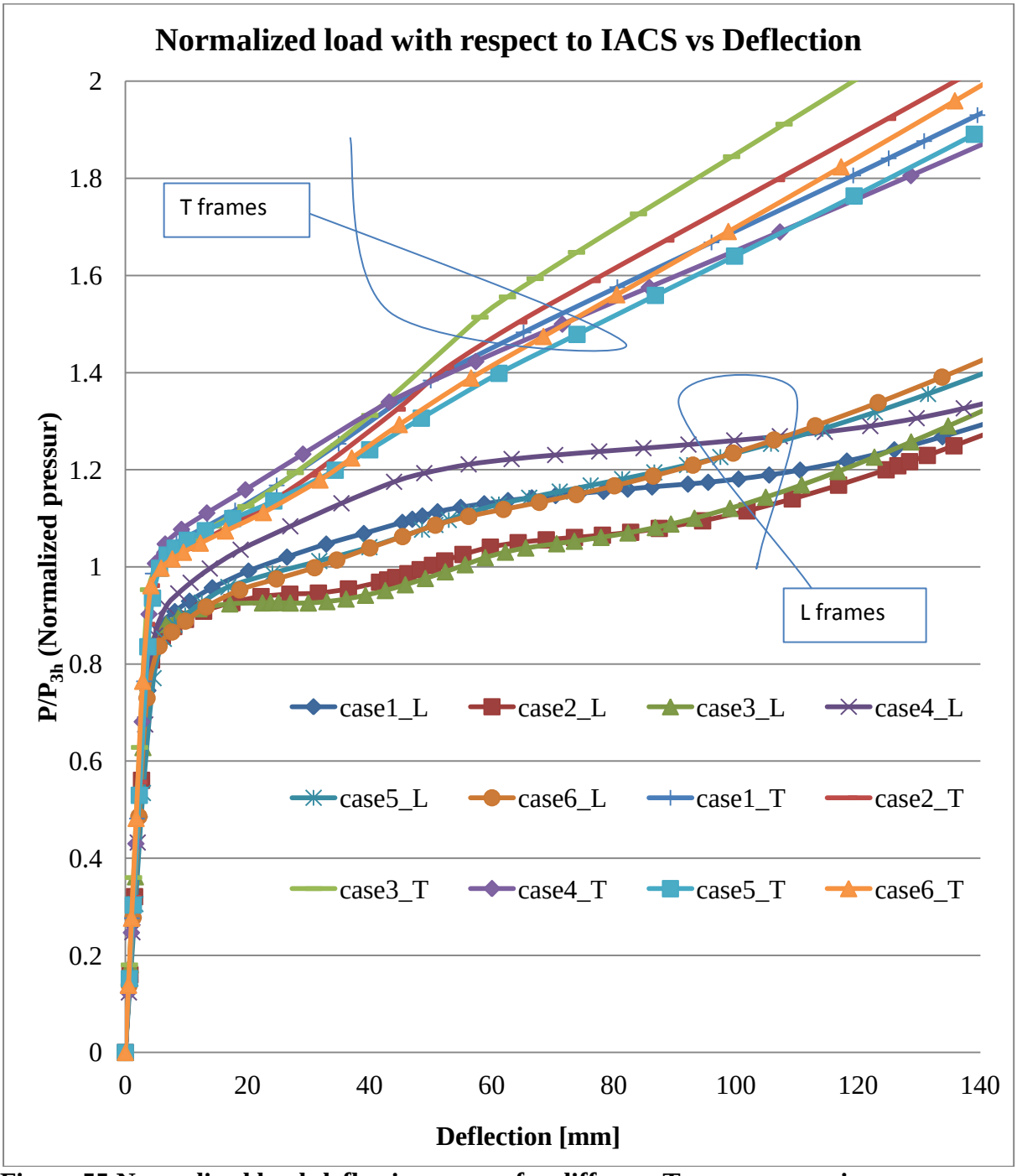

Figure 55 Normalized load-deflection curves for different Transverse sections

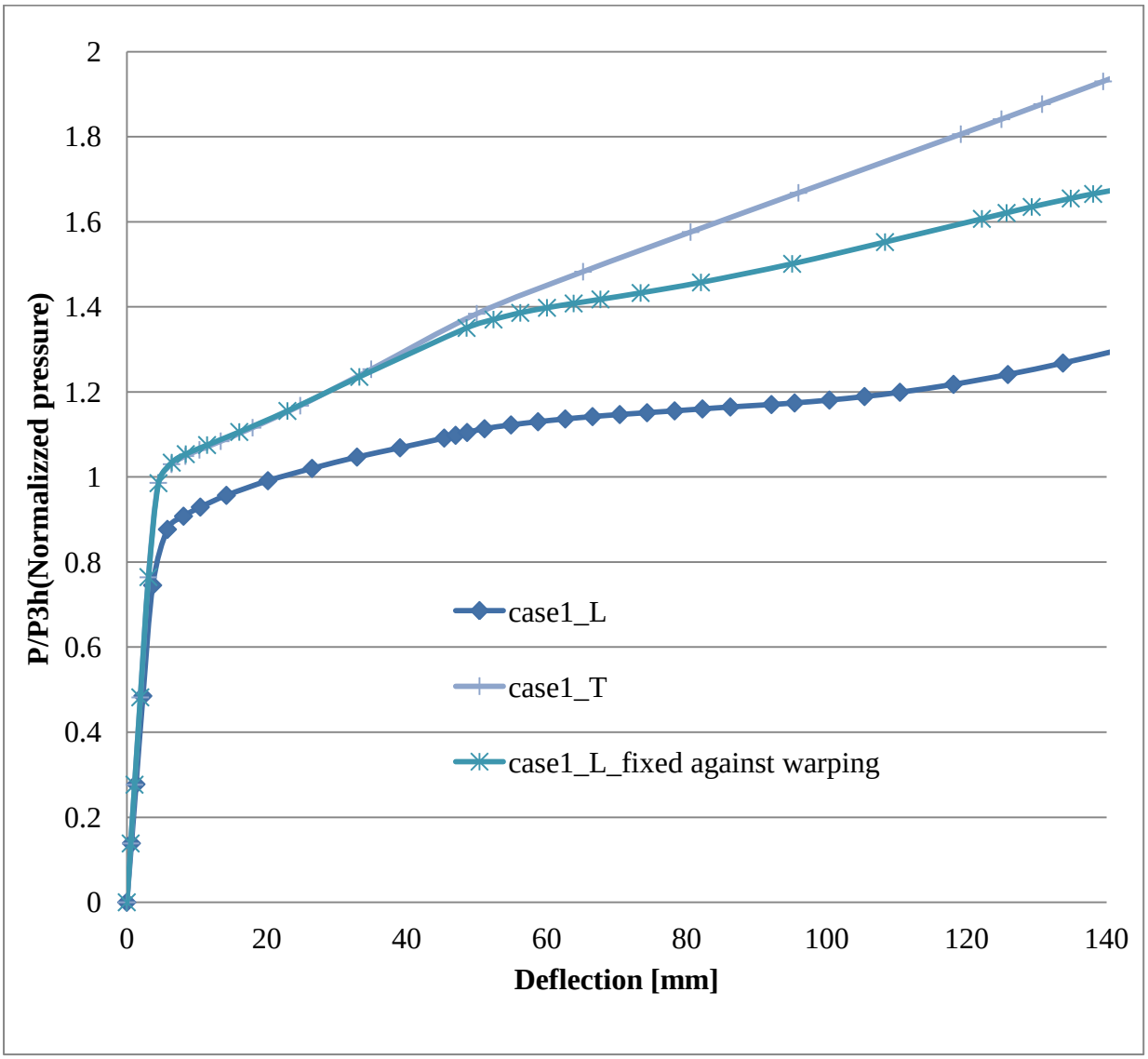

Figure 56 Normalized load (with respect to IACS UR)-deflection curves for frame cas1

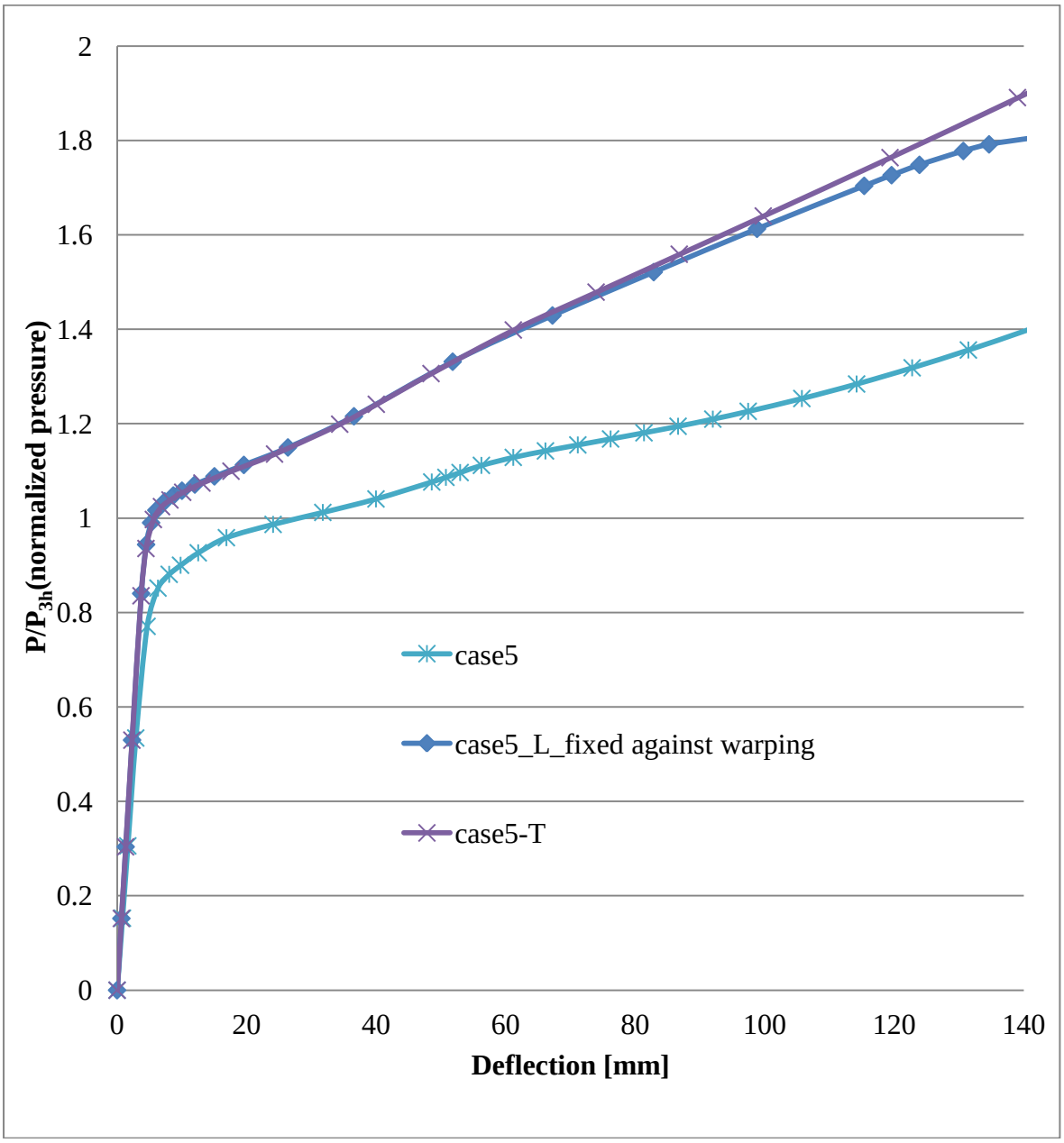

Figure 57 Normalized load (with respect to IACS UR)-deflection curves for frame cas5

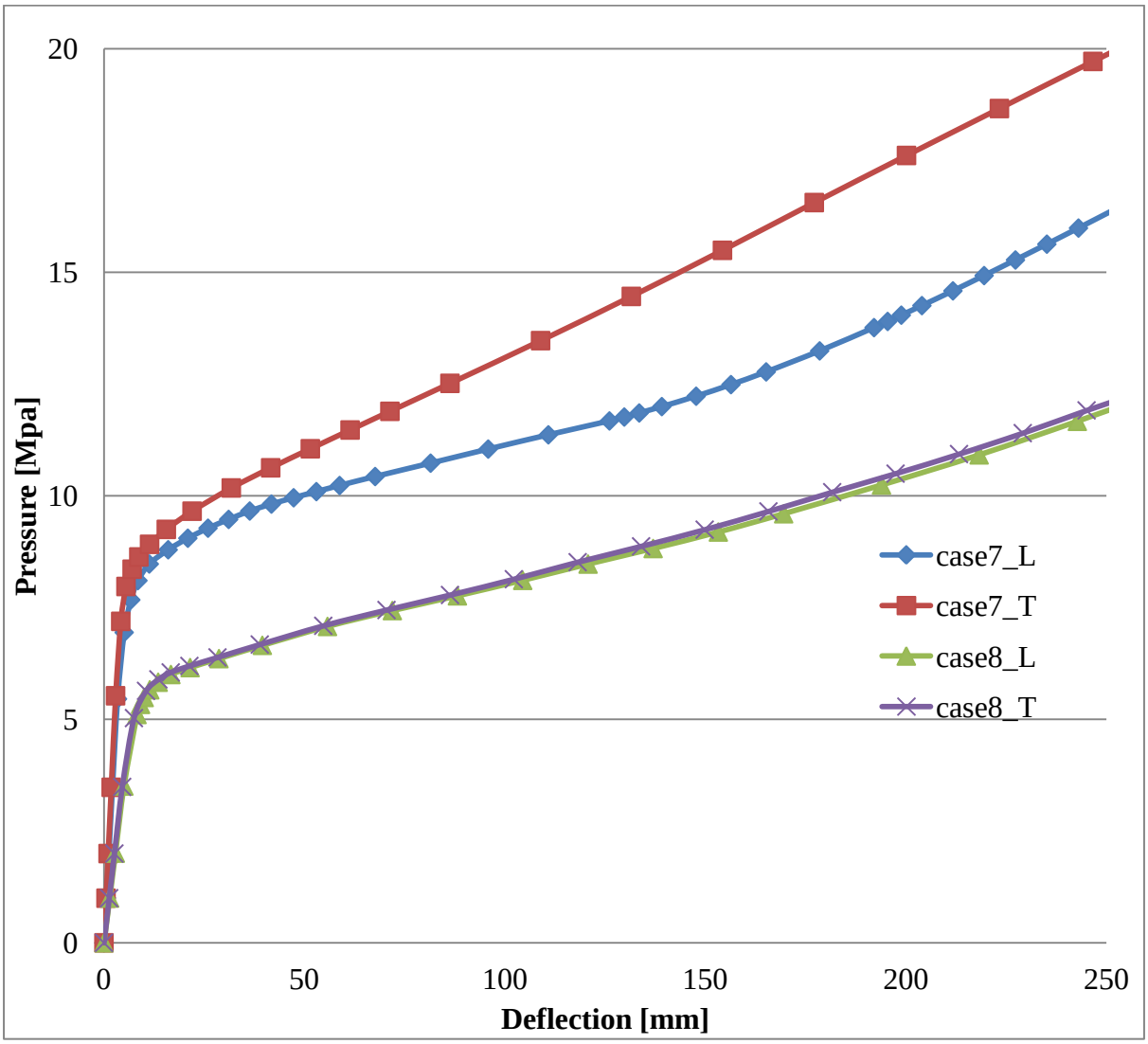

Figure 58 load-deflection curves for frame case7 and case8

7.3.1.1 Discussion of FE analysis results

It is observed from the transverse frame analysis that all the T frames in Table 4 (see Figure 55) have enough capacity to sustain IACS UR formulae design load, and maintain this capacity even at large deformations. Though L frames have similar cross sectional properties like T, they don't have enough capacity to sustain IACS UR design load. To understand this discrepancy in behavior of L and T frame, L frames were also analyzed by applying restriction against warping. It is clear from the figure 56 & 57 that warping causes the failure of L frame prior to achieve the capacity similar to that of T frame. It is been mentioned on chapter 3.7.1"warping effect" that warping resistance of a section depends on the following parameter

$$\beta = \frac{{t_w}^2 l^2}{80 h_{fc} {b_f}^2 t_f} + \frac{b_e}{b_f}$$

If the parameter β is greater than or equal to 0.5, there will be no loss of capacity in the section due to warping that means the stiffener web is strong enough to resist the unsymmetrical response of flange. The parameter β is directly proportional to the square power of the web thickness and the frame length. To understand this ideology, the web thickness of frame case 5 was increased to 16 mm (case 7) and run the FE analysis. The result has shown in figure 58. It is observed that capacity reduction due to warping decreases greatly due to the increased web thickness (see figure 57 & 58). To investigate the span length dependency of warping effect, the length of the case 7 was increased from 2400mm to 3600mm (case 8) and analyzed the frames in Abaqus. There is no significance difference of behavior found in the load deflection characteristics curves of L and T frames (see figure 58, case 58) meaning span length also has great impact on the warping effect.

It is resembled from the figures 60, 62, 63 & 64 that the L frames fail due to local web buckling at mid-span under patch load at IACS UR limit state load. Whereas at the same load T frame does not fail (see figure 59, 61 & 66). It is obvious that lateral pressure loads applied on frames will develop stresses in the flange of the stiffener. But the stresses in an unsymmetrical stiffener flange will create a second-order bending moment with respect to the web location. When the constraining capacity of the stiffener web does not have sufficient strength to counteract the unsymmetrical response of the flange, the web tends to buckle at mid span.

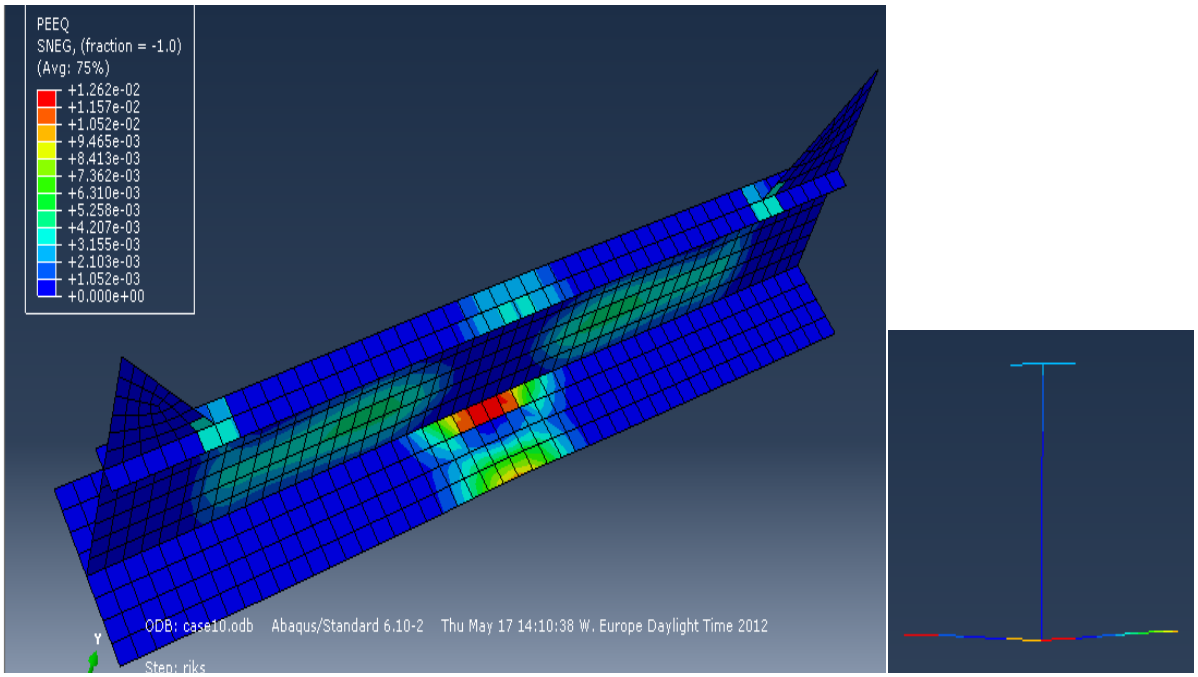

Figure 59 Plot of deformation (with equivalent plastic contour) and section at mid-span for case1_T frame at normalized pressure 1.05

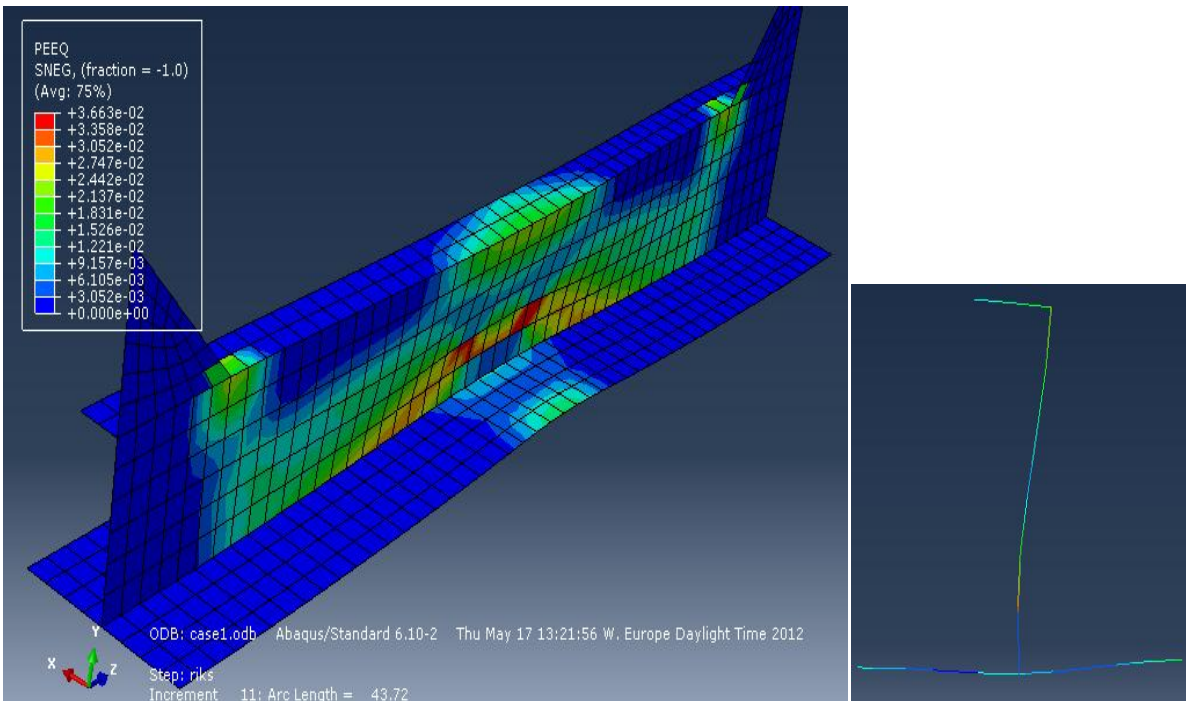

Figure 60 Plot of deformation (with equivalent plastic contour) section at mid-span for case1_L frame at IACS UR limit state load (Normalized load 1)

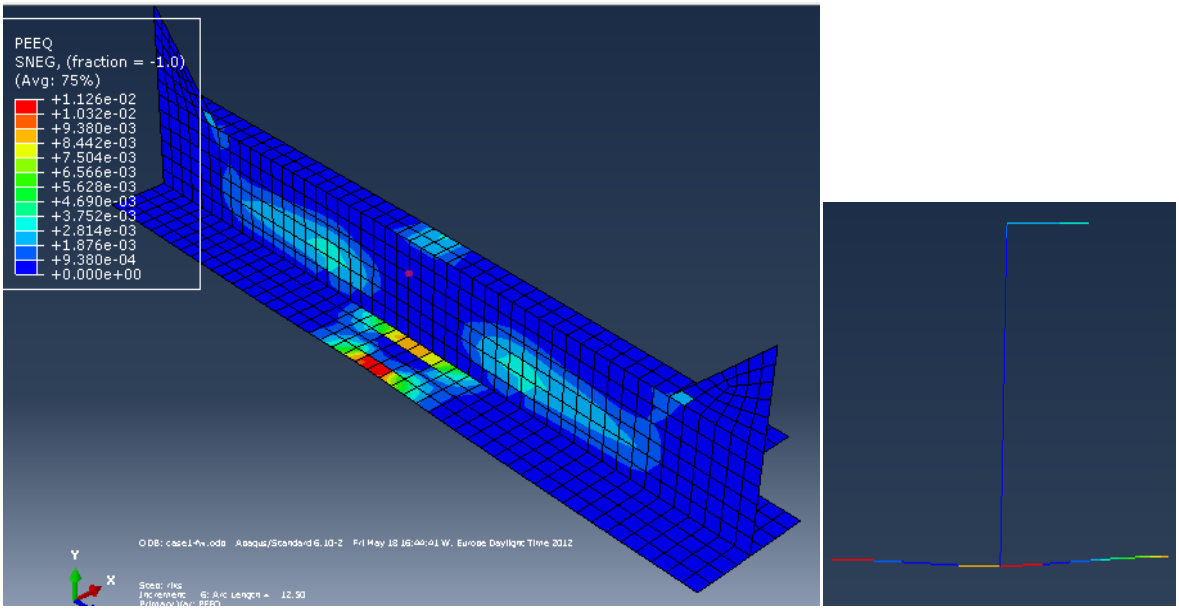

Figure 61 Plot of deformation (with equivalent plastic contour) section at mid-span for case1_L frame fixed against warping at Normalized load 1.033

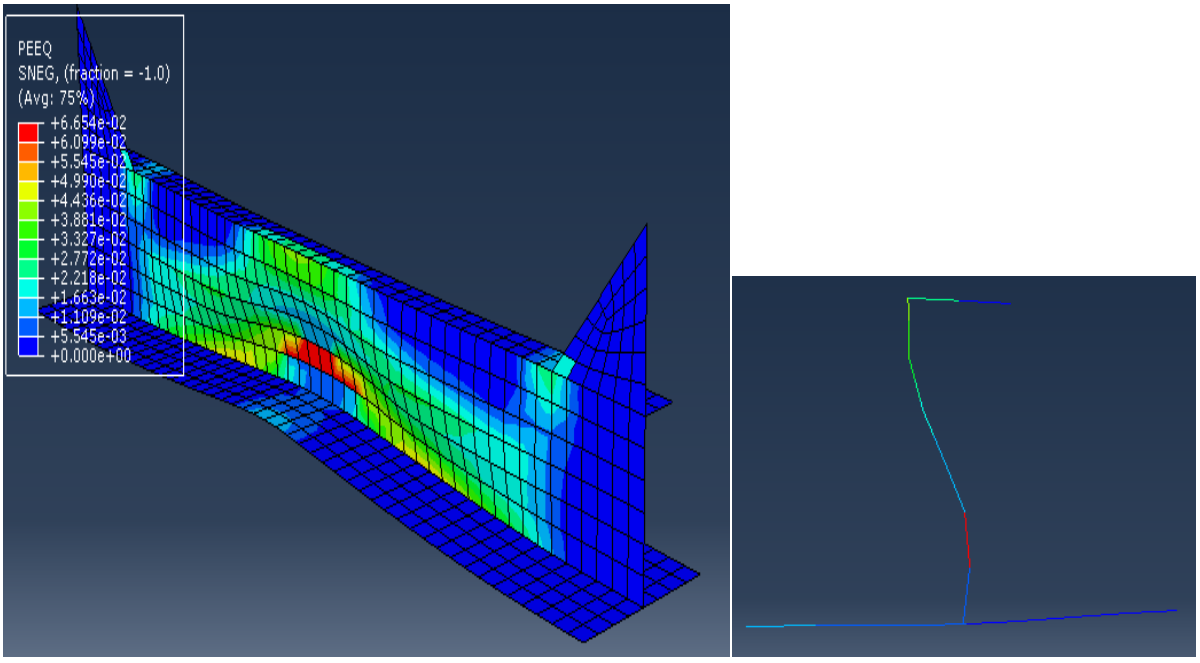

Figure 62 Plot of deformation (with equivalent plastic contour) and section at mid span for case2_L frame at IACS UR limit state load.

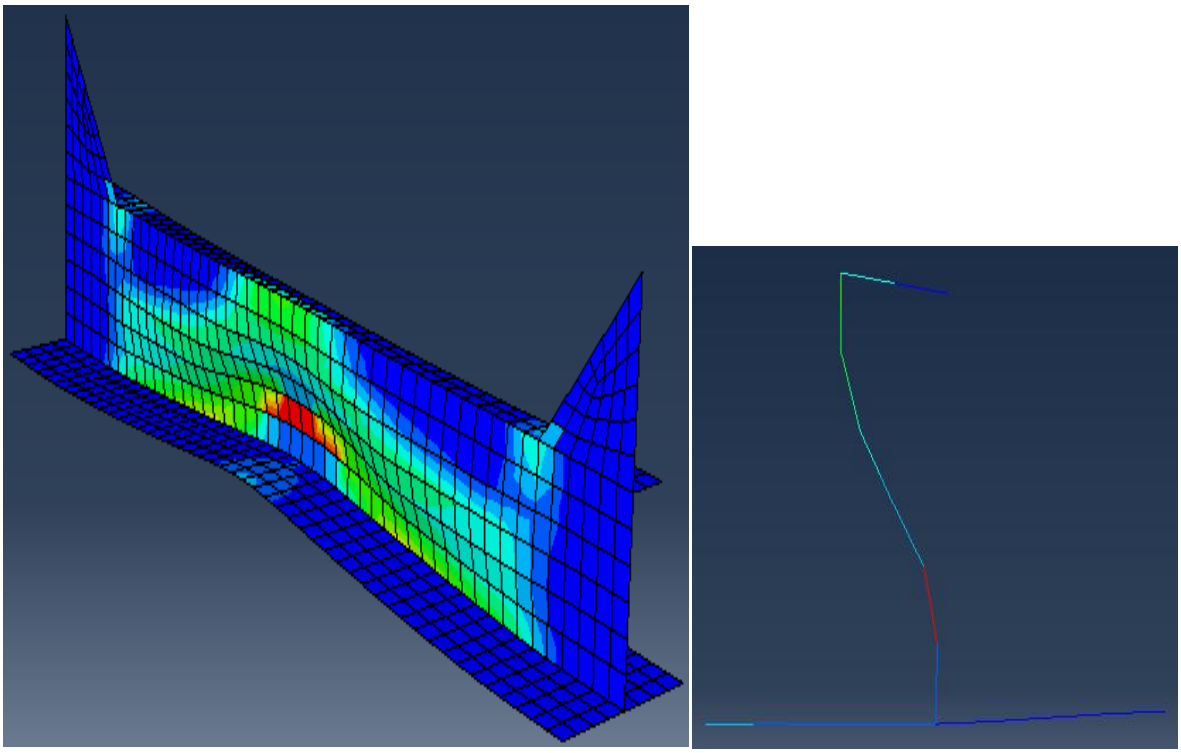

Figure 63 Plot of deformation (with equivalent plastic contour) and section at mid span for case3_L frame at IACS UR limit state load.

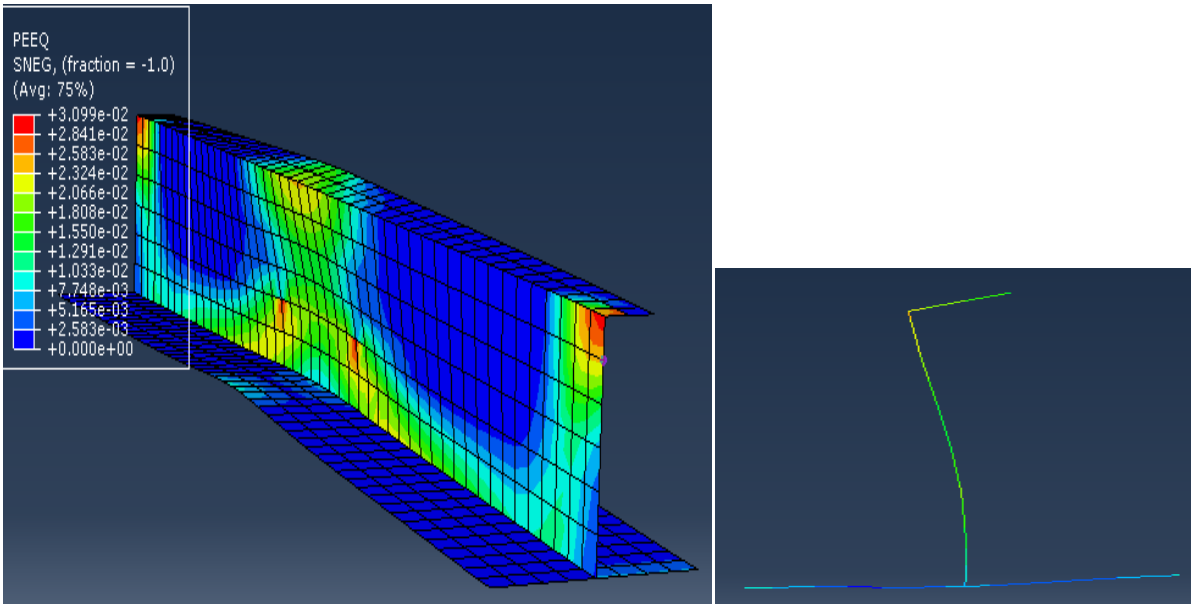

Figure 64 Plot of deformation (with equivalent plastic contour) and section at mid span for case5_L frame at IACS UR limit state load.

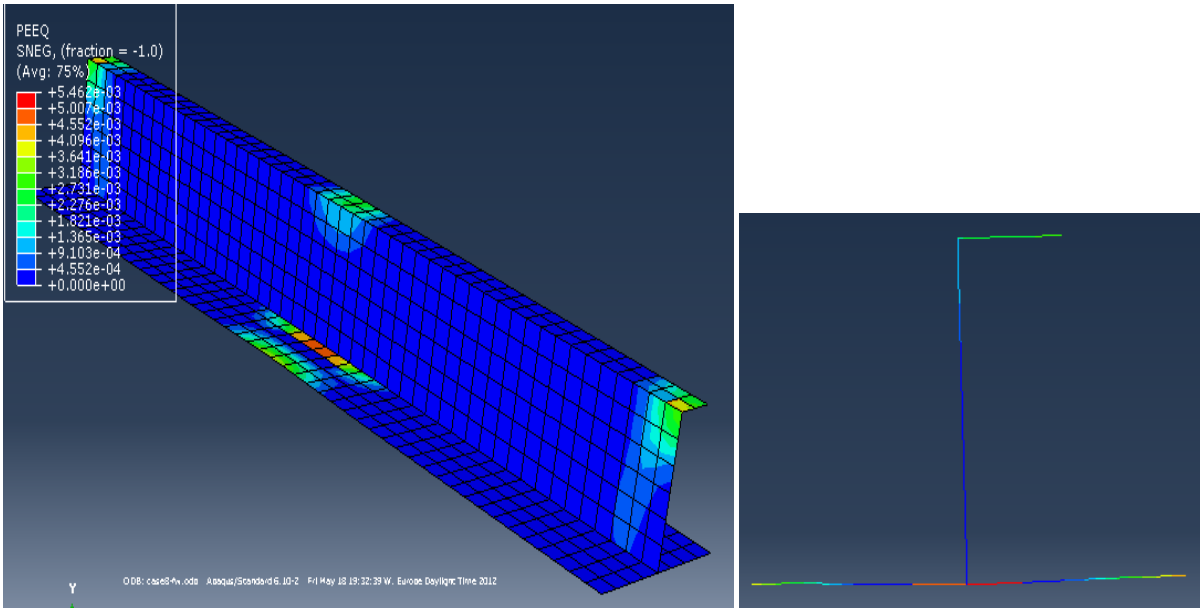

Figure 65 Plot of deformation (with equivalent plastic contour) and section at mid span for case5_L frame fixed against warping at IACS UR limit state load.

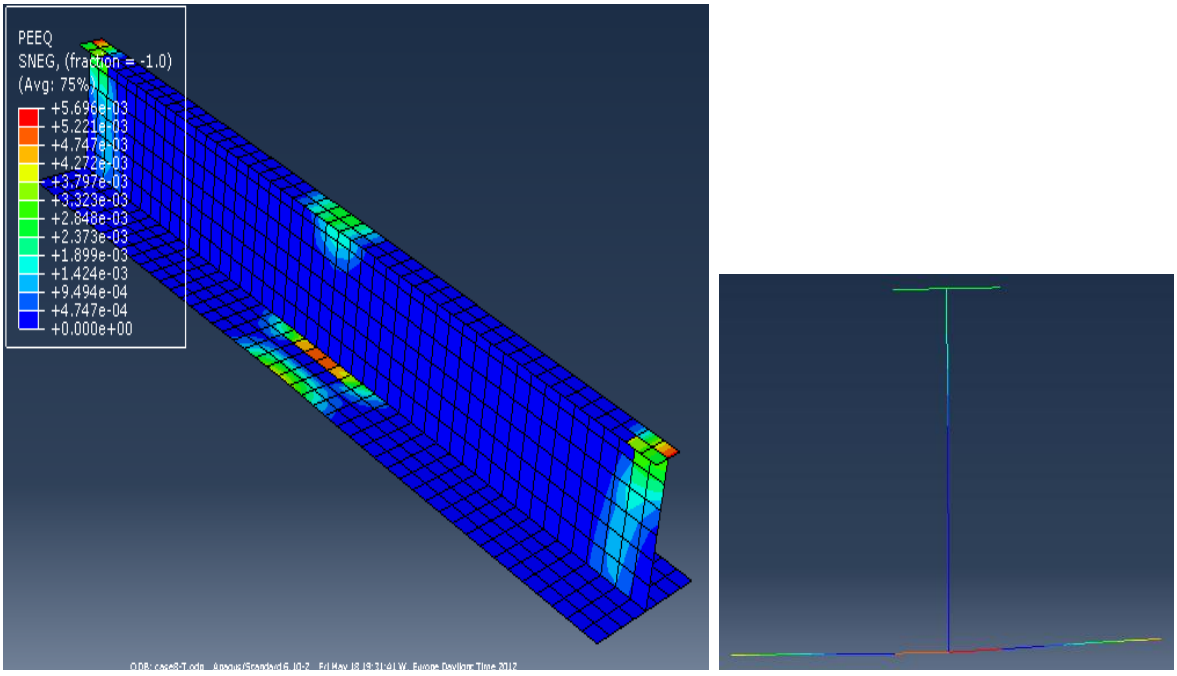

Figure 66 Plot of deformation (with equivalent plastic contour) and section at mid span for case5_T frame at IACS UR limit state load.

7.3.2 Effect of Inclination of stiffener web

The transverse frames case 5 and 7 were also analyzed with patch length 400mm and breadth equal to stiffener spacing for 65 degree web inclination with the plate flange. Angle of inclination is defined as the smallest angle between plate flange and stiffener web. The results have shown in the figure 67.

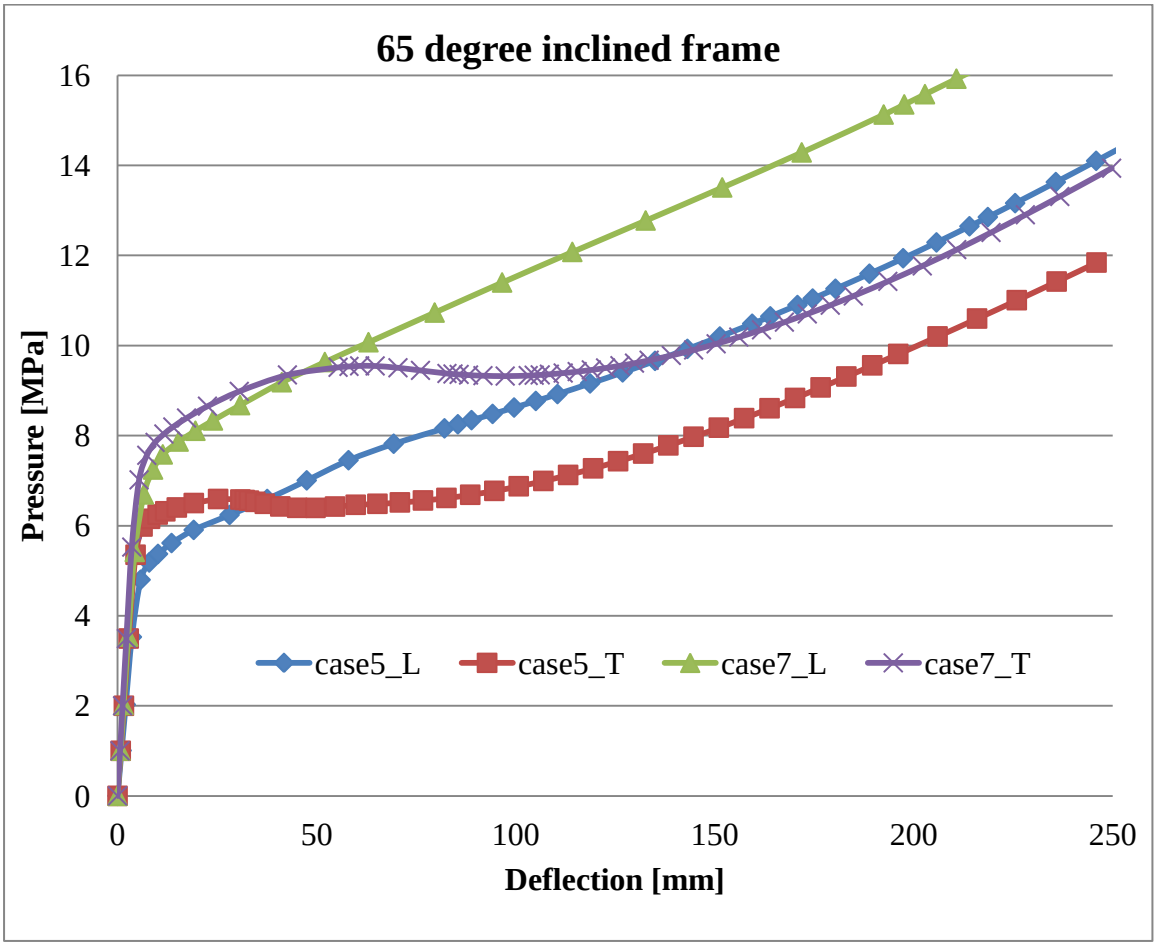

Figure 67 Transverse profiles case 5 & 7 inclined 65 degree with plate, normalized load deflection curves

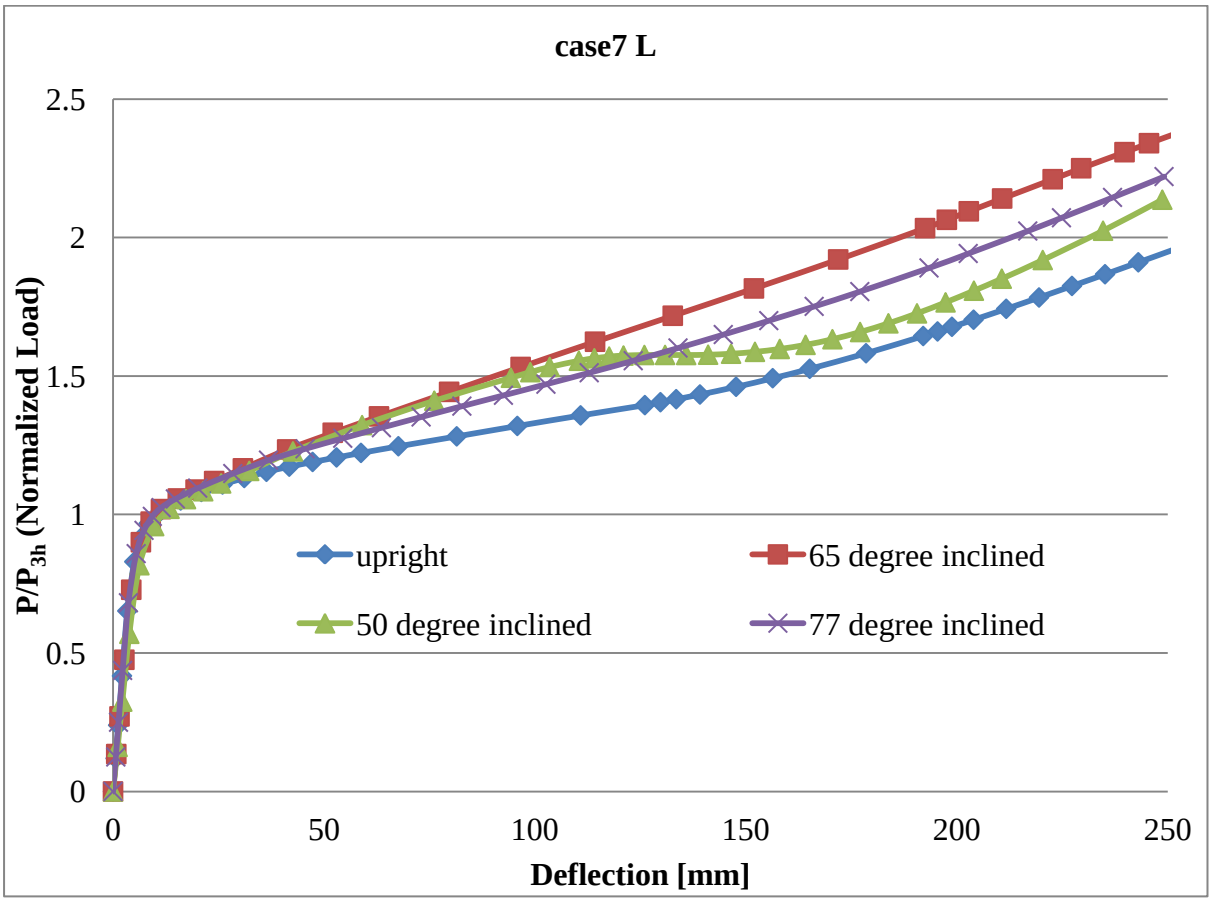

Figure 68 Transverse profile L (case7)-Normalized load deflection curves for different angle of inclination with plate flange.

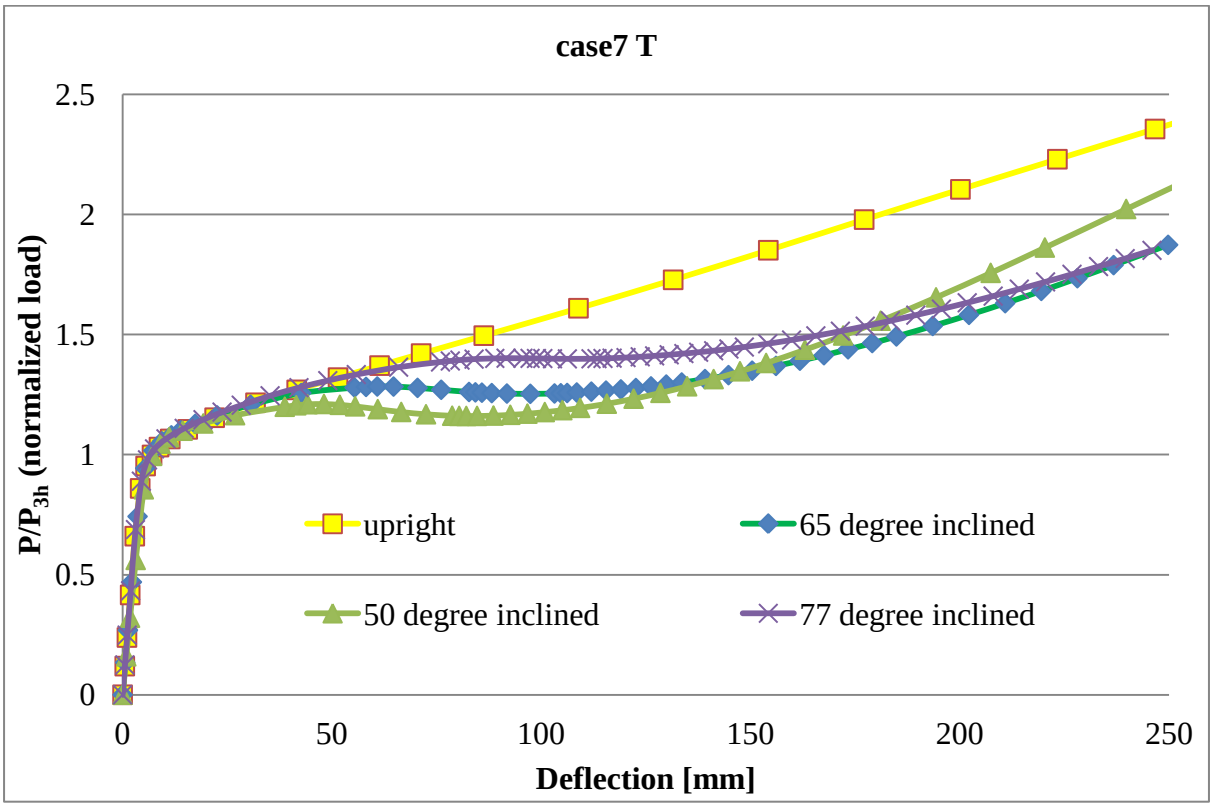

Figure 69 Transverse profile T (case7)-Normalized load deflection curves for different angle of inclination with plate flange.

The trend of capacity curve for L profile appears to be unaffected by the inclination angle (see figure 68) except slightly rising trend of capacity at large deformation. On the other hand, though the trend of capacity curve for inclined T profile is similar to that of upright T profile in the elastic range and onset of plastic deformation, drop of capacity is observed at moderate and large deformation for inclined T profile (see figure 69). The web angle itself possibly causes the stiffener of symmetrical cross-section to deflect sideways (see figure 70). Non uniform stress at the flange of stiffener of unsymmetrical cross-section in some extend resist the sideways deflection caused by web inclination (see figure 71).

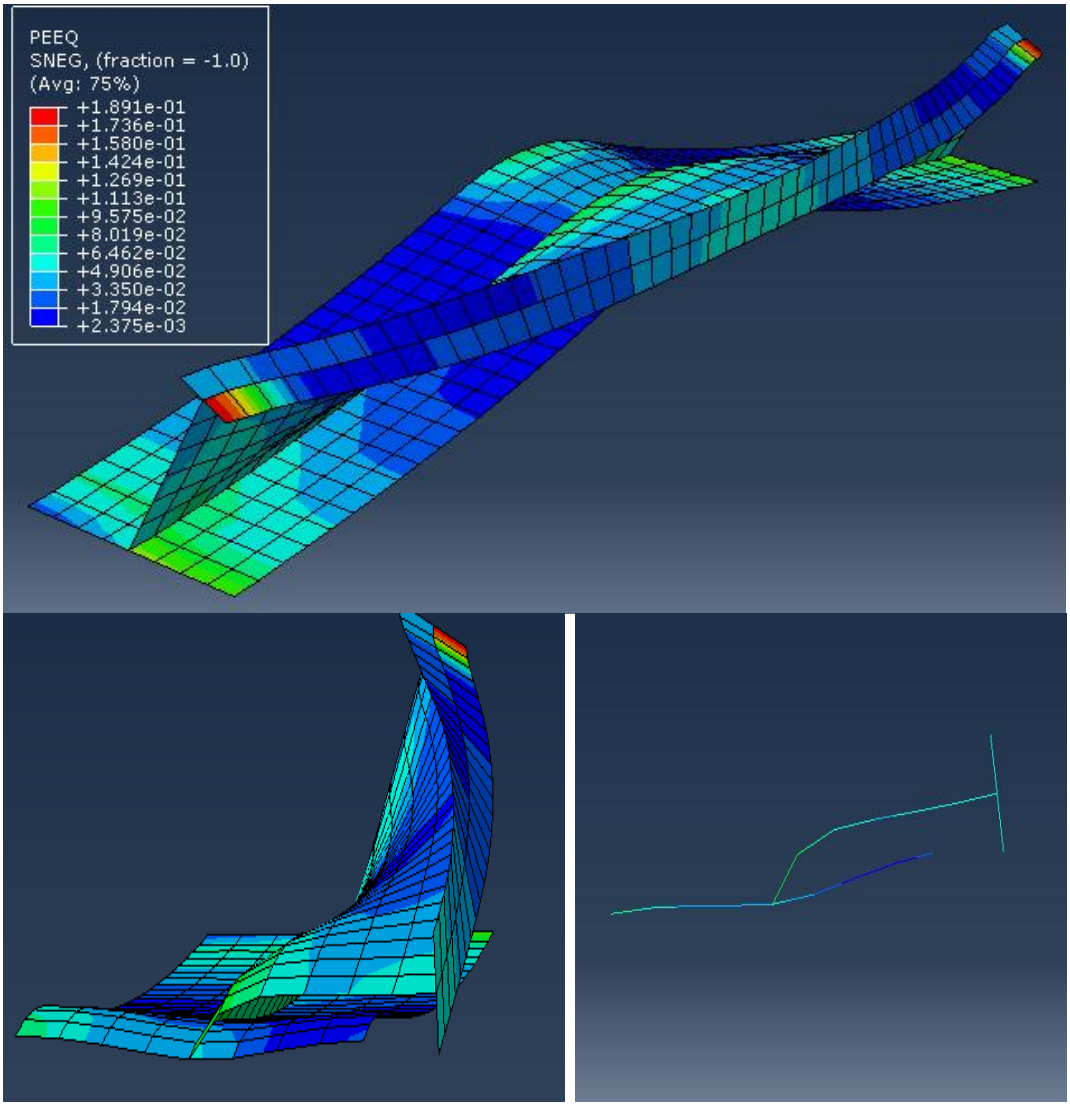

Figure 70 Plot of deformation (with equivalent plastic strain contour) for case7 T inclined 65 degree at pressure 13.3074 MPa; a) whole frame, b) section at midspan.

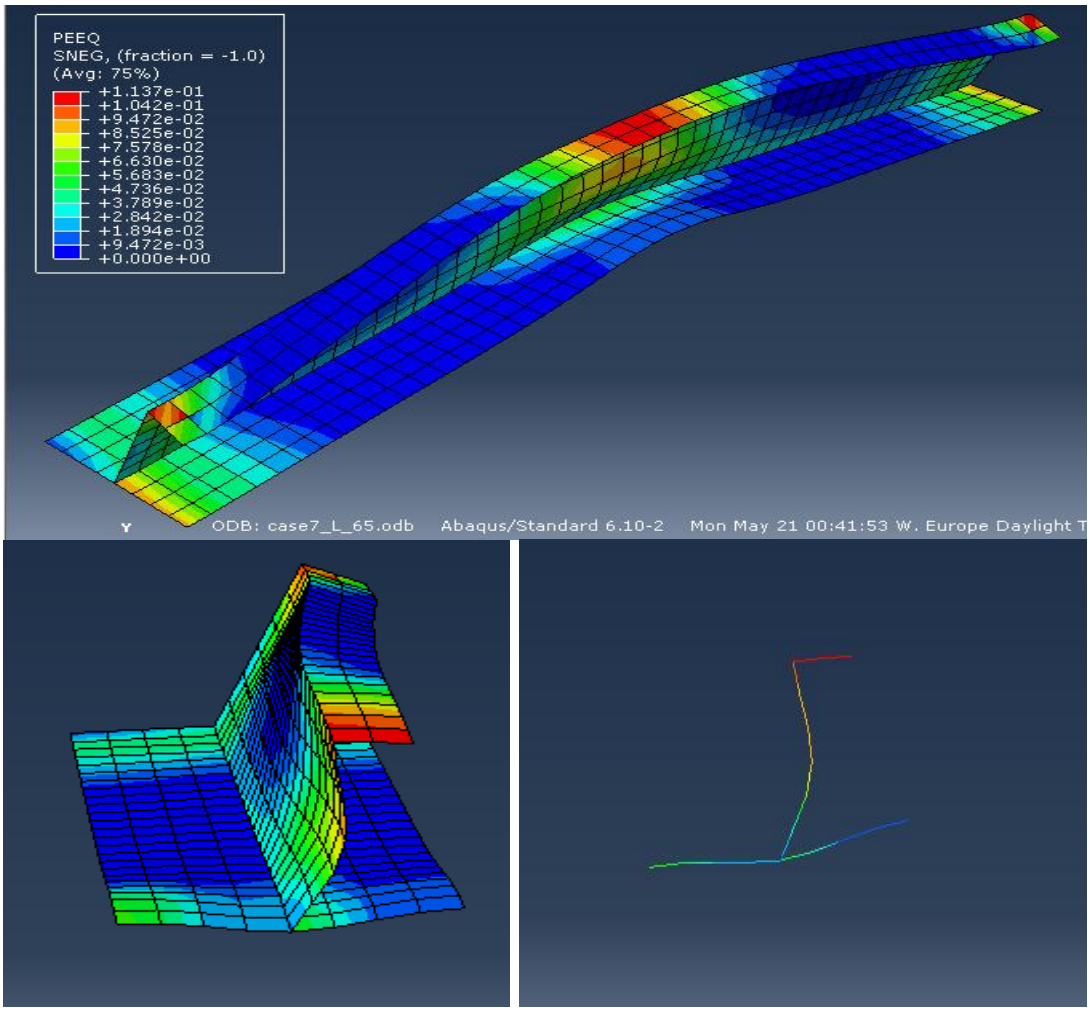

Figure 71 Plot of deformation (with equivalent plastic strain contour) for case7 L inclined 65 degree at pressure 13.5085 MPa; a) whole frame, b) section at midspan.

7.3.3 Effect of mid-span Tripping bracket

To understand the effect of mid-span tripping bracket on the load deflection characteristics of L and T frames, several cases from table 4 were simulated and analyzed in Abaqus with mid-span tripping bracket. The dimensions of mid-span tripping bracket were determined from the guideline of DNV common structural rules for ships structures. The angle of inclination of web was one of the main variants to the simulation of the frames.

For almost all angle of inclination (except greater than 80 degree) of stiffener web, Load deflection curve of T stiffener shows a significant improved lateral capacity to the non-linear response region (see figure 72, 73, 74) . But upright T stiffener does not show any improvement on the load deflection curves due to mid-span tripping bracket (see figure 75).

For the case of L stiffener the effect of having mid-span tripping bracket can be divided into two categories as:

1. Stiffener which doesn't have sufficient capacity to counteract warping effect:
   Significant improved lateral capacity is found for upright L stiffener. For all angle of web inclination, load deflection curve shows significant improved lateral capacity in the elastic region, onset of plastic deformation and in large deformation.

2. Stiffener which has sufficient capacity to counteract warping effect:
   For all angle of web inclination, load deflection curve does not show any improvement on lateral capacity in the elastic region and onset of plastic deformation. Effect of Tripping bracket in large deformation can be described as
   - Upright: Load deflection curve shows significant improved lateral capacity.
   - Inclined: Slightly improved lateral capacity is found for about 45-80 degree angle of inclination. Moderately improved capacity is found for small angle of inclination.

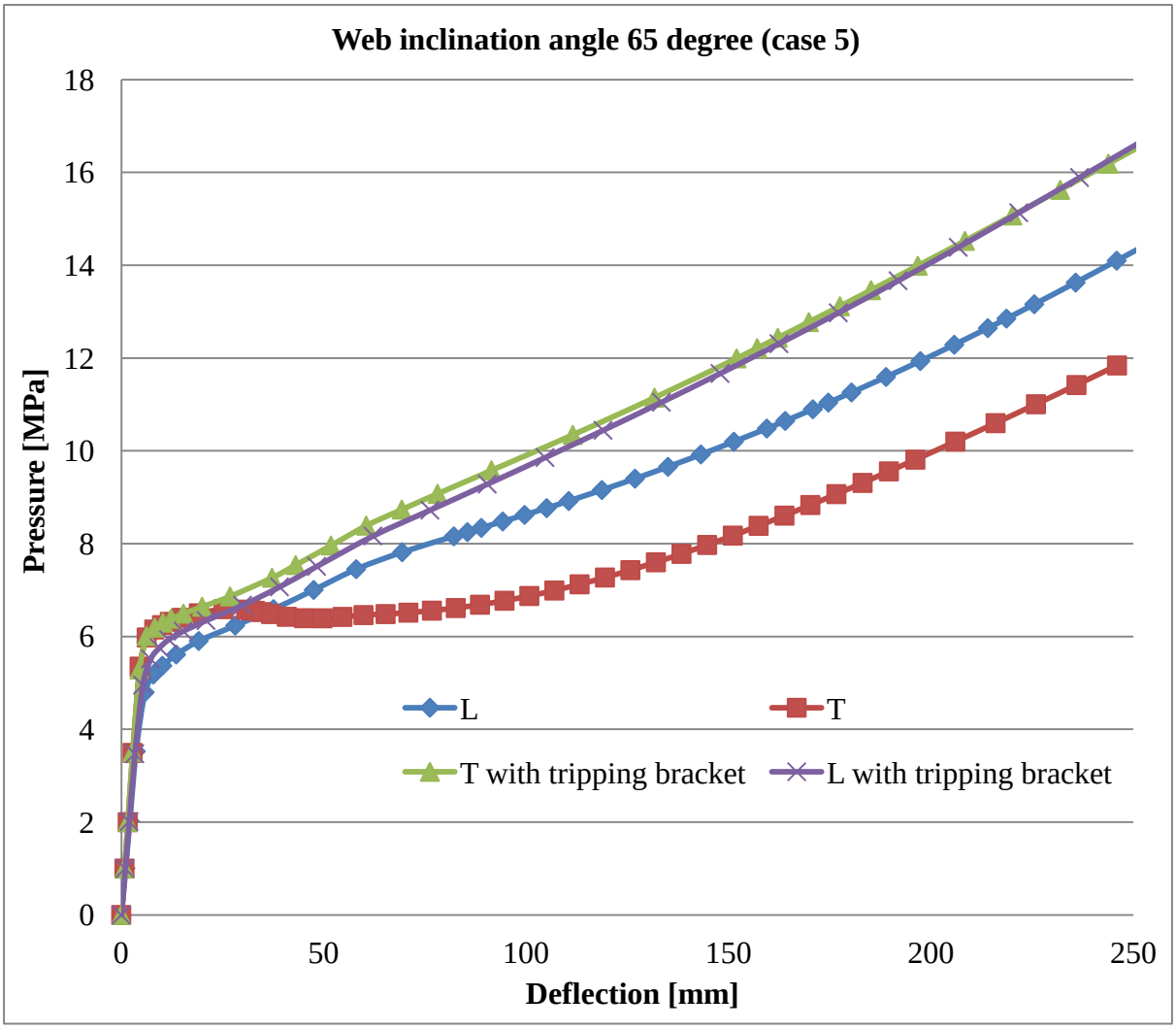

Figure 72 Load deflection curves for 65 degree inclined frames - case 5 with and without tripping bracket

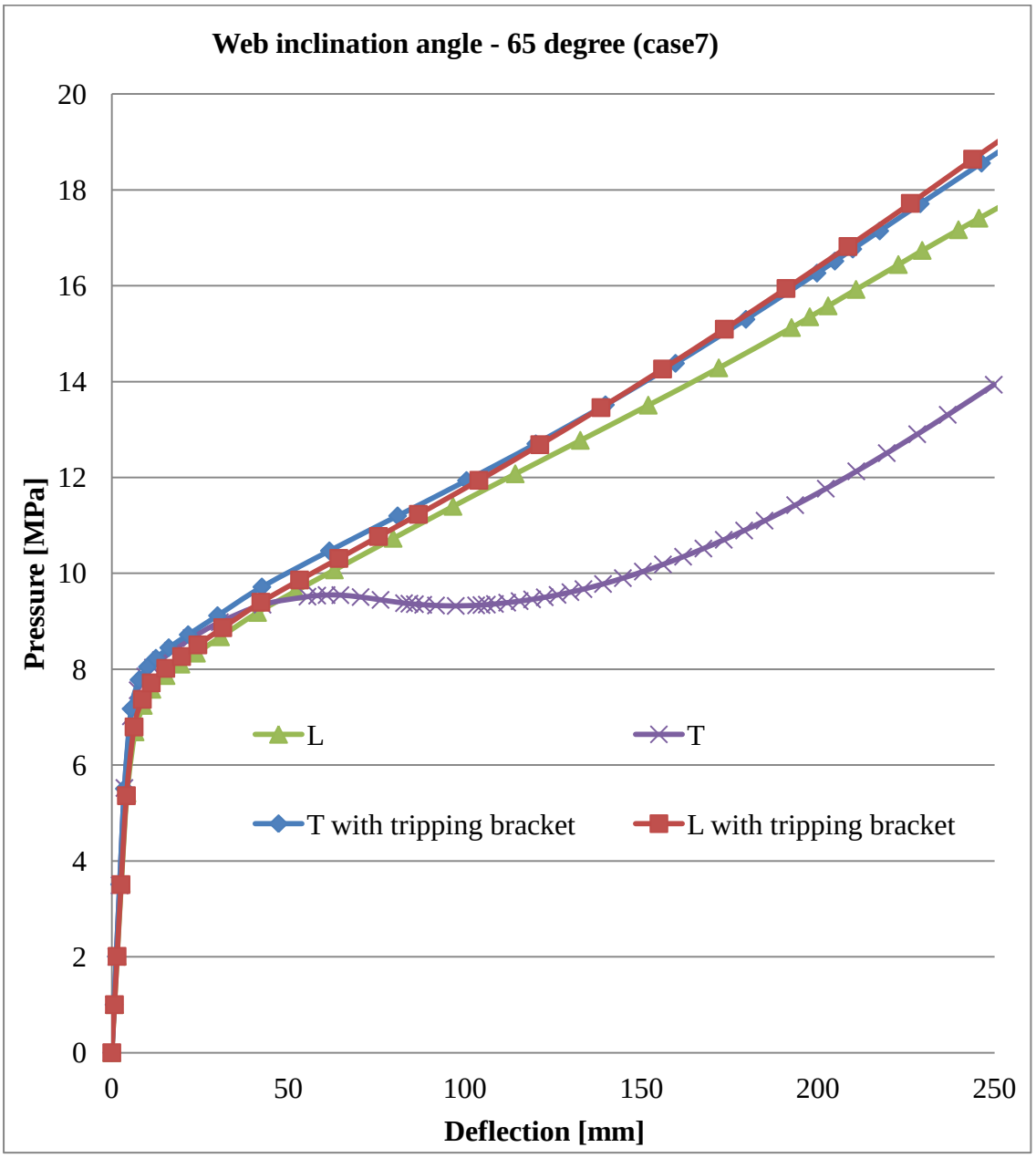

Figure 73 Load deflection curves for 65 degree inclined frames - case 7 with and without tripping bracket

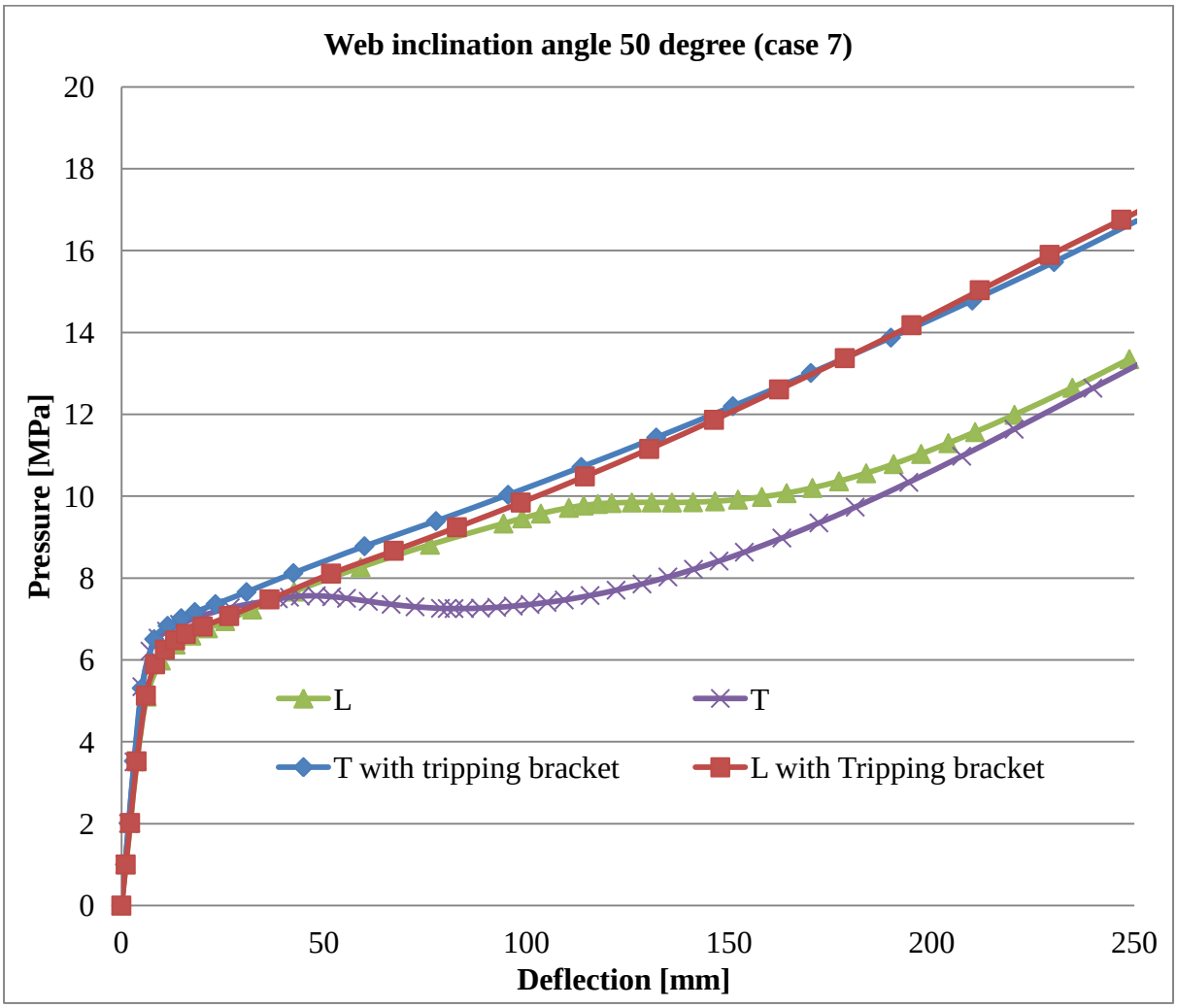

Figure 74 Load deflection curves for 50 degree inclined frames - case 7 with and without tripping bracket

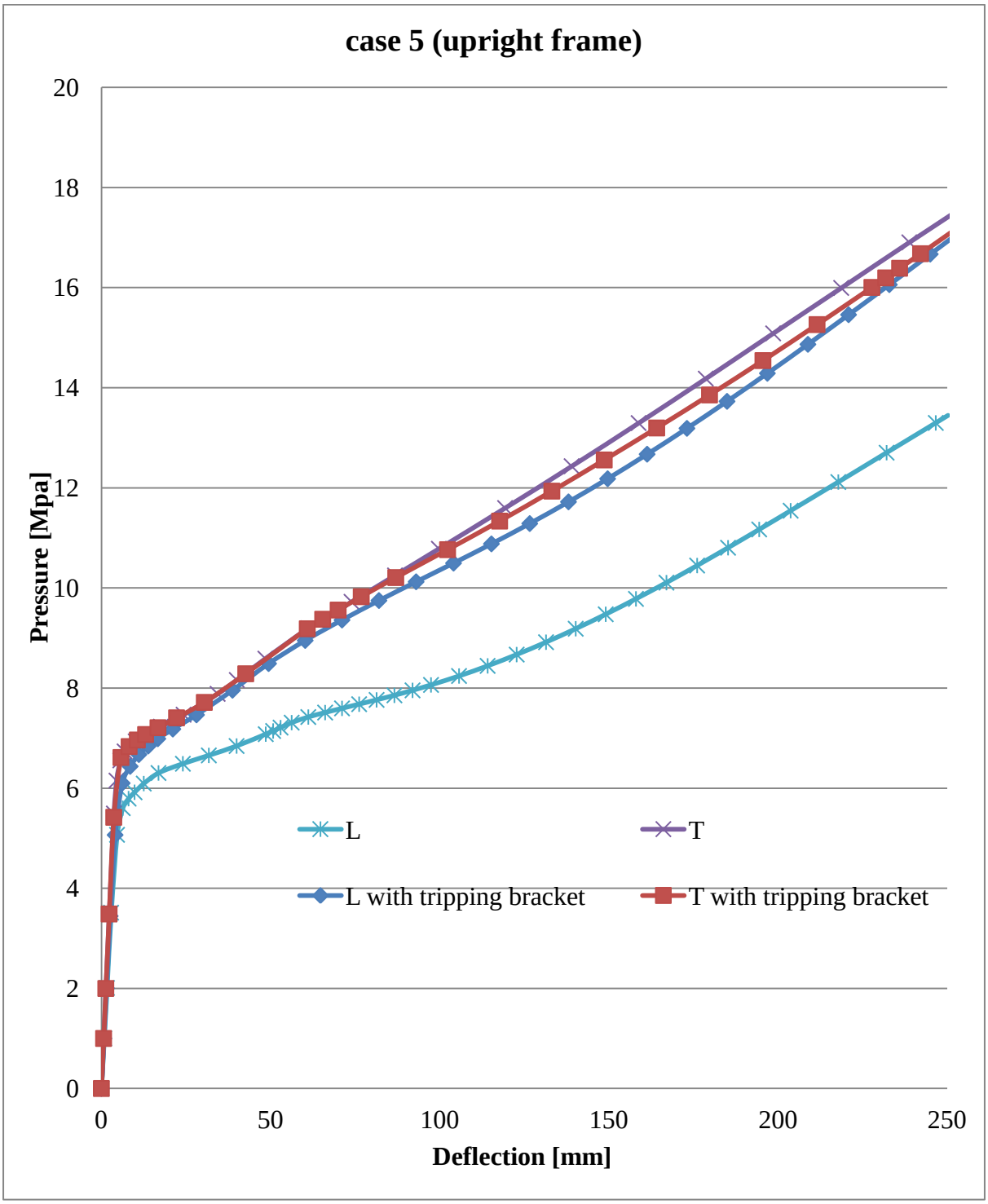

Figure 75 Load deflection curves for frames - case 5 with and without tripping bracket

7.4 Non linear Finite element Analysis of Frame and Panel

The stiffened panel shown in figure 44-48 was chosen from bow part of an existing ice strengthen offshore vessel. Simulations were perform for a single frame (see figure 32-36), a ½+1+½ frames (see figure 37-42) and a grillage (see figure 44-48). Both L and T section were used to perform simulations.

Table 5 Frames in a grillage structure

	T	L
Web height, h_w	400 mm	400 mm
Web thickness, t_w	18 mm	18 mm
Flange width, b_f	100 mm	100 mm
Flange thickness, t_f	11 mm	11 mm
Plate thickness, t_p	20 mm	20 mm
Frame spacing, S	400 mm	400 mm
Frame span, L	1650 mm	1650 mm
Yield strength	315 MPa	315 MPa
Web angle inclination	65 degree	65 degree
Patch load length	1000 mm	1000 mm
Patch load breadth	Stiffener spacing	Stiffener spacing
Capacity (IACS), P_{3h} [MPa]	6.386 MPa	6.386 MPa

7.4.1 Determination of Patch load length

Several analyses were performed for the above mentioned T stiffener considering the patch load length shown in Table 6. Pressure applied to the stiffener is determined from the DNV pressure area relationship for polar vessel described in topic "ice pressure and contact area relationship" in chapter 2. The results of the analysis have been shown in figure 76. By observing the figure 76, patch load lengths 1m and 1.2 m were found to be most critical patch load length for the considered stiffener. In this study, patch load length 1m was chosen to perform the simulations in consultation with supervisor.

Table 6 Determination of patch load length

Patch load length, b [m]	Total Area [m^2]	P=k*A^-0.5 (k=5)
1.65	0.66	6.154575
0.7	0.28	9.449112
1	0.4	7.905694
0.4	0.16	12.5
0.9	0.36	8.333333
0.8	0.32	8.838835
1.2	0.48	7.216878

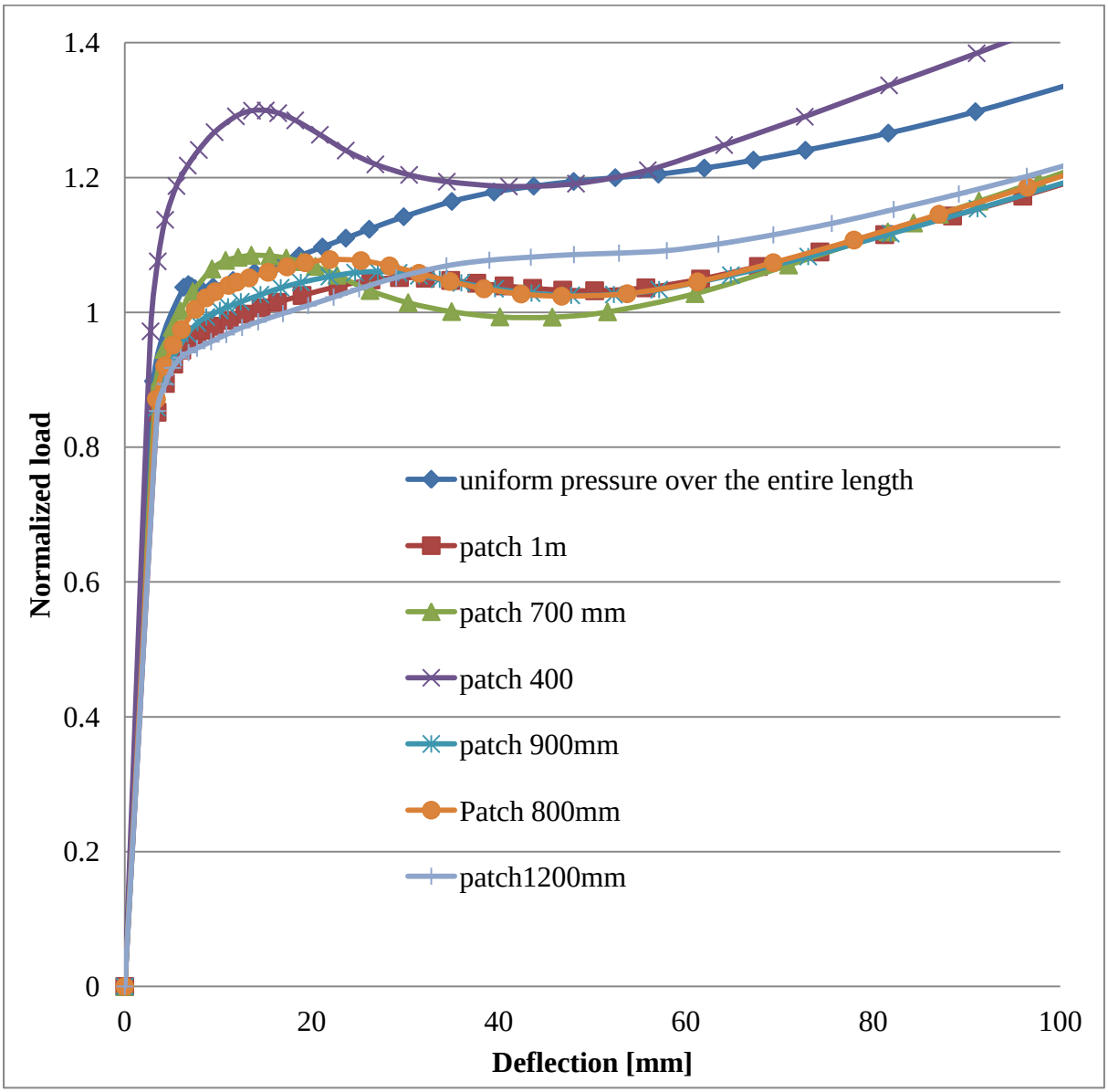

Figure 76 Non linear FE analysis of frame for different patch load length – single T frame

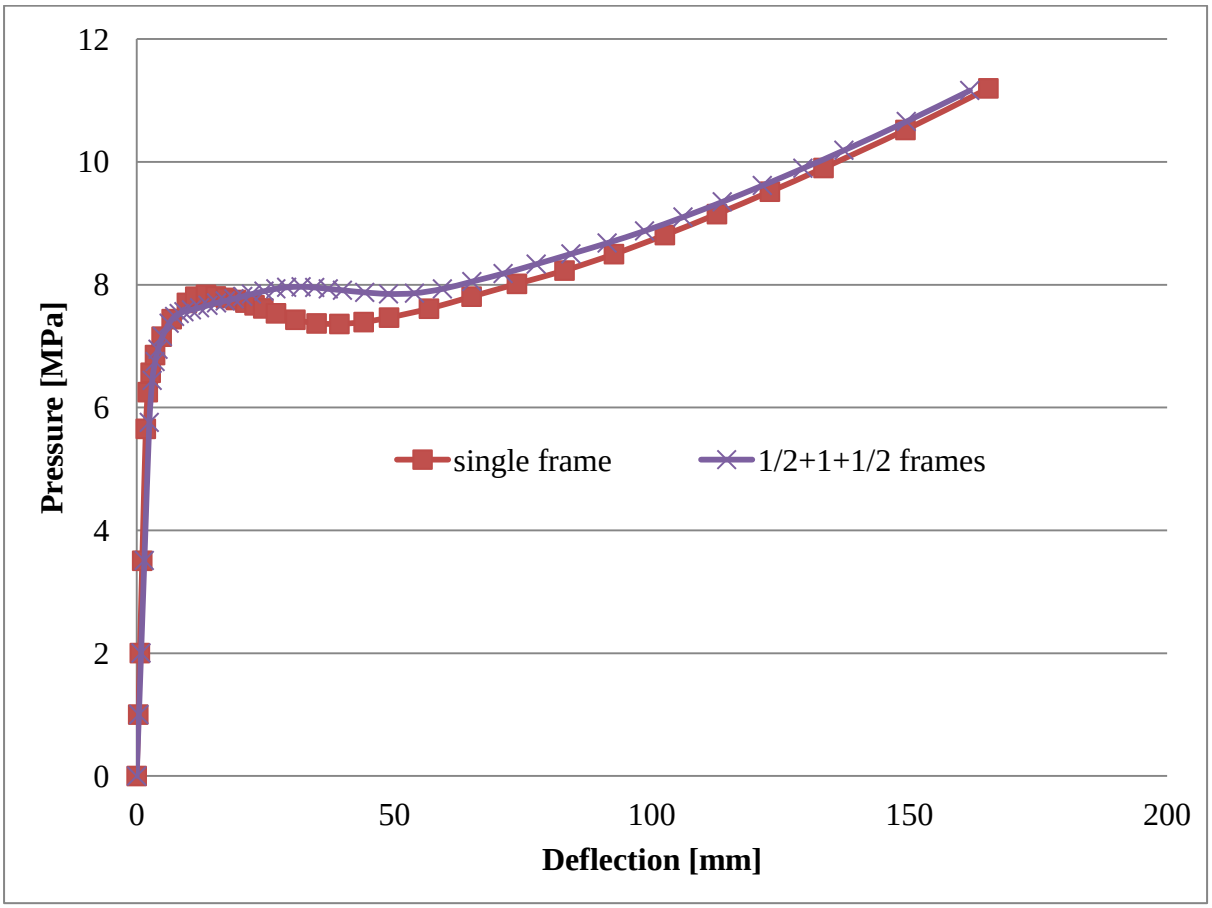

Figure 77 Load deflection curves.

As capacity curves for the stiffener in isolation and as part of a ½+1+½ frames matches pretty closely (see figure 77) and ½+1+½ frames model simulates transverse boundary condition more accurately than that of single frame model, ½+1+½ frames model were used to determine the capacity of the stiffener in a single frame instead of using single frame model.

7.4.2 Capacity of a frame

The capacity of a structure can be defined as the load corresponding to a limit state. One of the limit states for a frame is the formation of three hinges. In an ideal case this is a situation where the deformation or strain increases infinitely without any appreciable increase in load. This hypothetical situation can be reached by an elastic perfectly plastic structure with no membrane effects. In real structures, this limit state does not occur due to strain hardening and membrane action of the plate. Therefore, various methods are used to determine the limit load value. Examples are the twice elastic slope method, tangent intersection method and 0.1% residual strain method.

7.4.2.1 Twice Elastic Slope Method (TES)

In the TES criterion, the structural response is characterized by plotting a load parameter against a deformation parameter. A straight collapse limit line is then drawn from the origin of the characteristic curve with slope conventionally referred to as twice the slope of the initial elastic response relative to the load axis. This corresponds to half the stiffness of the initial response, as shown in Fig. 78. The plastic load PP is defined as the load corresponding to the intersection of the collapse limit line and the load-deformation curve. It is to some extent arbitrary and does not relate the specified plastic load to any specific event in the evolution of the plastic deformation mechanism.

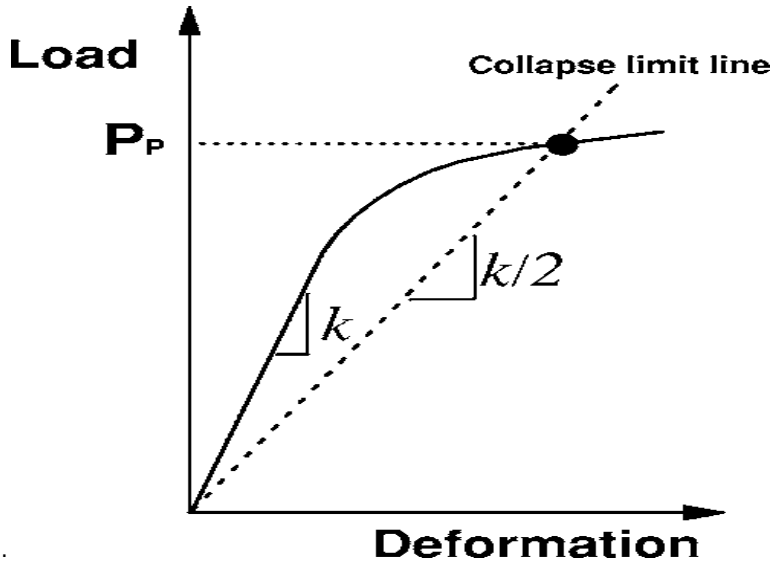

Figure 78 Definition of capacity using twice elastic slope method

7.4.2.2 Tangent intersection criterion (TI)

Tangent intersection method describes the limit load as the load at which the elastic and plastic tangents intersect (see figure 79). This method is also arbitrary as the slope in the plastic region is not constant and the there can be infinite number of possible tangents in the plastic region [24].

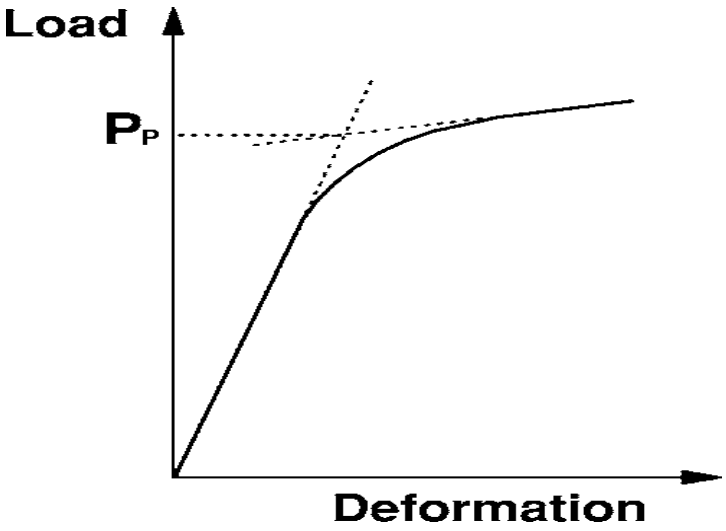

Figure 79 Definition of capacity using Tangent intersection method

7.4.2.3 0.1% residual strain method

A line is drawn with a slope equivalent to the elastic slope at a location which is offset from the origin by 0.1% of frame span. The intersection of this line with the force displacement curves is defined as the capacity (see figure 80). It is also known as 0.1%-offset-strain method. The capacity is equivalent to a force which causes a permanent strain of 0.1% of span.

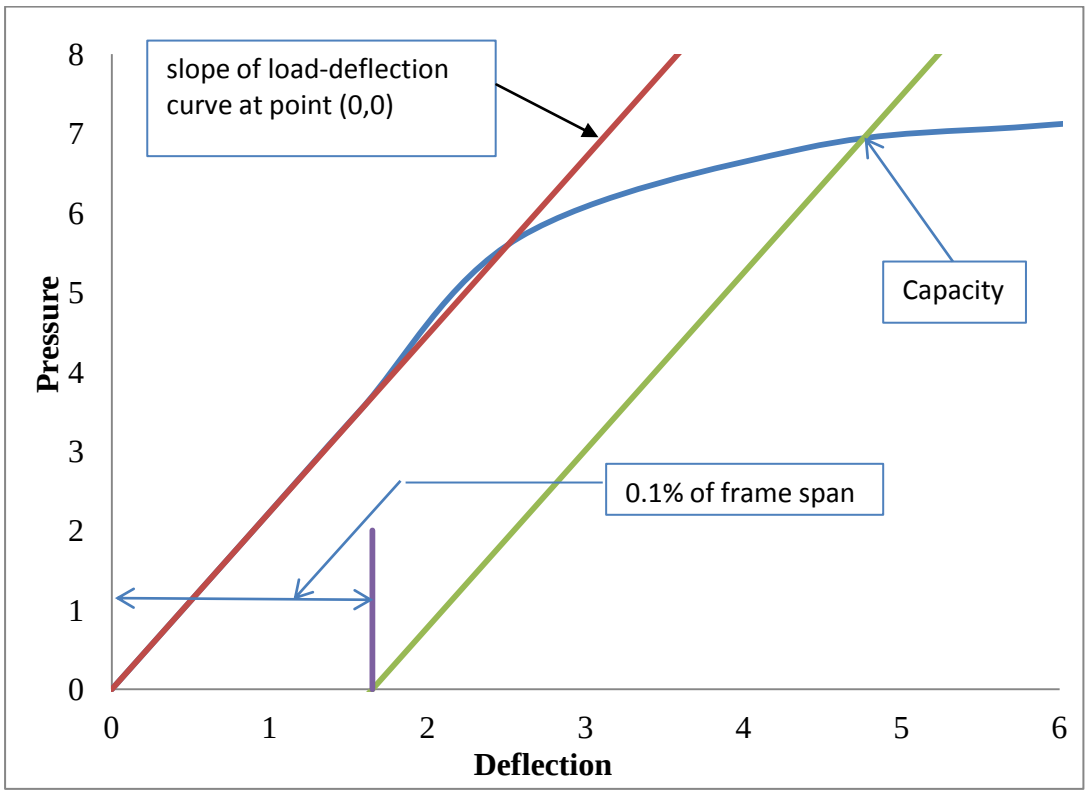

Figure 80 Definition of capacity using 0.1% residual strain method

7.4.3 ULS design loads

In determining ULS design loads shown in table 7, 0.1% residual strain method has been used.

Table 7 ULS design load

	T frame			L frame		
	Capacity [MPa]	**Obtained from**	**Plot of deformation**	**Capacity [MPa]**	**Obtained from**	**Plot of deformation**
Single frame	7.16	Figure 82	Figure 92 & 93	6.94	Figure 84	Figure 94 & 95
Grillage case1	10.55		Figure 96 & 97	10.2013		Figure 98 & 99
Grillage case2	8.44		Figure 100 & 101	8.058		Figure 102 & 103
Grillage case3	9.8		Figure 104 & 105	9.25		Figure 106 & 107
Capacity factor to grillage case 1	1.47			1.47		
Capacity factor to grillage case 2	1.18			1.161		
Capacity factor to grillage case 3	1.37			1.33		

Slightly higher ULS design load (around 3% to 5.6%) is found for T profile than that of L profile. The plot of deformation (with Von Mises stress and equivalent plastic strain) of frames subjected to ULS load presented in Table 7 has been shown in Appendix A.

Capacity factor is defined as the ratio of capacity of the center stiffener in a grillage to that of a single frame. It seems from the capacity factor that the capacity of the stiffener as part of a grillage is 15% to 50% high than that of frame in isolation. As grillage structure is the representation of real structure, design capacity based on single frame seems to be very conservative.

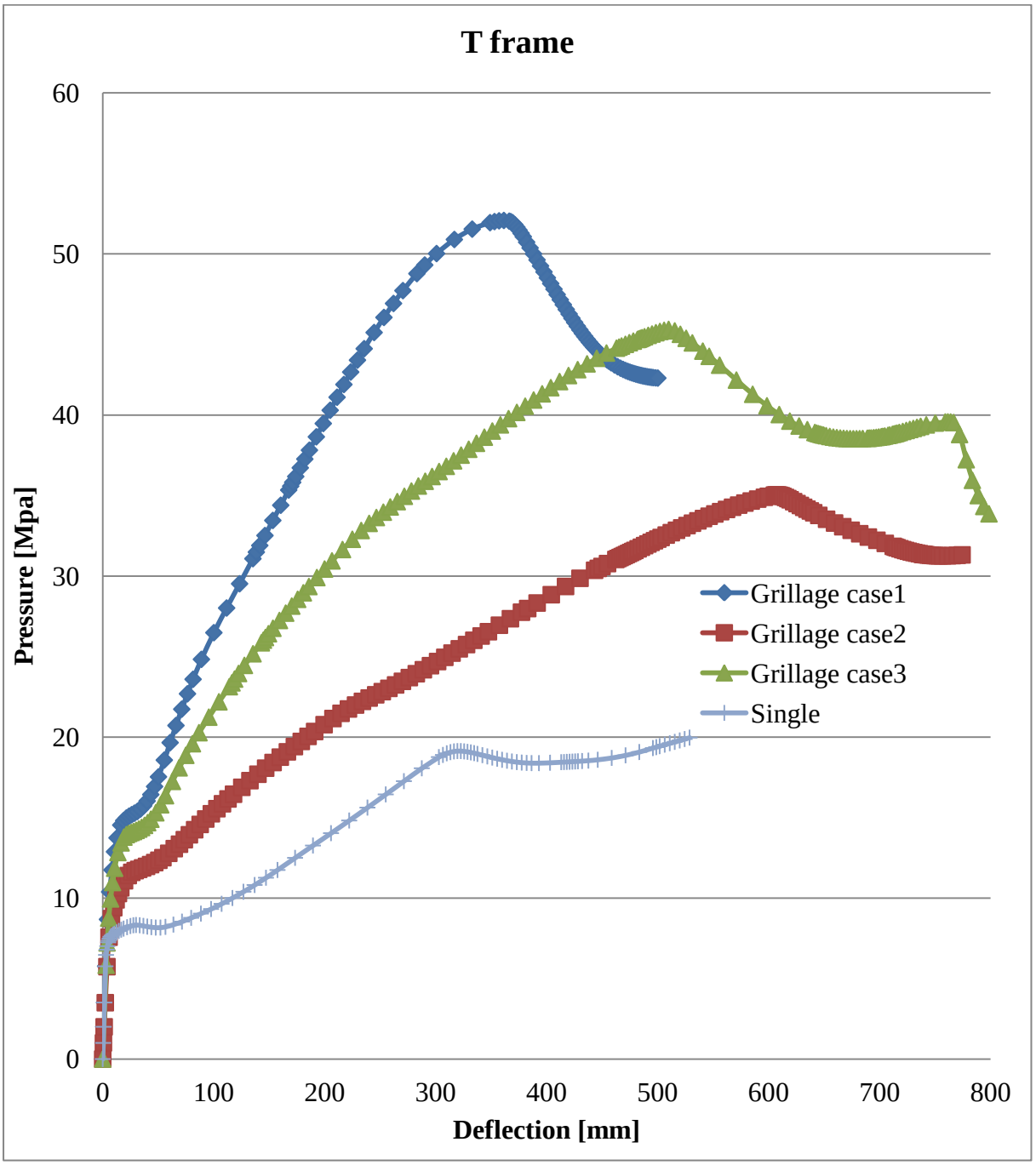

Figure 81 Load deflection curves – Frame T

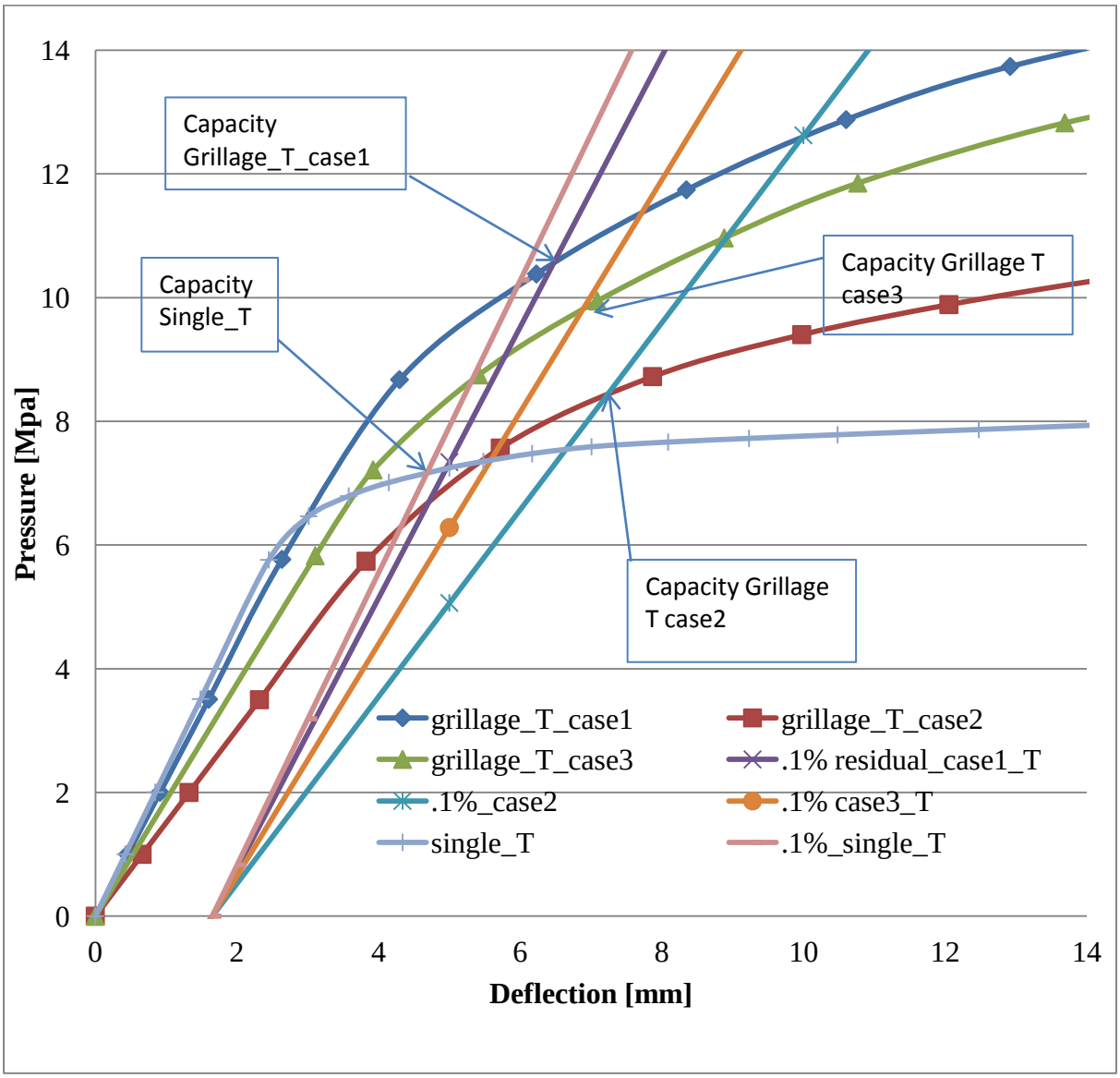

Figure 82 Capacity of T frame according to 0.1% residual strain method

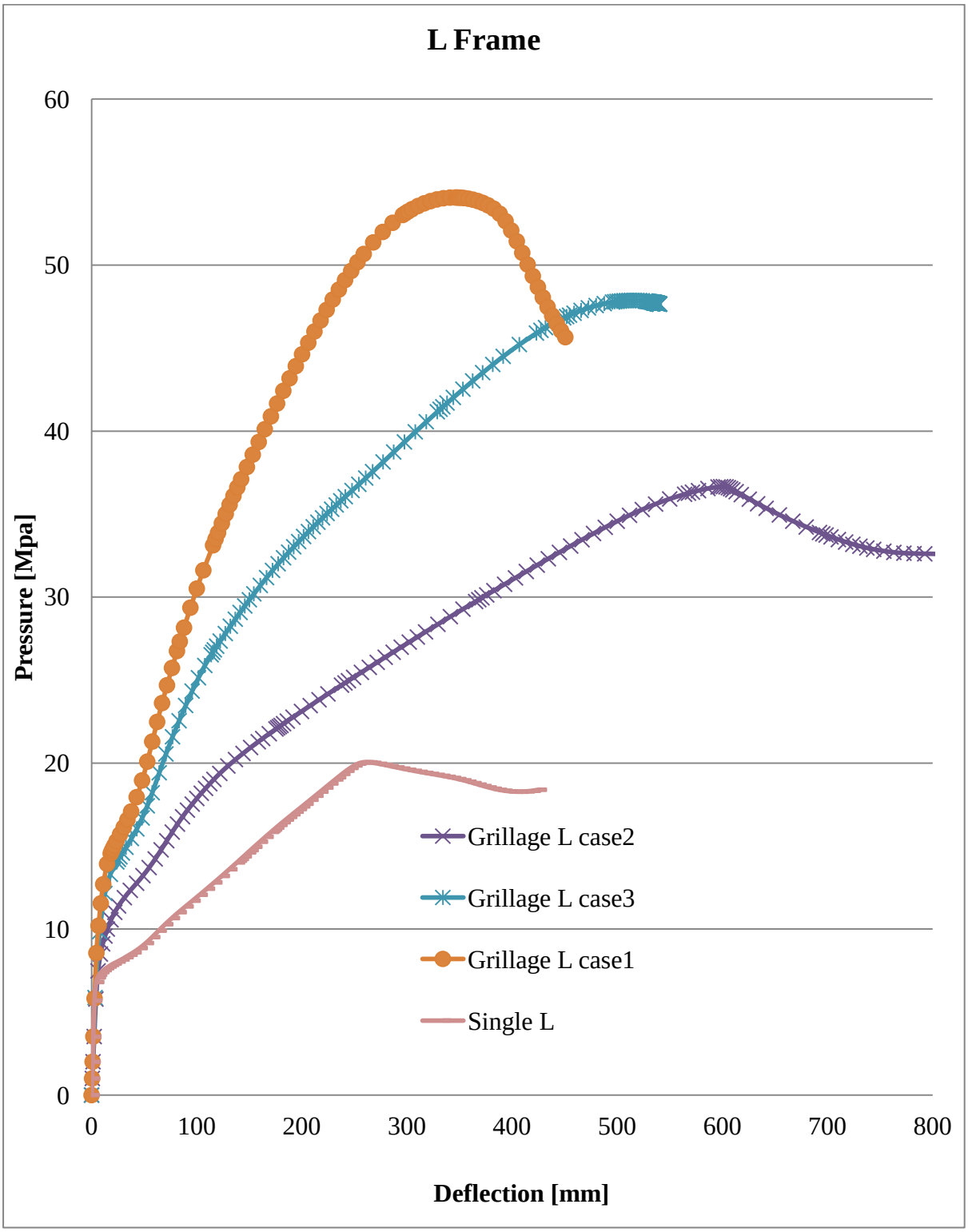

Figure 83 Load deflection curves – Frame L

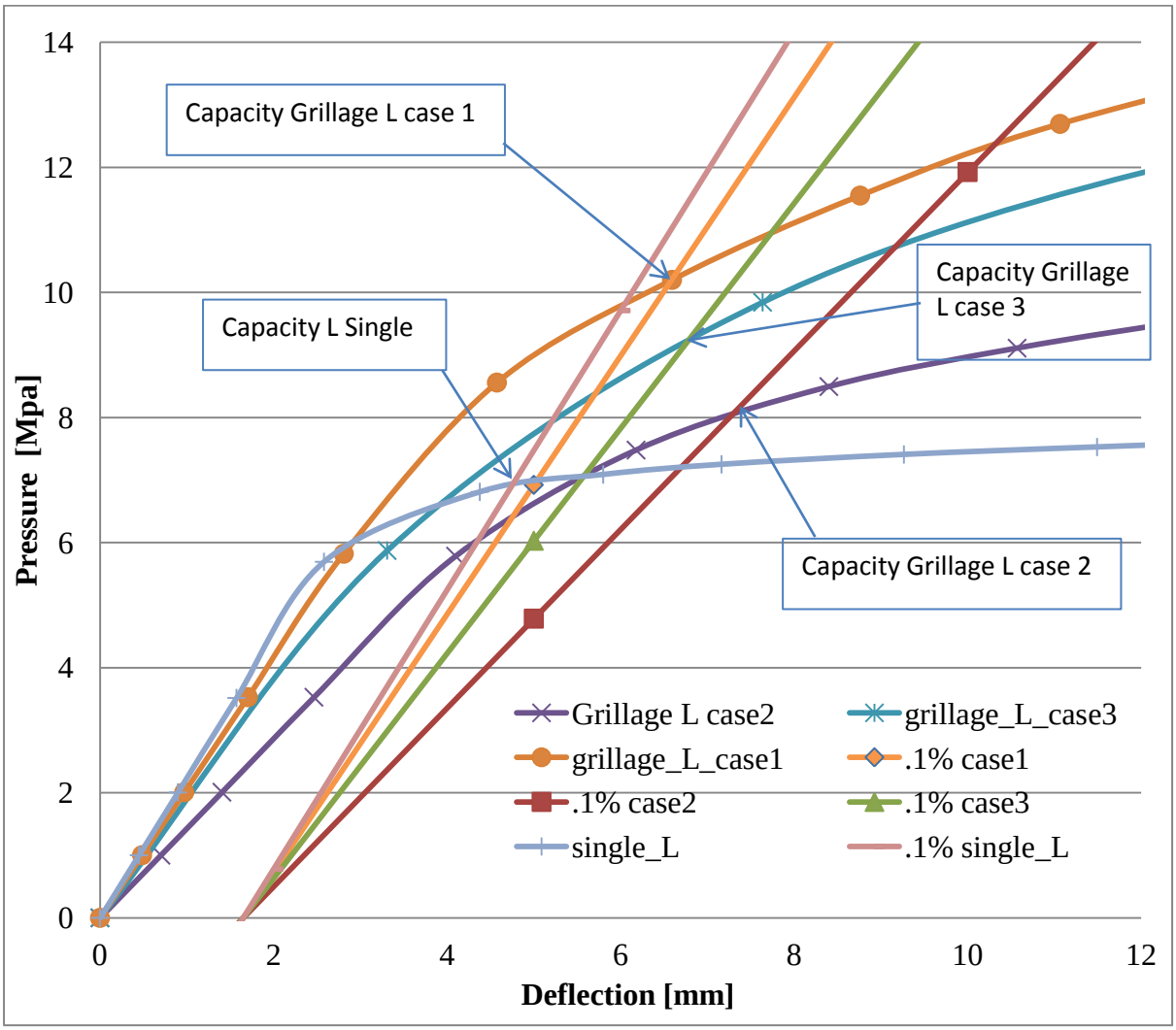

Figure 84 Capacity of L frame according to 0.1% residual strain method

7.4.4 ALS design Loads

NORSOK proposed critical strain value of 15% for steel with yield strength 355 MPa. Though here in this study all analyses were performed with steel of yield strength 315 MPa, 15% plastic equivalent strain is used to determine the ALS design load (see Table 8). To study the difference in load carrying capacity at large deformation between frames L and T, loads at 10% equivalent strain are obtained and presented in Table 9.

Table 8 ALS design load at 15% equivalent plastic strain

ALS loads	T frame			L frame		
	Pressure [MPa]	Obtained from	Plot of deformation	Pressure [MPa]	Obtained from	Plot of deformation
Single frame	17.094	Figure 85	Figure 108	18.5305	Figure 85	Figure 109
Grillage case1	45.8	Figure 86	Figure 110	51.245	Figure 86	Figure 111
Grillage case2	29.37	Figure 87	Figure 112	29.47	Figure 87	Figure 113
Grillage case3	38.77	Figure 88	Figure 114	44.56	Figure 88	Figure 115

Note: Plot of deformation of L and T frames for different loading conditions subjected to ALS design load at 15% equivalent strain has been shown in Appendix B.

Table 9 ALS design load at 10% equivalent plastic strain

Limit loads	T frame		L frame	
	Pressure [MPa]	Obtained from	Pressure [Mpa]	Obtained from
Single frame	14.94	Figure 85	19.1	Figure 85
Grillage case1	40.425	Figure 86	48.425	Figure 86
Grillage case2	24.55	Figure 87	27.945	Figure 87
Grillage case3	32.9	Figure 88	41.533	Figure 88

From the Table 8 and 9 it can be concluded that Inclined L stiffener is stronger than inclined T stiffener (see figure 85, 86, 87 & 88). Similar results were found for Transverse frame analysis described on the topic “Analysis of Transverse stiffener”. In figure 89 and 90, plot of deformation (with Von Mises stress contour) has been shown. From those figure it seems that under same load inclined T stiffener deflects more than inclined L stiffener.

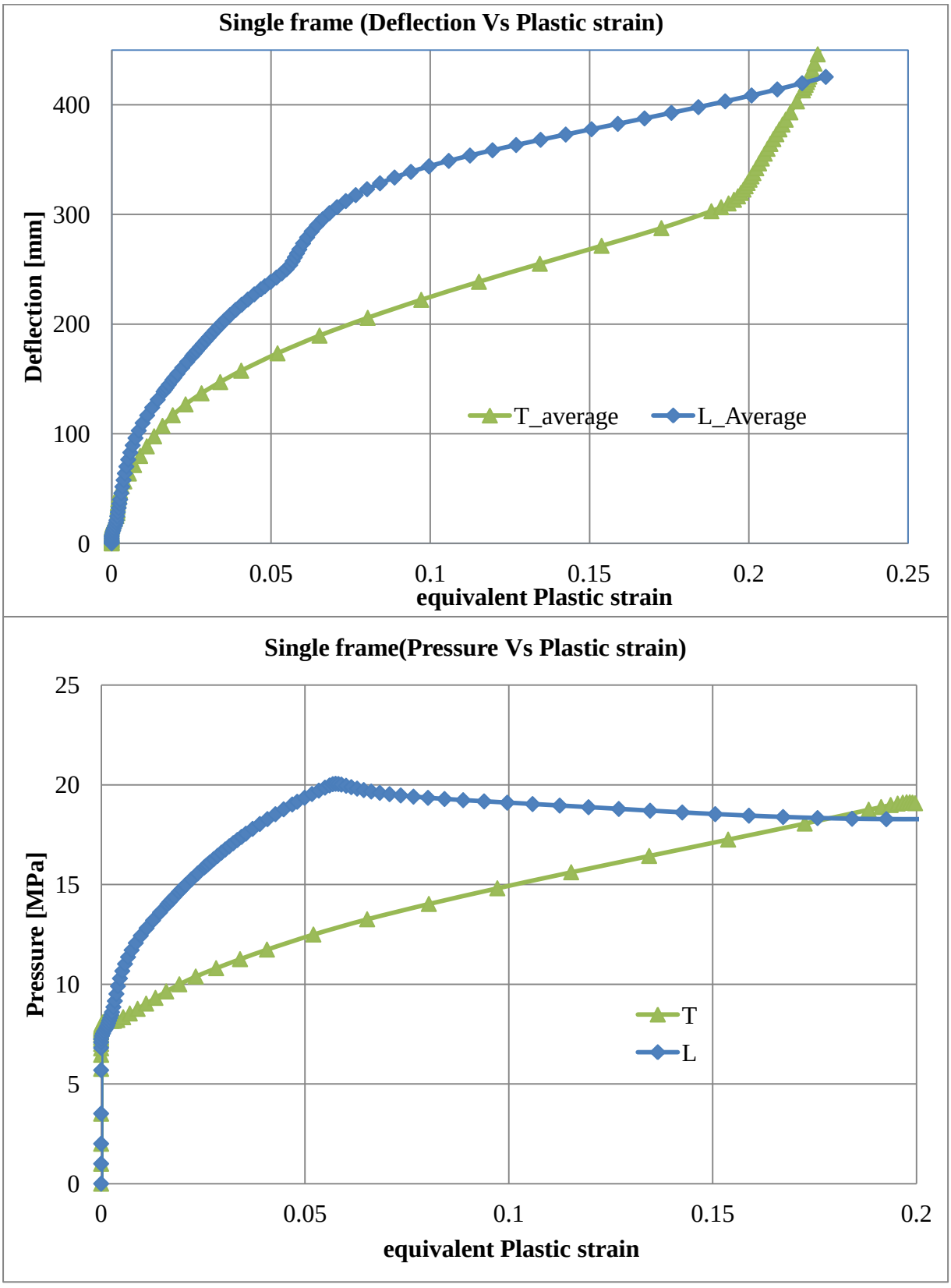

Figure 85 Comparison of capacity at large deformation – single frame

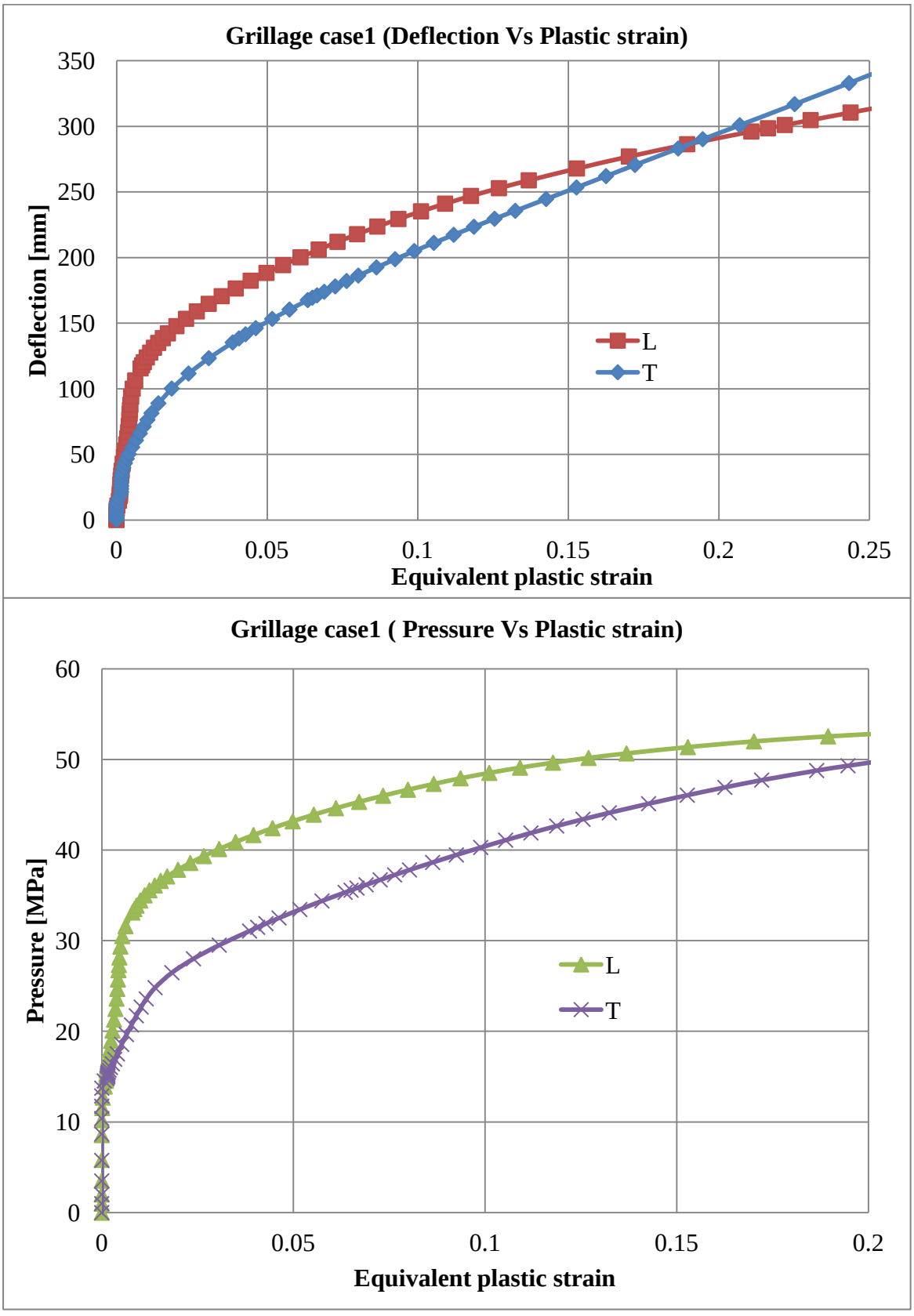

Figure 86 Comparison of capacity at large deformation – Grillage case1

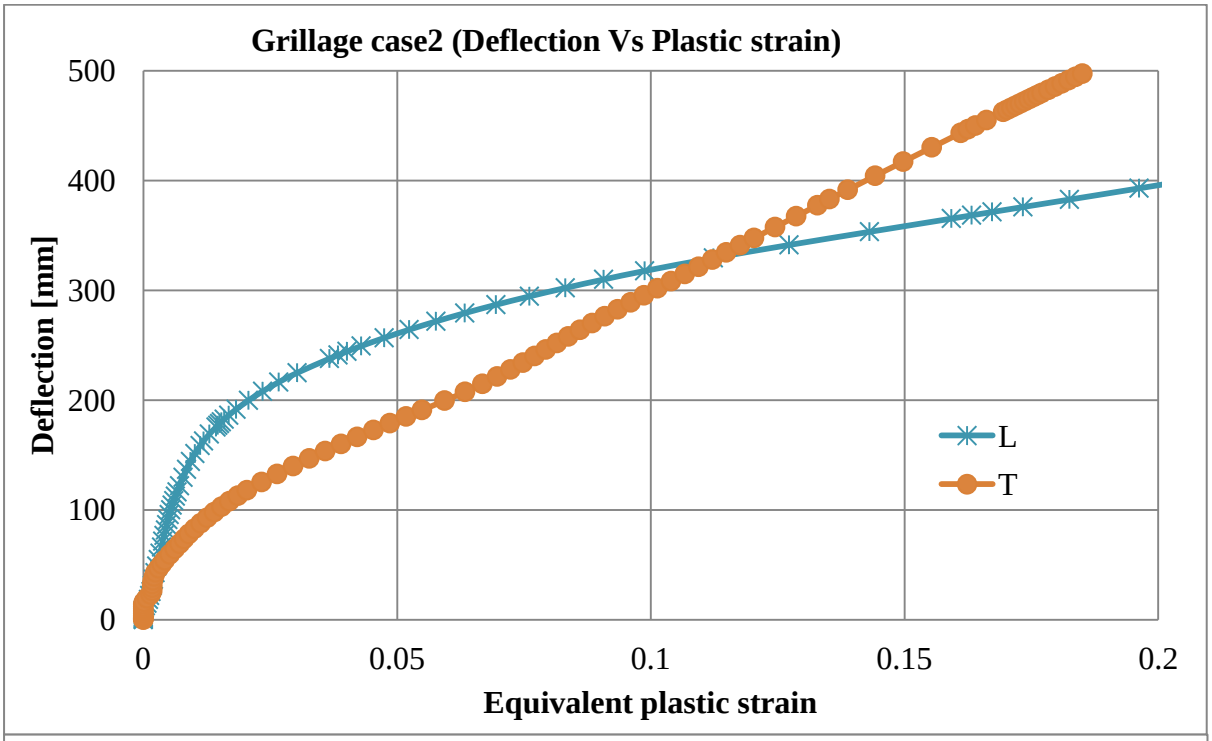

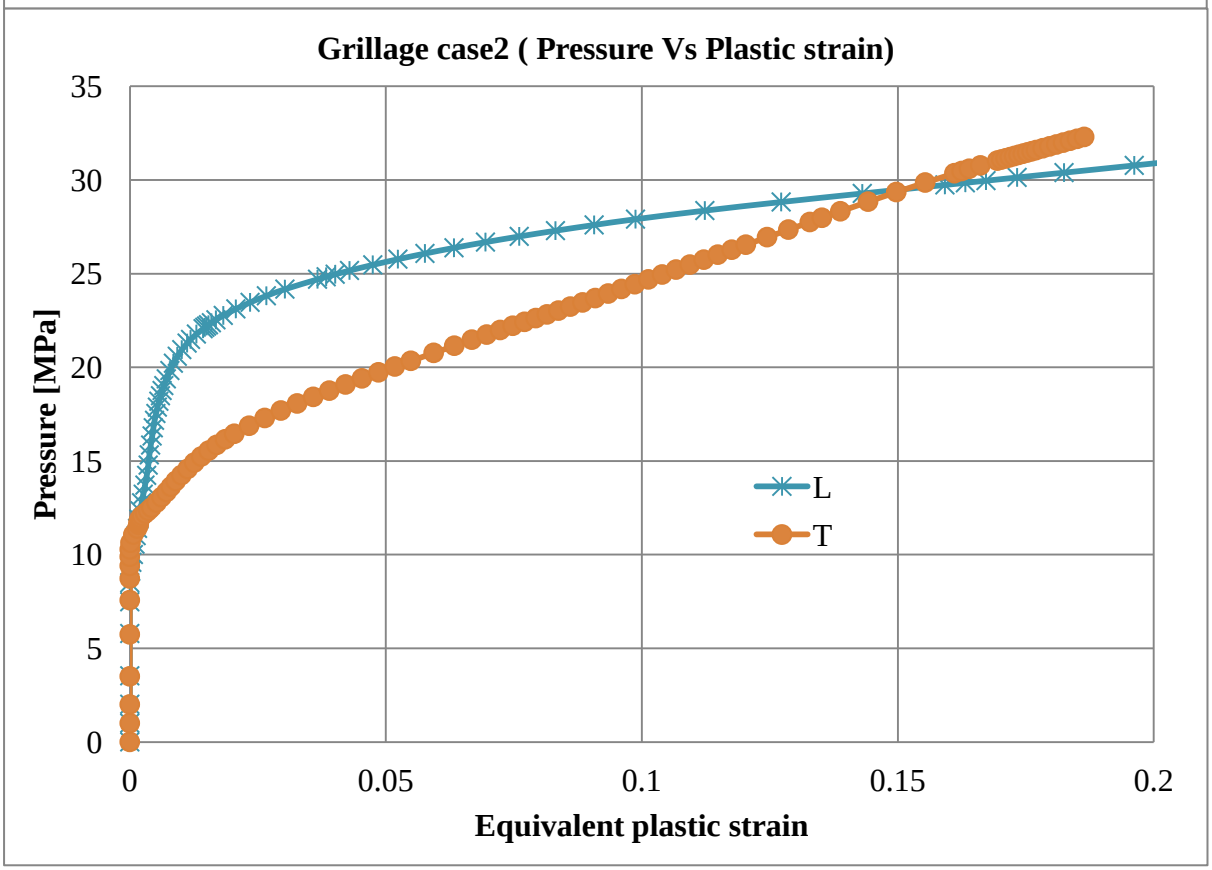

Figure 87 Comparison of capacity at large deformation – Grillage case2

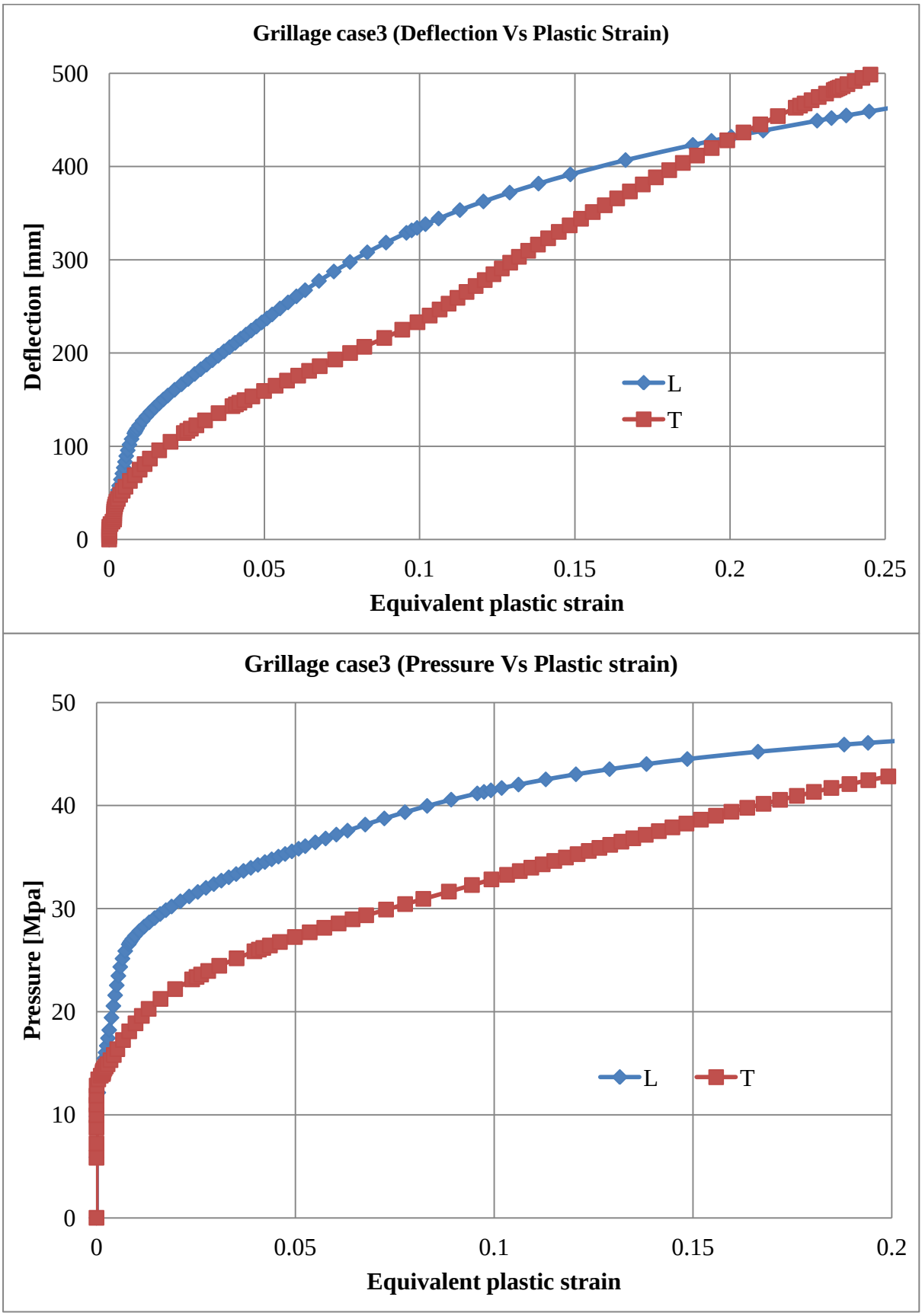

Figure 88 Comparison of capacity at large deformation – Grillage case3

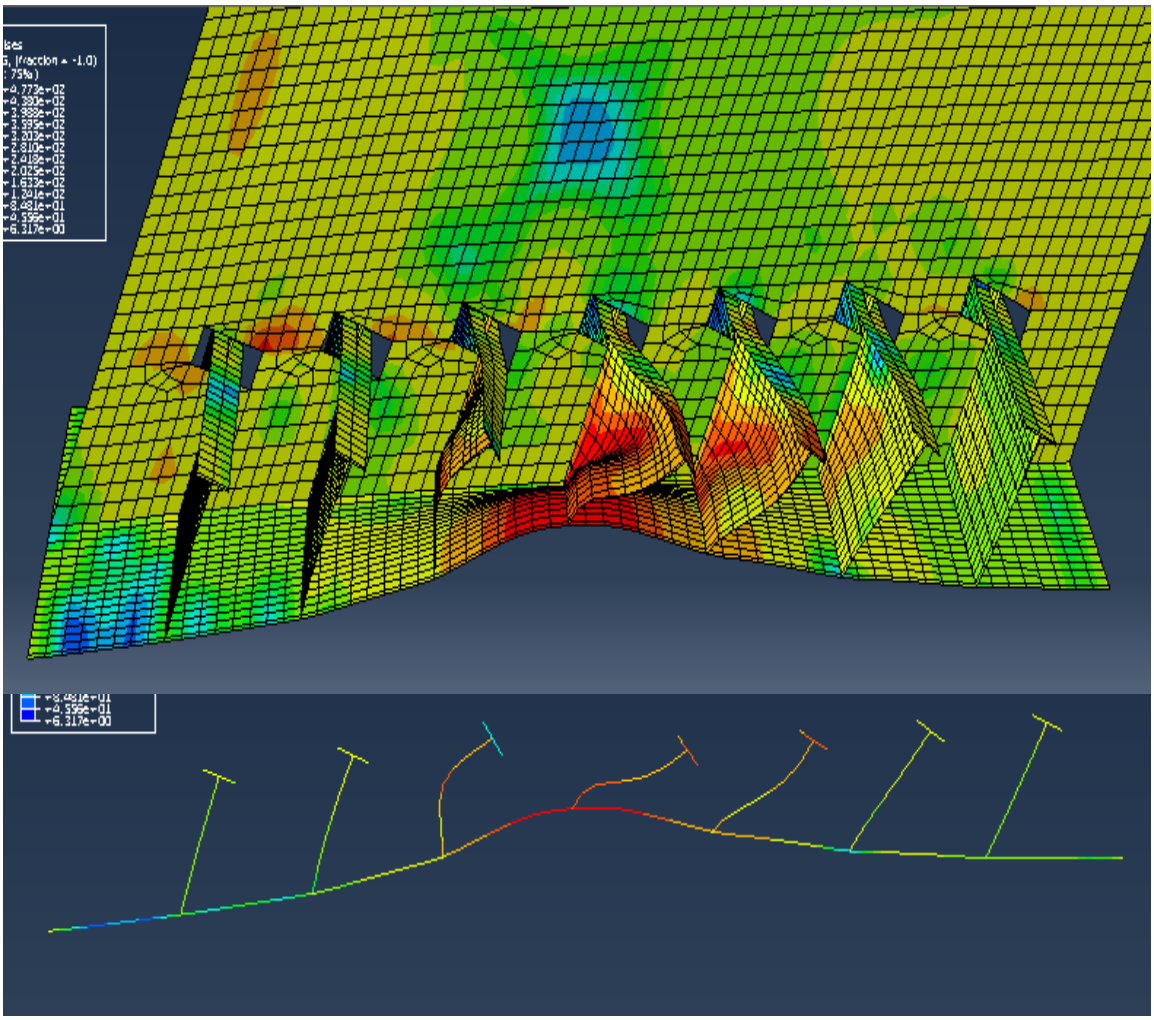

Figure 89 Mid span section of grillage T case3 (with Von Mises stress) subjected to load 32.8255 MPa

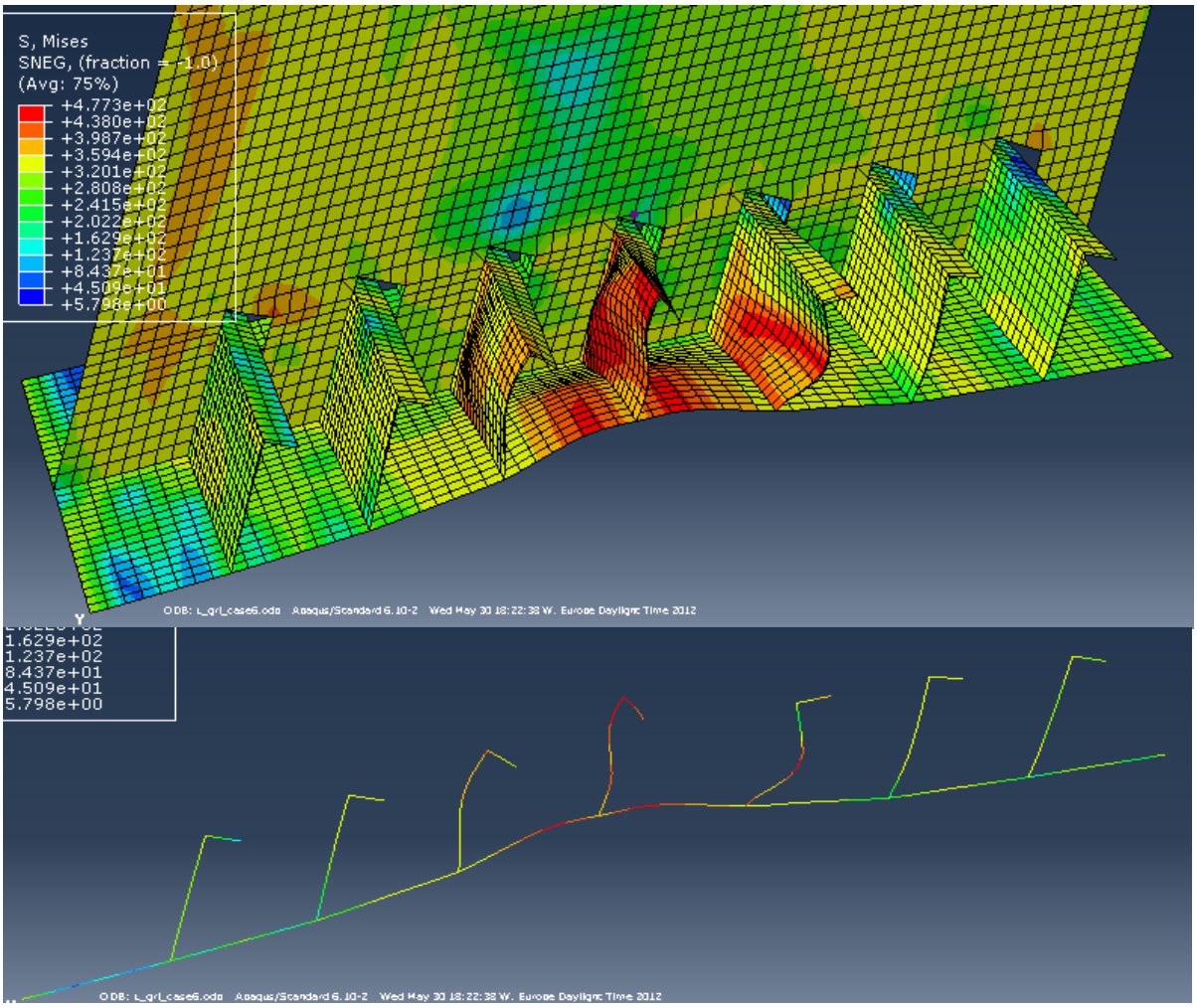

Figure 90 Mid span section of grillage L case3 (with Von Mises stress) subjected to load 33.03182 MPa

7.4.5 Assessment of limit loads when fracture in the plating likely to take place

Table 10 shows the limit loads assessed on the basis of simulation when fracture in the plating is likely to take place.

Table 10 Limit loads when fracture in the plating likely to take place

	T frame		L frame	
	Limit load [MPa]	**Plot of deformation**	**Limit load [MPa]**	**Plot of deformation Figure**
Single frame	18.0593	Figure 116	20.0527	Figure 117
Grillage case1	51.542	Figure 118	54.0724	Figure 119
Grillage case2	29.8577	Figure 120	35.273	Figure 121
Grillage case3	44.7622	Figure 122	47.876	Figure 123

Note: Plot of deformation of L and T frames for different loading conditions subjected to load when fracture in plating likely to take place has been shown in Appendix C.

From the Table 10 it is clear that inclined L stiffener can sustain higher lateral loads than inclined T stiffener.

Chapter 8

8 Conclusion and Recommendation

8.1 Conclusion

Normally a single frame is considered as a representative of the entire grillage structure when the loading is uniform. The symmetric boundary conditions take care of the support provided by the adjacent structure in a single frame. In case of ice loading which is non symmetric, the symmetric boundary condition might not accurately represent the true structural behavior. This concept can be supported by the comparison of FE analysis results of frame in isolation and frame as center stiffener in a grillage presented in the previous chapter. Where it is been found that stiffener in grillage (grillage case3) is around 30% stronger than single frame. Although the analysis of grillage structure was performed for three different load cases, the grillage case-3 represents appropriately the characteristics load of ship ice interaction. So, the design of polar vessel structure based on a single frame seems to be very conservative.

It is also found from the analysis of frames in isolation that in most cases single frame possess higher ULS design load than IACS UR limit state load. One possible reason could be the way IACS UR takes into account the effect of shear on the plastic bending moment capacity is conservative. The concept which has been used in IACS UR to take into account the shear effect on the plastic bending capacity of a frame is shown in figure 91. One of the main drawbacks to this concept is that it does not satisfy the equilibrium conditions of stresses at transition of stresses. And where it is been considered the shear stress uniformly distributed over the web of stiffener but it is known that the effect of shear stress is higher at and near the neutral axis of the section.

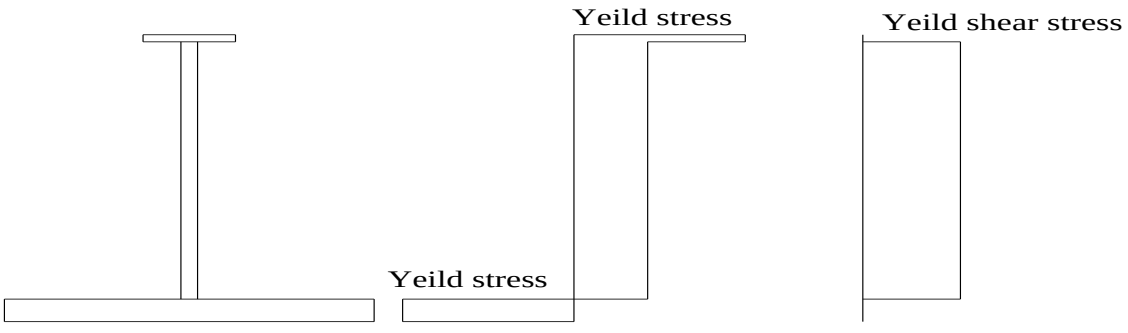

Figure 91 Effect of shear stress on bending stresses used in IACS UR

From the analysis it is observed that the load deflection characteristics of L and T stiffener is almost similar in the region of elastic and small deformation, when the L stiffener is strong enough to resist warping effect due to unsymmetrical stress in the flange. But discrepancy of load deflection characteristics for L and T stiffener was found at moderate and large deformation. It is also found that in all cases the capacity of T stiffener fitted perpendicularly to plate is higher than that of L stiffener fitted perpendicularly to plate at moderate and large deformation. But for moderate web angle inclination (about 45 degree to 80 degree), L stiffener shows better performance than that of T stiffener at moderate and large deformation. Load-deflection characteristic of moderately (45 degree to 80 degree) inclined T stiffener at moderate and large deformation can be greatly improved by introducing tripping bracket at mid-span of the frame. But the use of tripping bracket will have affect on the weight of the structure and consequently in the economy of building the structure. So, to achieve higher ALS design load for the case of 45 degree to 80 degree angle of web inclination, it is better to use L stiffener which has sufficient capacity to resist warping effect.

Although for moderate angle of web inclination, ALS design load of L stiffener is greater than that of T stiffener , in the case of small web angle of inclination (up to 40 degree) the load-deflection characteristic of frames predicts almost similar ALS design load for L and T frame (see figure 125). Possible reason could be the excessive difference between section modulus of the L and T-stiffener due to the small web angle inclination.

8.2 Recommendations for further work

In the analysis of transverse frame it is been observed that L frames from table 4 don't sustain IACS UR limit state load. It is been found that local buckling of web at mid span under the patch load causes the frame to fail prior to reach the IACS UR load, though all the frames satisfy the IACS UR local buckling requirement. So, further work need to be done in this regard.

From the analysis of the frames it is been observed that almost all cases, except the cases where failure due to local buckling occur prior to reach the IACS UR limit state load, frame possess about 5% to 40% higher lateral capacity at the onset of plastic deformation than IACS UR limit state load. So, IACS UR for capacity of frame needed to be revised in order to predict limit state design load precisely close to onset of plastic deformation.

From the analysis of longitudinal frames for both L and T section it is found that shorter frames seem to have higher design capacity (see figure 51 & 53) and it also appear that above a certain length, the capacity falls. It indicates that certain behavior occurs in frames longer than a critical value. It is recommended that further study should be carried out on understanding this behavior of frames.

From the difference in load carrying capacity between frames in isolation and frames as part of a grillage, it appears that frames as part of grillage case3 which is appropriate

representation of structure subjected to ice loads, show about 30% to 40% higher capacity than that of frames in isolation. IACS UR design rule for framing which is based on single frame needs to be revised in order to take into account the effect of adjacent structure.

The available reliable methods to estimate ALS design capacity of ice strengthen structures are either to conduct full scale experiment or a nonlinear finite element analysis. These methods are either very expensive or too complex. Further work might be done in order to develop simplified resistance expression to account for the influence of membrane stresses for the structure subjected to large deformations.

9 References

[1] T.H. Søreide, Ultimate load analysis of Marine Structures, Tapir, Trondheim, May 1981.

[2] Kmiecik M. Usefulness of the yield line theory in design of ship plating. Mar Struct 1995;8(1):67–79.

[3] Sawczuk A. On initiation of the membrane action in rigid-plastic plates. J Mech 1964;3(1):15–23.

[4] Jones N. A theoretical study of the dynamic plastic behavior of beams and plates with finite-deflections. Int. J Solids Struct 1971; 7:1007–29.

[5] H. Nyseth, Structural resistance of polar ships subjected to ice loads, master thesis. Department of Marine Technology, NTNU, 2003.

[6] IACS, I2 Structural requirements for polar class ships. IACS requirements, 2010.

[7] C. D. A. Kendrick, Derivation and use of formulations for framing design in the polar class unified requirements. IACS Ad-hoc Group on Polar Class Ships, Transport Canada, 2000.

[8] L. Hong and J. Amdahl, Plastic design of laterally patch loaded plates for ships. Elsevier, 2007.

[9] Daley CG, Kendrick A, Appolonov E. Plating and framing design in the unified requirements for polar class ships. In: Proceedings of the 16th international conference on port and ocean engineering under arctic conditions, vol, 3, Ottawa, Canada, 2001. p. 779–91.

[10] Kendrick, A. and C. Daley (2000). Derivation and use of formulations for framing design in the polar class unified requirements.

[11] D. Beghin, Ultimate Strength of Laterally Loaded Stiffeners, July 1999 Discussion Paper to IACS Ad-hoc Group

[12] DNV, Rules for classification of ships, ships for navigation in Ice. Det Norske Veritas, Høvik, 2010.

[13] J. Amdahl, TMR 4205 compendium, Buckling and ultimate strength of marine structures, Marine technology, NTNU, 2007.

[14] C.Daley and A. Bansal, Discussion of plastic capacity of plating subject to patch loads, 2009.

[15] A. Kendrick, background to definition of polar classes. IACS Ad-hoc group on polar class ships, Transport Canada, 2000.

[16] C. Daley, Background notes to Design Ice Loads, IACS Ad-hoc group on Polar Class ships, Transport Canada, 2000.

[17] K. Riska, Design of ice breaking ships, ILS Oy, Helsinki, FINLAND and University of Science and Technology, Trondheim, NORWAY.

[18] Popov, Yu. et. al. Strength of Ships Sailing in Ice (Translation) U.S. Army Foreign Science and Technology Center, FSTC-HT-23-96-68, Washington DC, USA, 1969.

[19] RISKA, K. & RANTALA, H. & JOENSUU, A. 1990. Full Scale Observations of Ship-Ice Contact. Helsinki University of Technology, Lab. of Naval Architecture and Marine Eng., Report M-97, Espoo, 1990.

[20] T. Moan, Finite element modeling and Analysis of Marine structures, Compendium TMR 4190, Department of Marine Technology, NTNU, September 2003.

[21] Finnish-Swedish Ice Class Rules, The structural design and engine output required of ships for navigation in ice.

[22] G. Holtsmark and H. Strømme, The capacity of panel stiffeners subjected to lateral Pressure loads, report No 2004-0168, Maritime Development centre DNV, 2004.

[23] H. Larsen, Structural resistance of polar ships subjected to ice loads, master thesis. Department of Marine Technology, NTNU, 2005.

[24] J. Abraham, Plastic response of ship structure subjected to ice loading, master thesis, Faculty of engineering and applied science, Memorial University of Newfoundland, September, 2008.

[25] D. Mackenzie and H. Li, A Plastic Load Criterion for Inelastic Design by Analysis, Journal of pressure vessel technology, February 2006.

[26] Claude Daley, Mihailo Pavic, Amgad Hussein, Greg Hermanski (2004). Ship Frame Research Program - A Numerical Study of the Capacity of Single Frames Subject to Ice Load. OERC Report 2004-02

Appendices

Appendix A: Plot of deformation for frames and stiffened plate subject to ULS design load presented in Table7

Plot of deformation of frames from table5

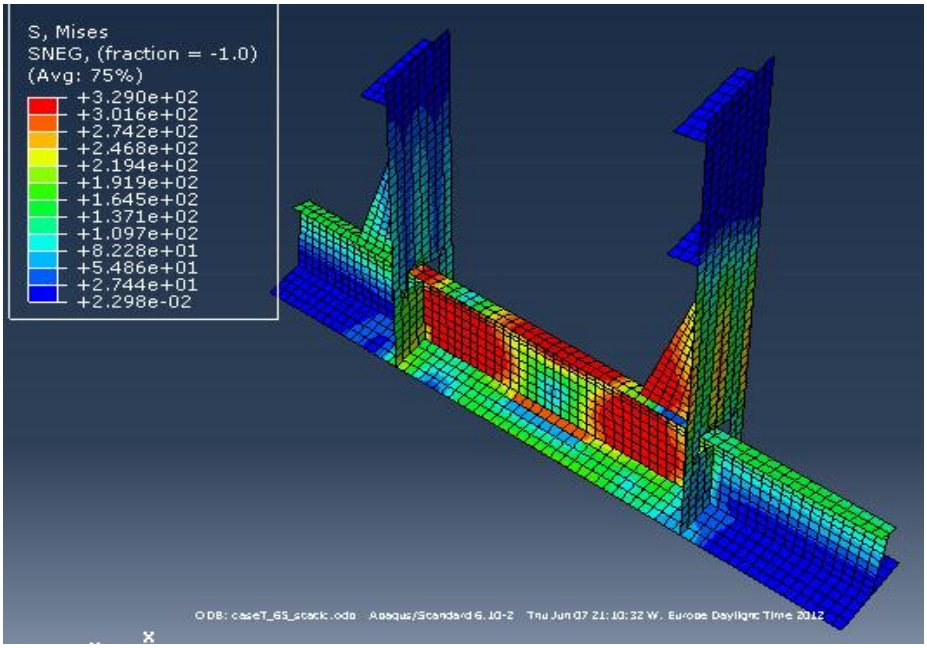

Figure 92 Plot of deformation (with Von Mises stress) for single T at 7.16 MPa

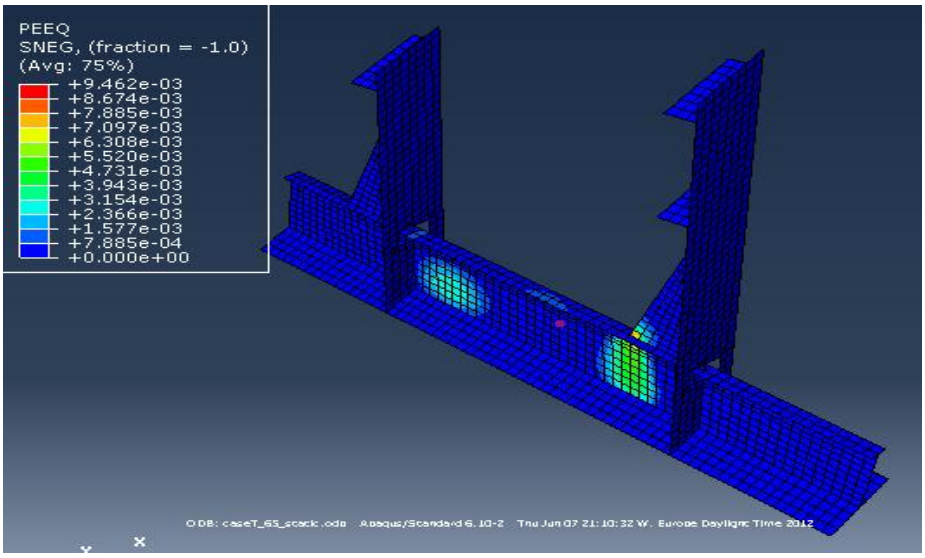

Figure 93 Plot of deformation (with equivalent plastic strain) for single T at 7.16 MPa

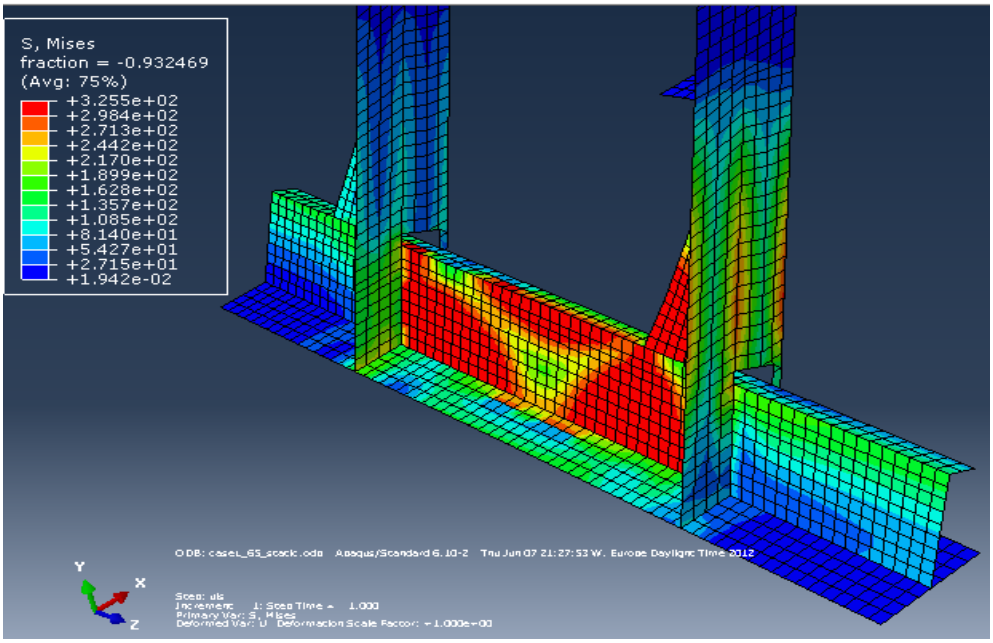

Figure 94 Plot of deformation (with Von Mises stress) for single L at 6.94 MPa

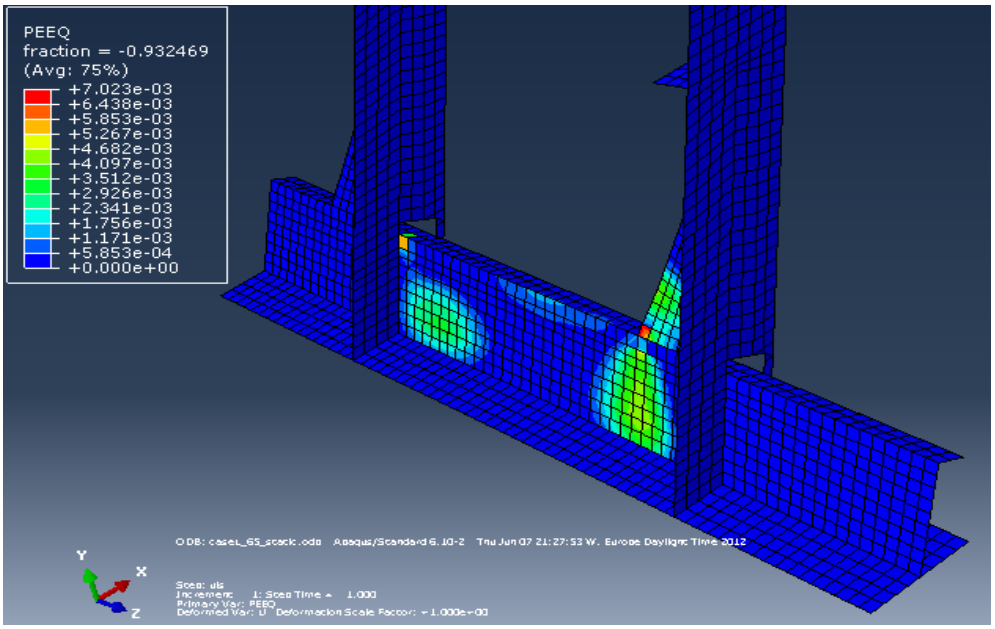

Figure 95 Plot of deformation (with equivalent plastic strain) for single L at 6.94 MPa

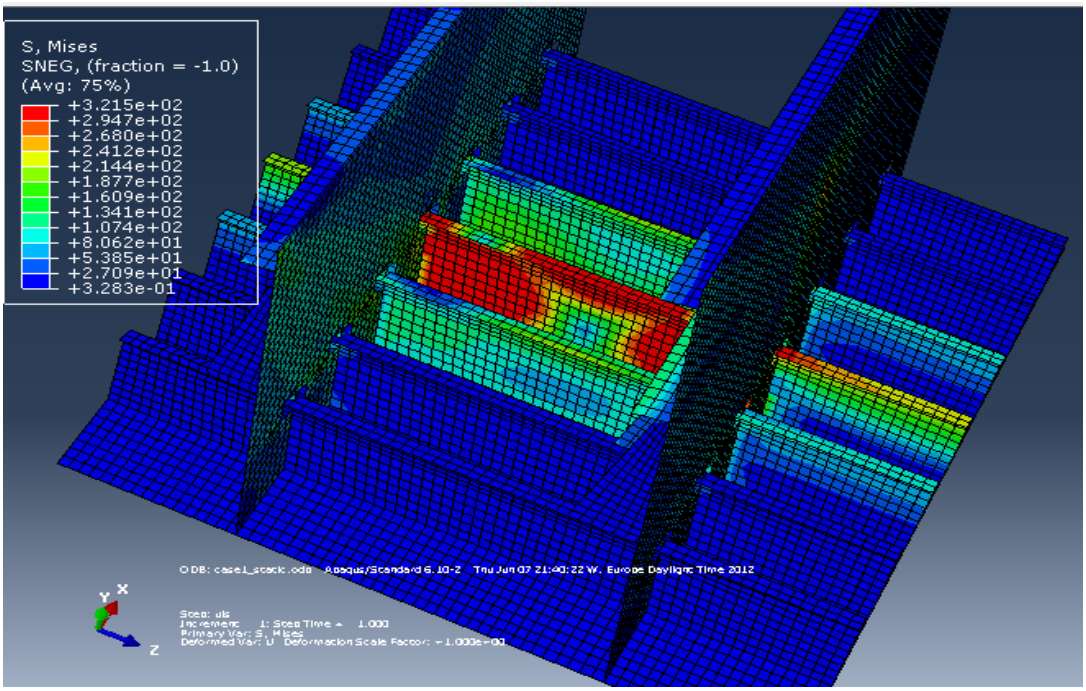

Figure 96 Plot of deformation (with Von Mises stress) for Grillage_1 T at 10.55 MPa

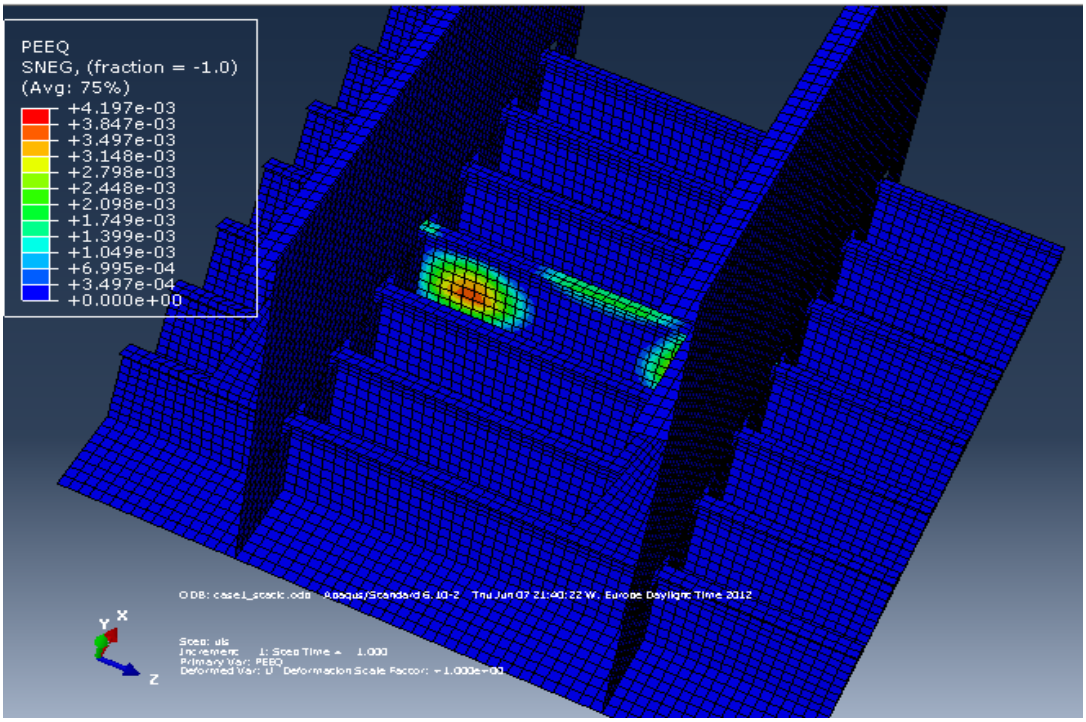

Figure 97 Plot of deformation (with equivalent plastic strain) for Grillage_1 T at 10.55 MPa

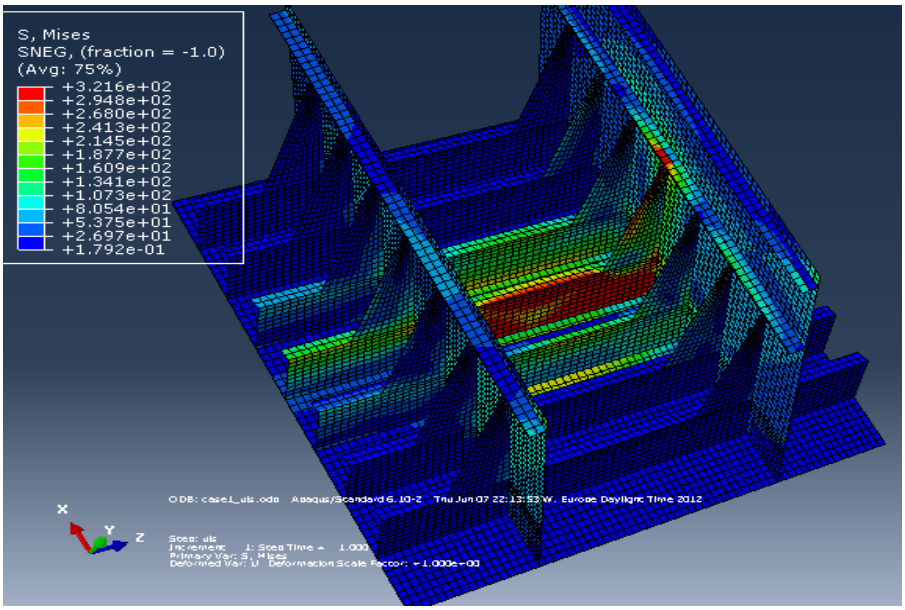

Figure 98 Plot of deformation (with Von Mises stress) for Grillage_1 L at 10.2013 MPa

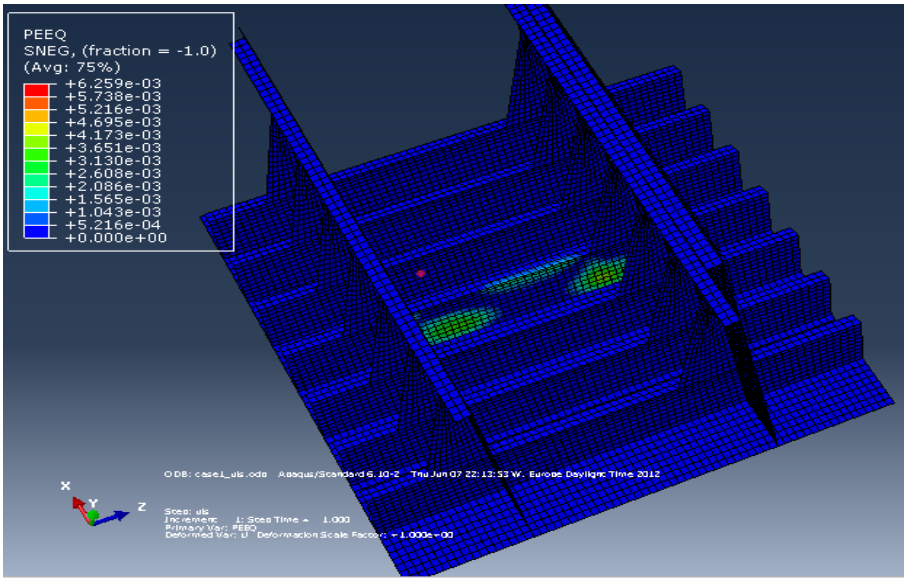

Figure 99 Plot of deformation (with equivalent plastic strain) for Grillage_1 L at 10.2013 MPa

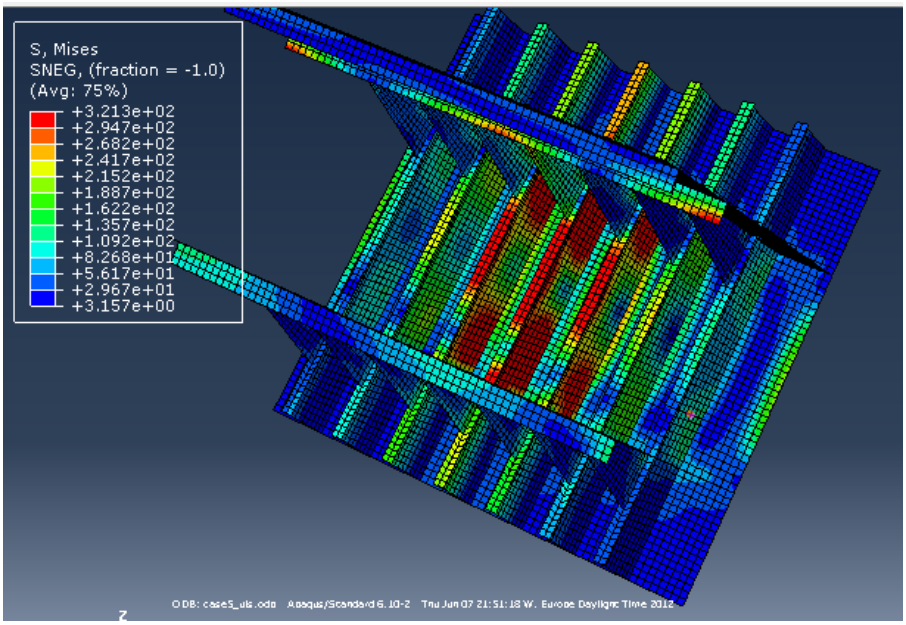

Figure 100 Plot of deformation (with Von Mises stress) for Grillage_2 T at 8.44 MPa

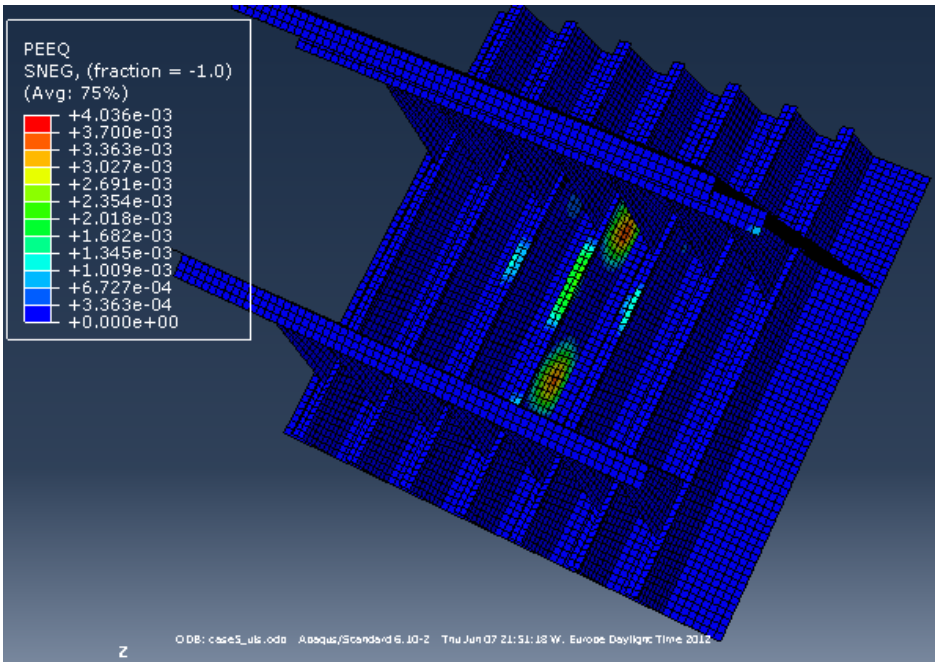

Figure 101 Plot of deformation (with equivalent plastic strain) for Grillage_2 T at 8.44 MPa

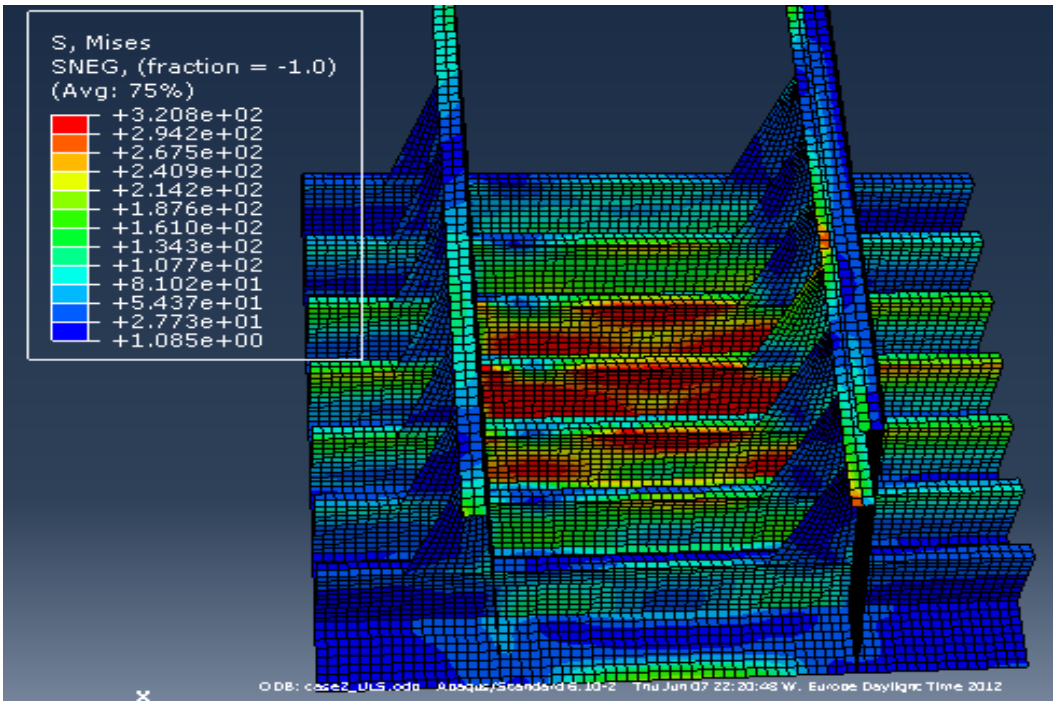

Figure 102 Plot of deformation (with Von Mises stress) for Grillage_2 L at 8.058 MPa

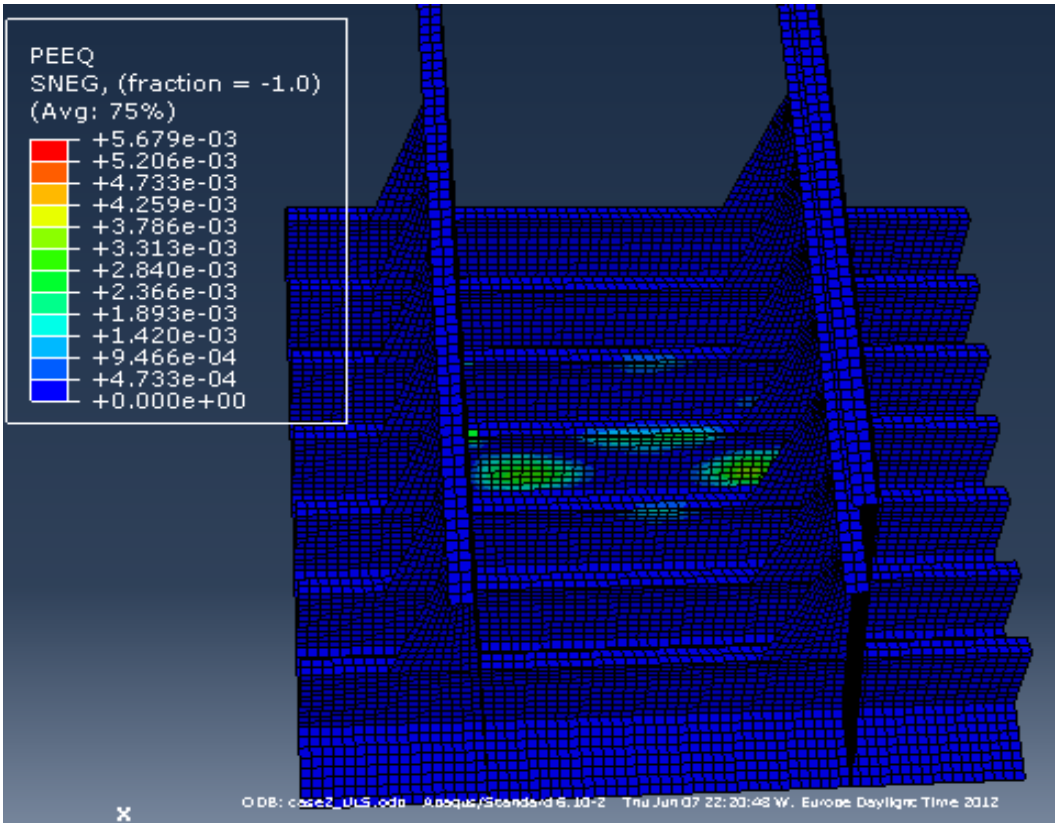

Figure 103 Plot of deformation (with equivalent plastic strain) for Grillage_2 L at 8.058 MPa

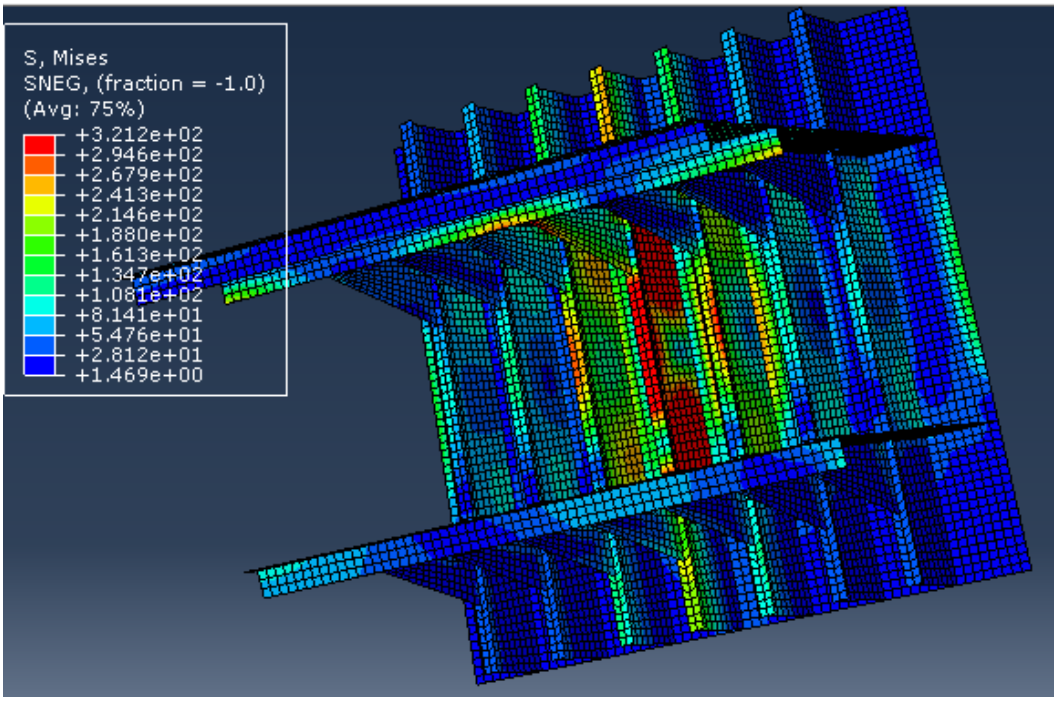

Figure 104 Plot of deformation (with Von Mises stress) for Grillage_3 T at 9.8 MPa

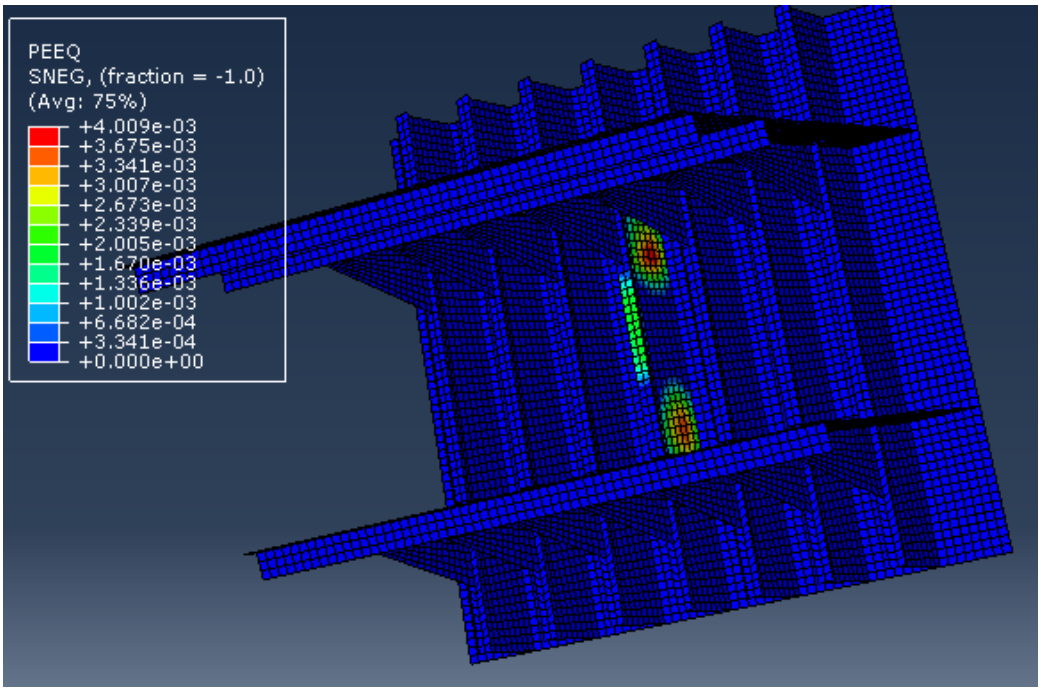

Figure 105 Plot of deformation (with equivalent plastic strain) for Grillage_3 T at 9.8 MPa

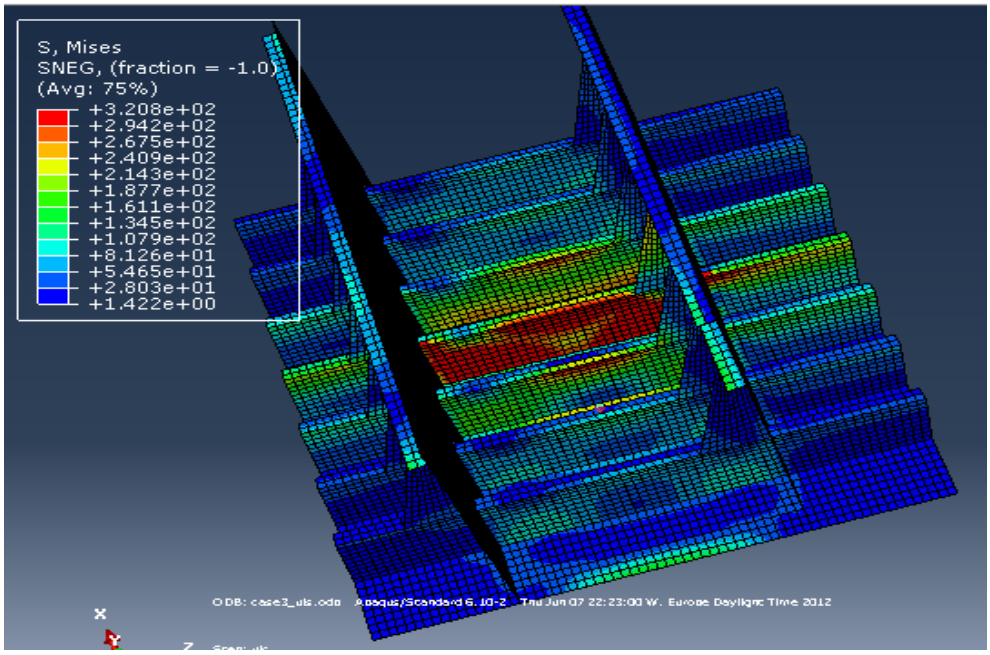

Figure 106 Plot of deformation (with Von Mises stress) for Grillage_3 L at 9.25 MPa

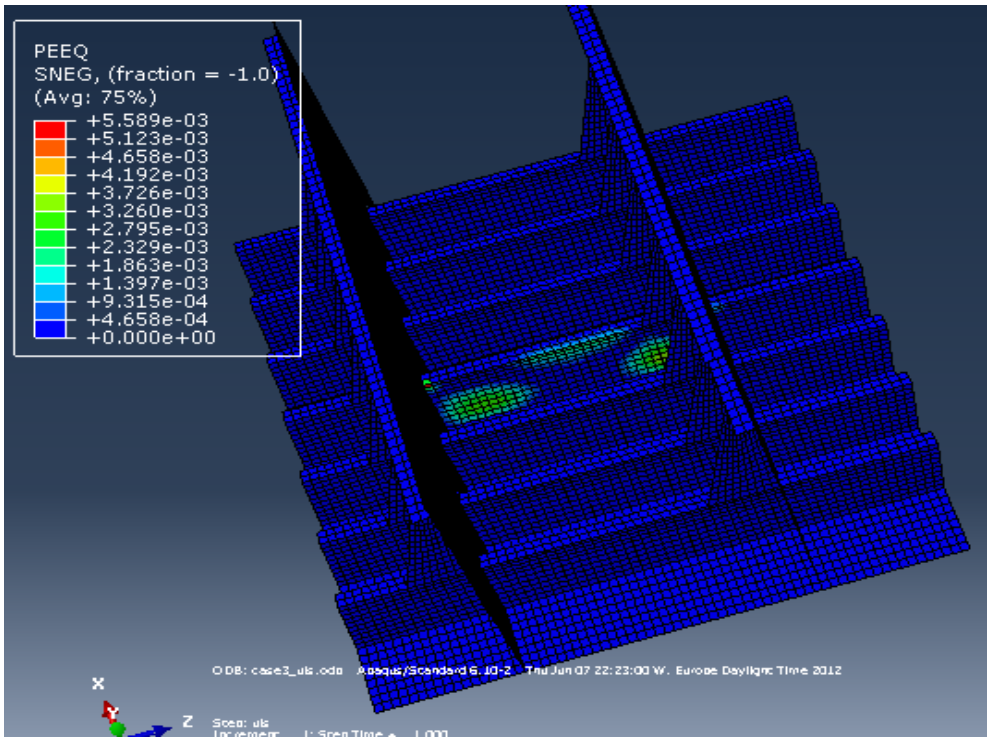

Figure 107 Plot of deformation (with equivalent plastic strain) for Grillage_3 L at 9.25 MPa

Appendix B: Plot of deformation for frames and stiffened plate subject to ALS design load presented in Table8

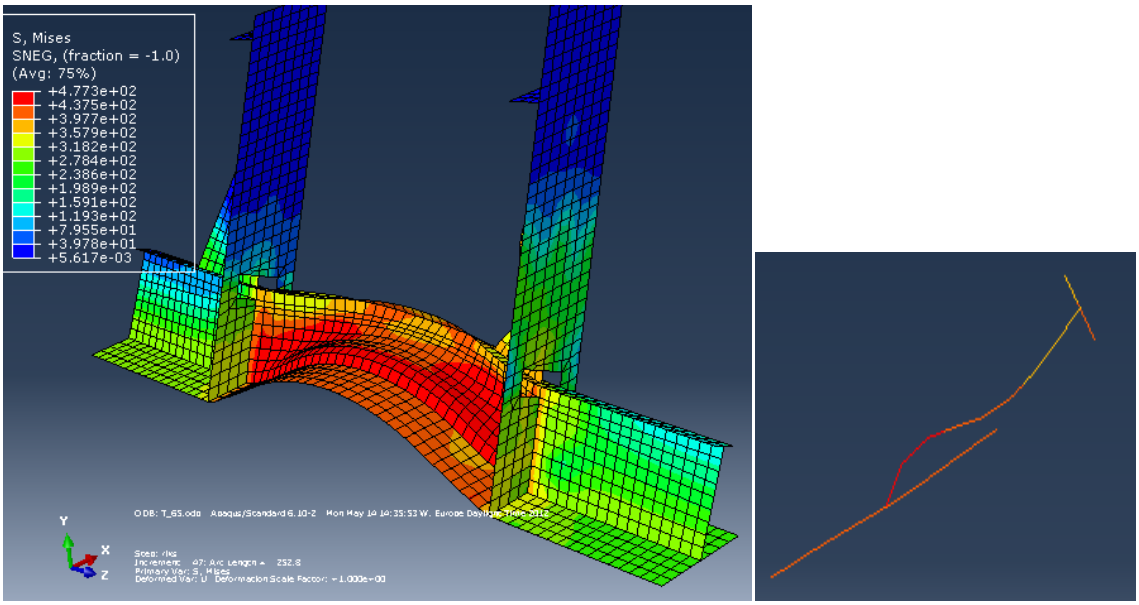

Figure 108 Plot of deformation (with Von Mises stress) for single T at 16.5 MPa

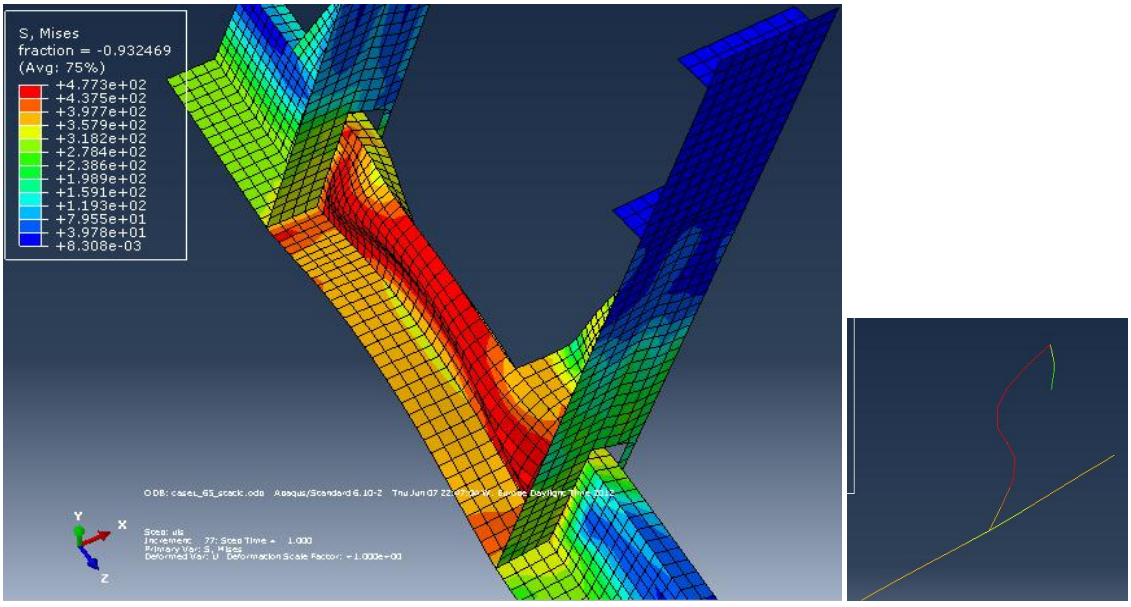

Figure 109 Plot of deformation (with Von Mises stress) for single L at 18.5305 MPa

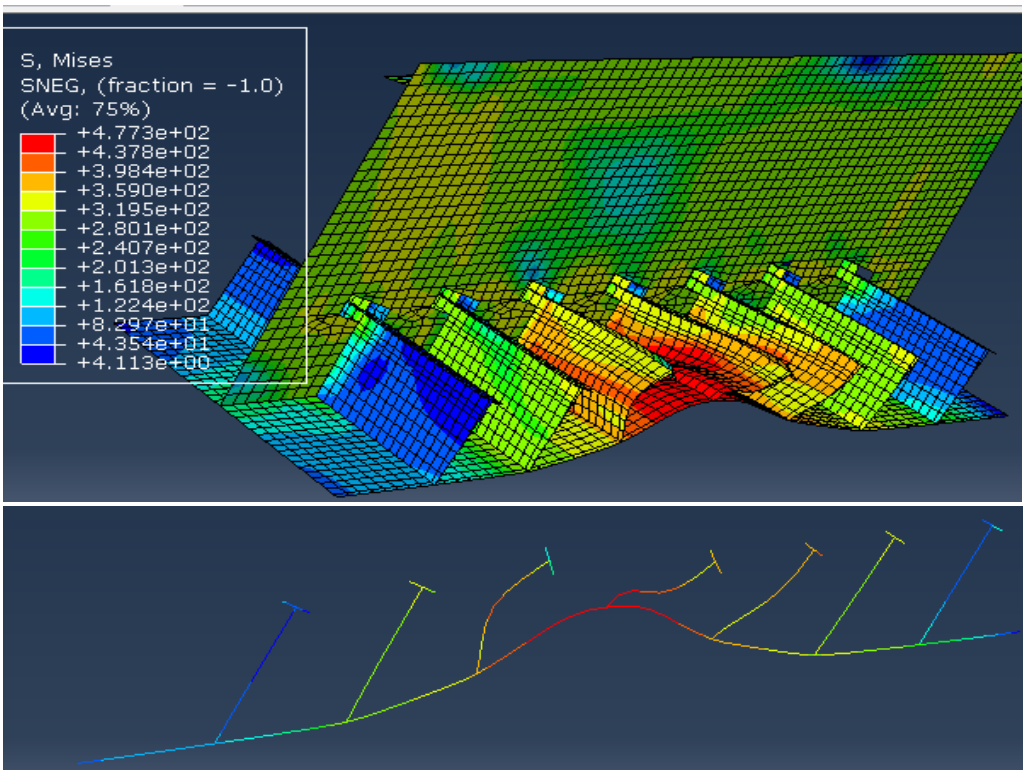

Figure 110 Plot of deformation (with Von Mises stress) for Grillage_1 T at 46.05 MPa

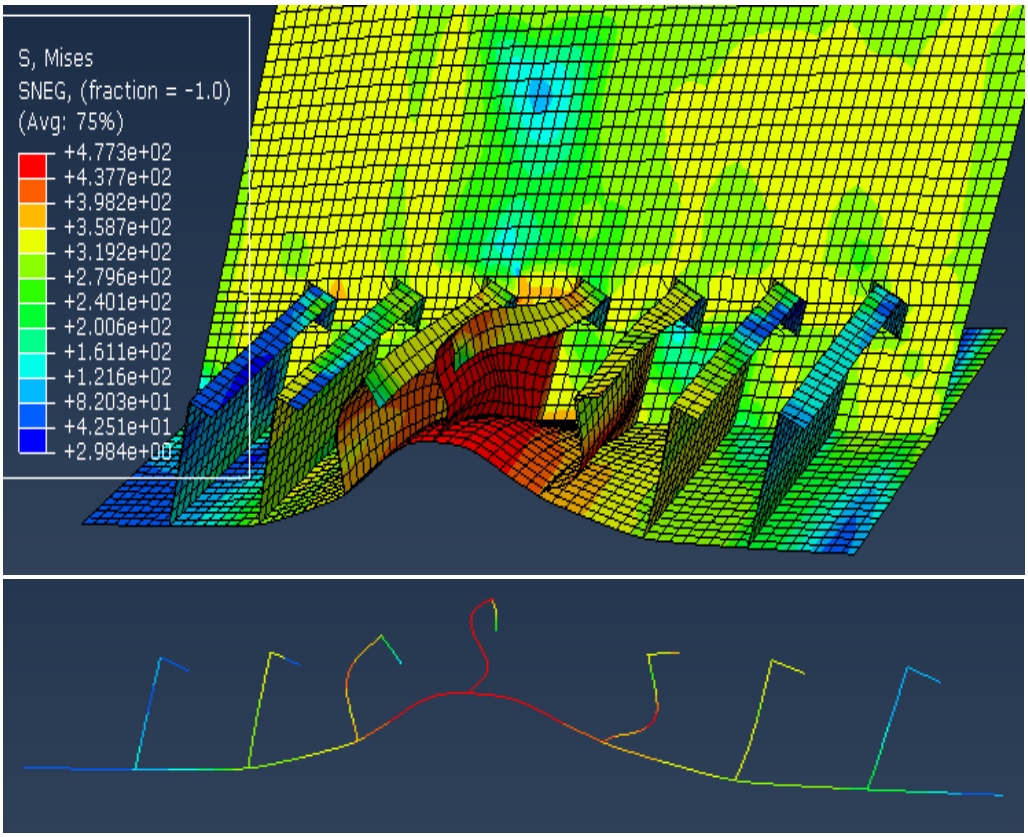

Figure 111 Plot of deformation (with Von Mises stress) for Grillage_1 L at 51.3661 MPa

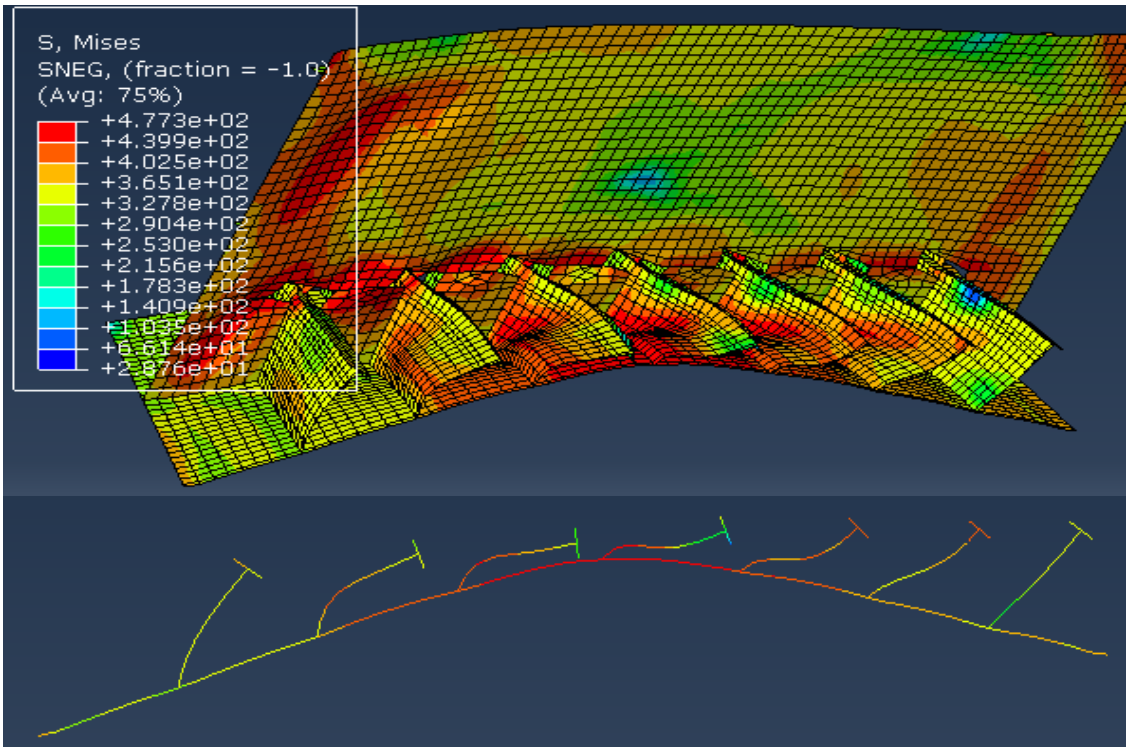

Figure 112 Plot of deformation (with Von Mises stress) for Grillage_2 T at 29.35 MPa

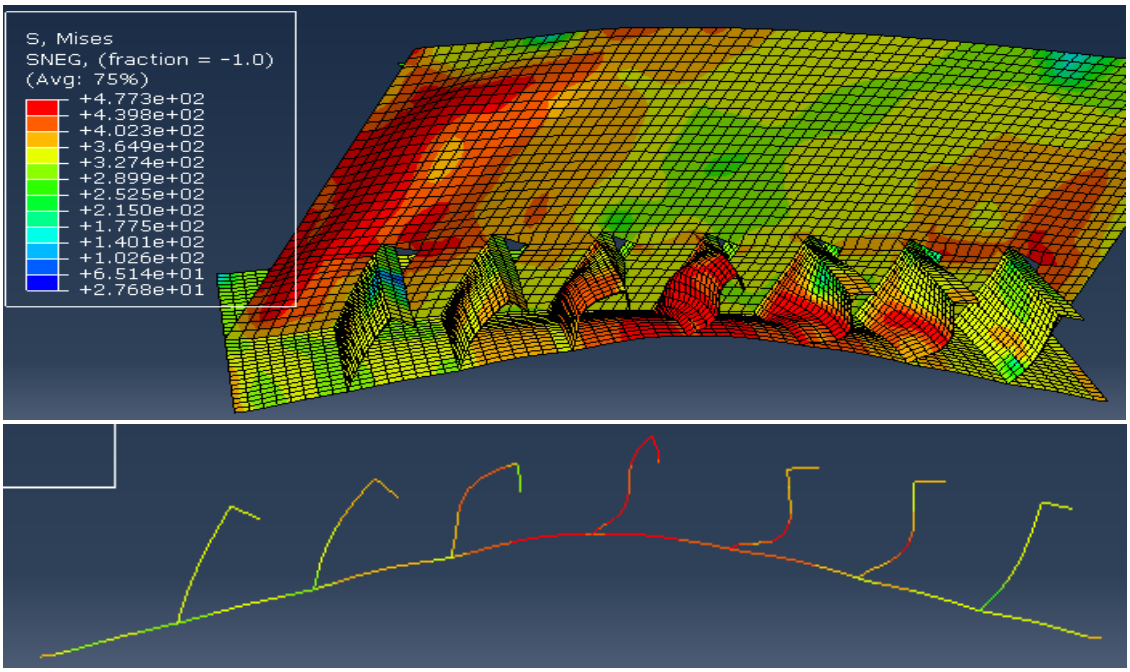

Figure 113 Plot of deformation (with Von Mises stress) for Grillage_2 L at 29.73 MPa

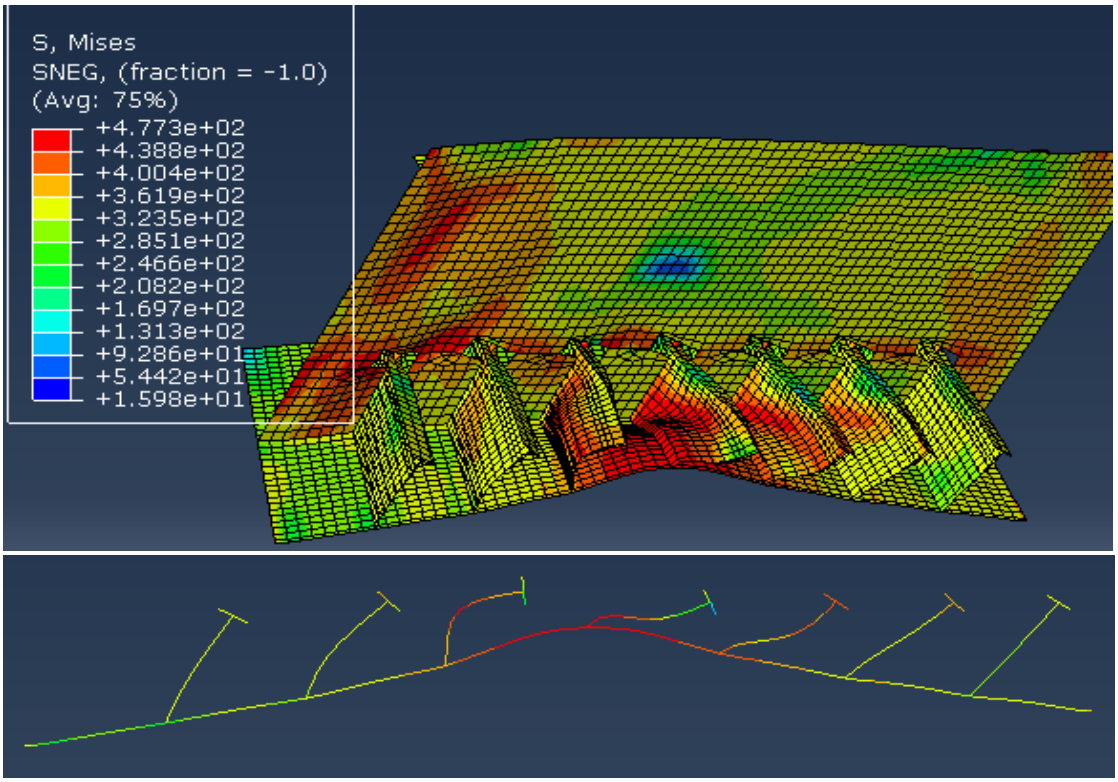

Figure 114 Plot of deformation (with Von Mises stress) for Grillage_3 T at 39 MPa

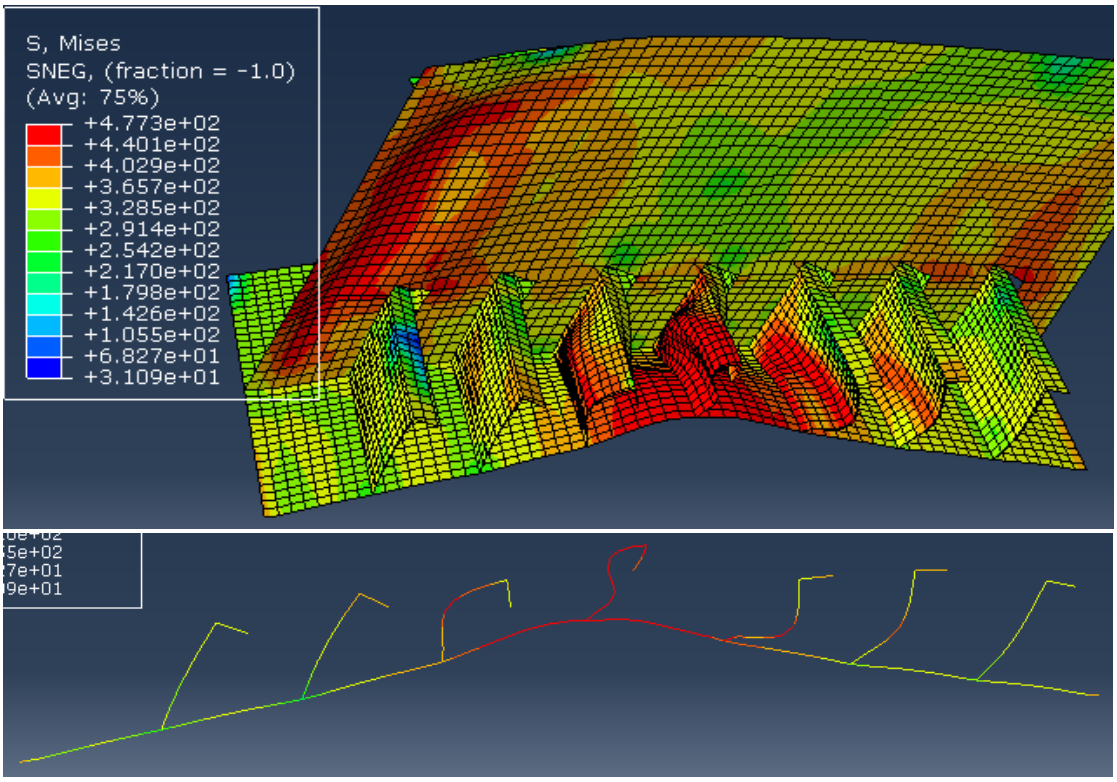

Figure 115 Plot of deformation (with Von Mises stress) for Grillage_3 L at 44.5 MPa

Appendix C: Plot of deformation for frames and stiffened plate subject to limit load when fracture in the plating likely to take place presented in Table10

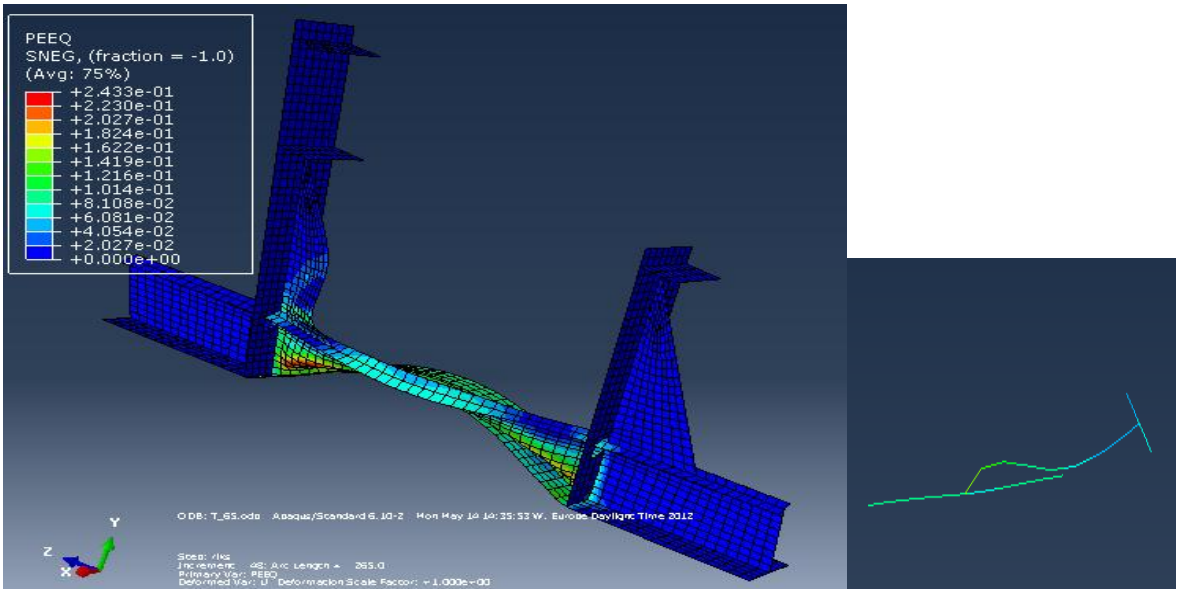

Figure 116 Plot of deformation subjected to limit load 18.0593 MPa – T frame

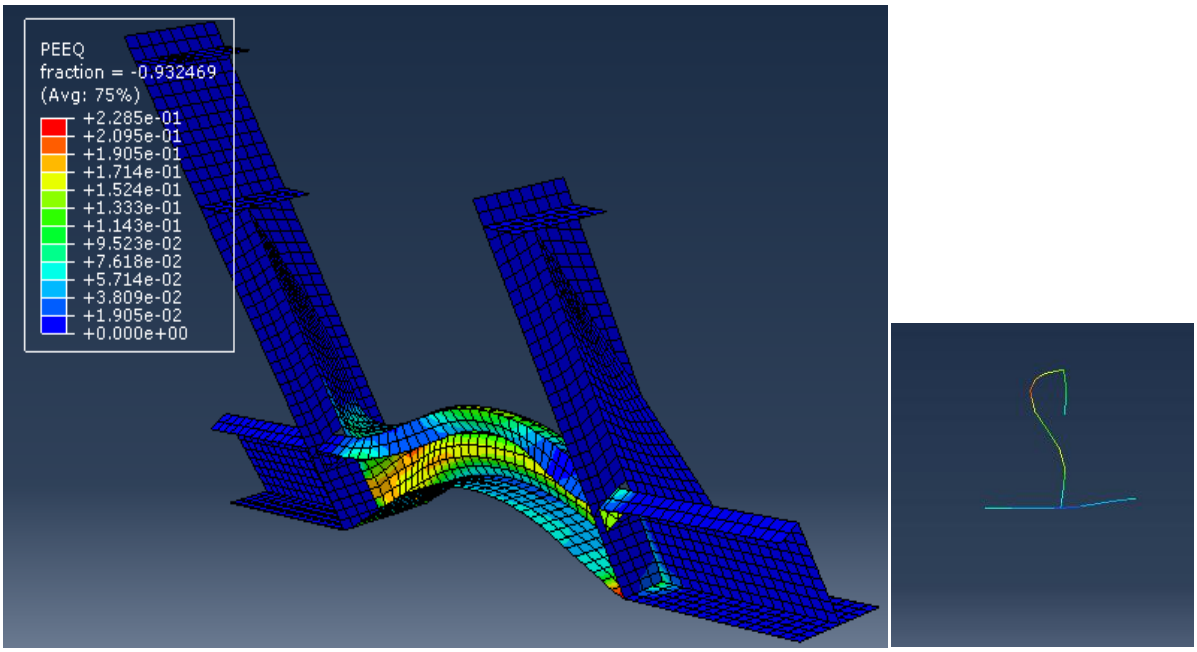

Figure 117 Plot of deformation subjected to limit load 20.0527 MPa – L frame

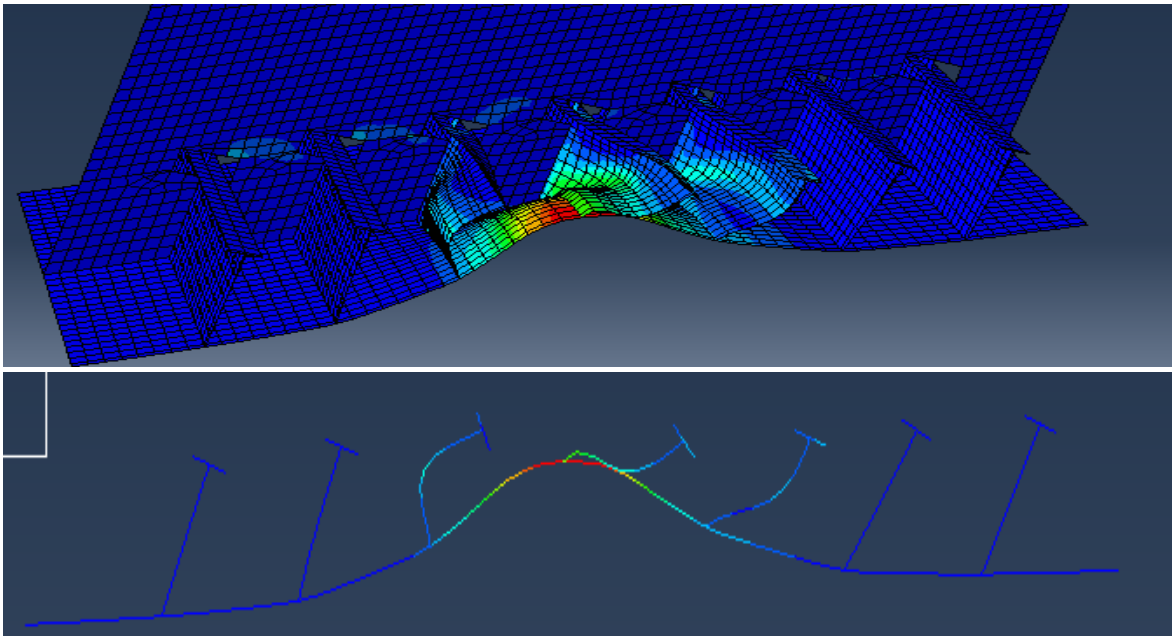

Figure 118 Plot of deformation subjected to limit load 51.542 MPa –T grillage case 1

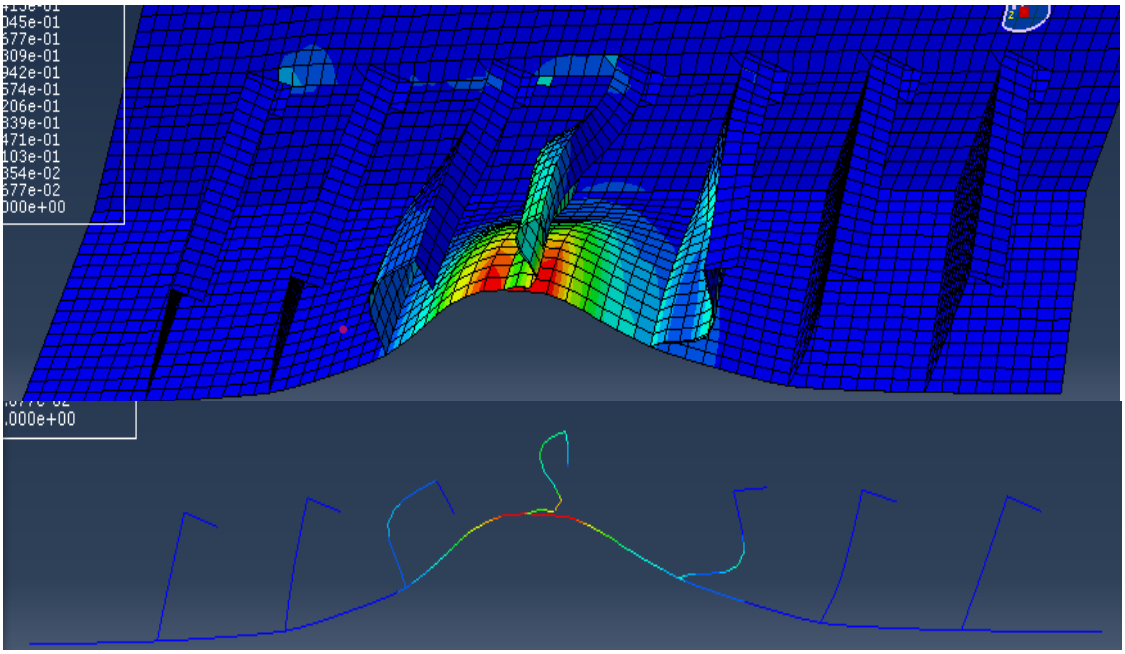

Figure 119 Plot of deformation subjected to limit load 51.542 MPa –L grillage case 1

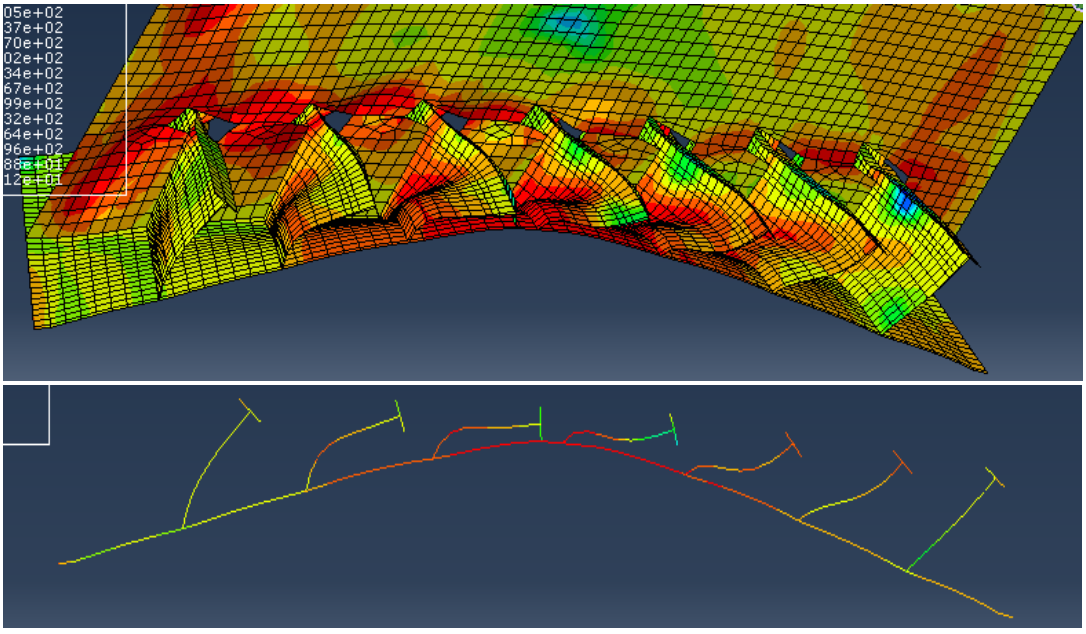

Figure 120 Plot of deformation subjected to limit load 29.8577 MPa –T grillage case 2

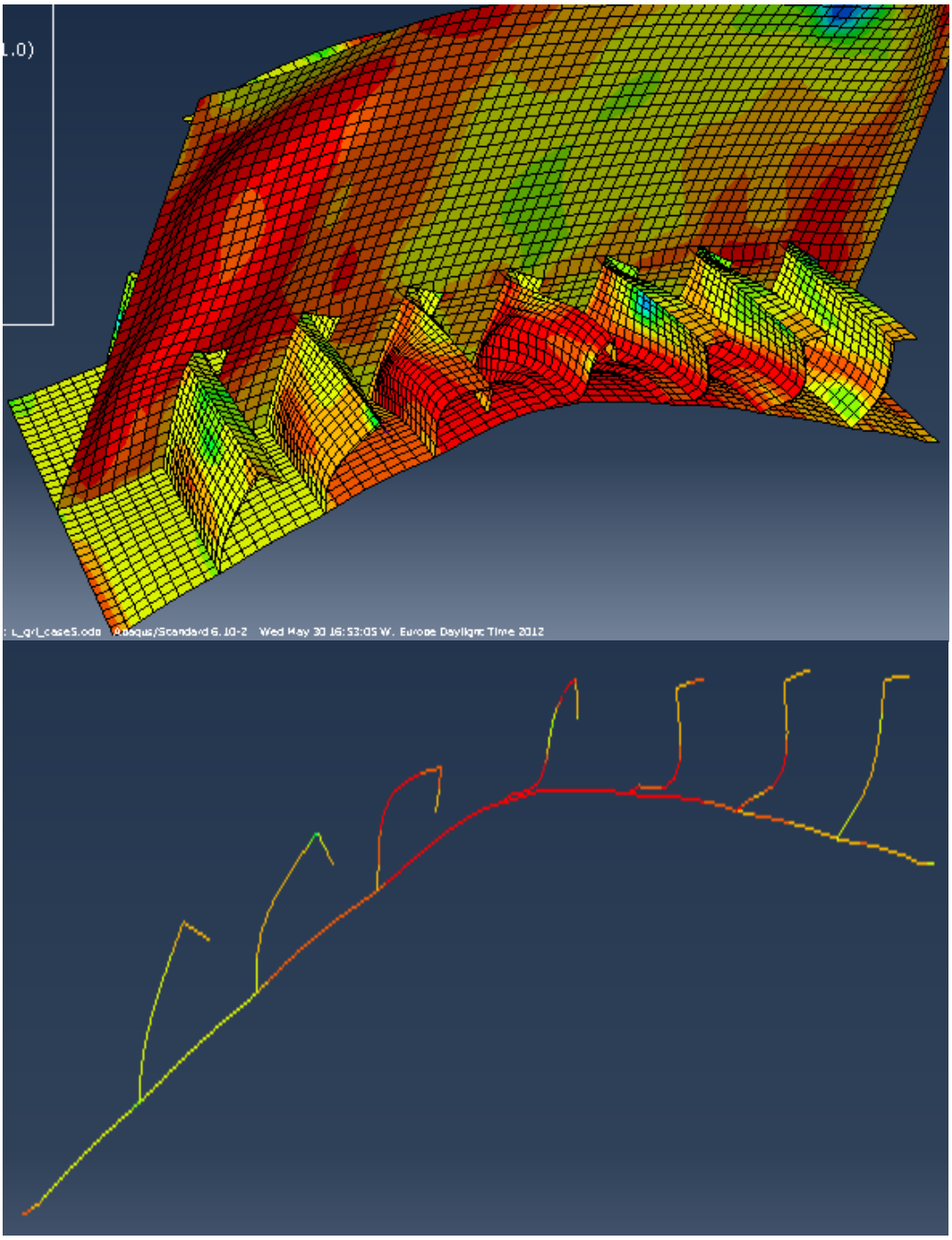

Figure 121 Plot of deformation subjected to limit load 35.273 MPa –L grillage case 2

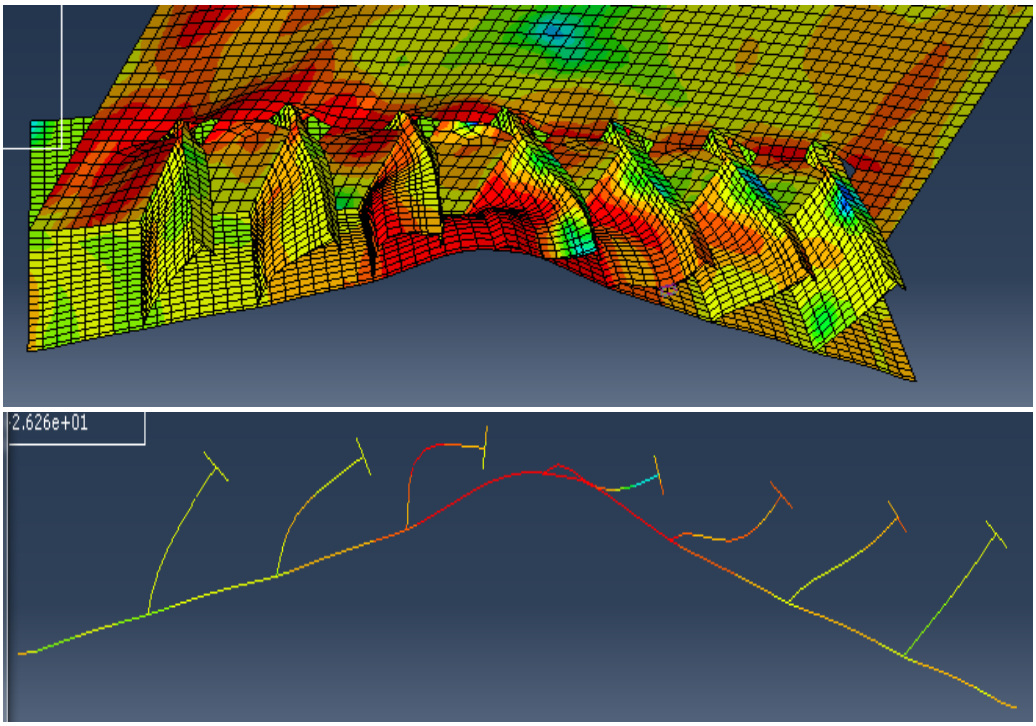

Figure 122 Plot of deformation subjected to limit load 44.7622 MPa –T grillage case 3

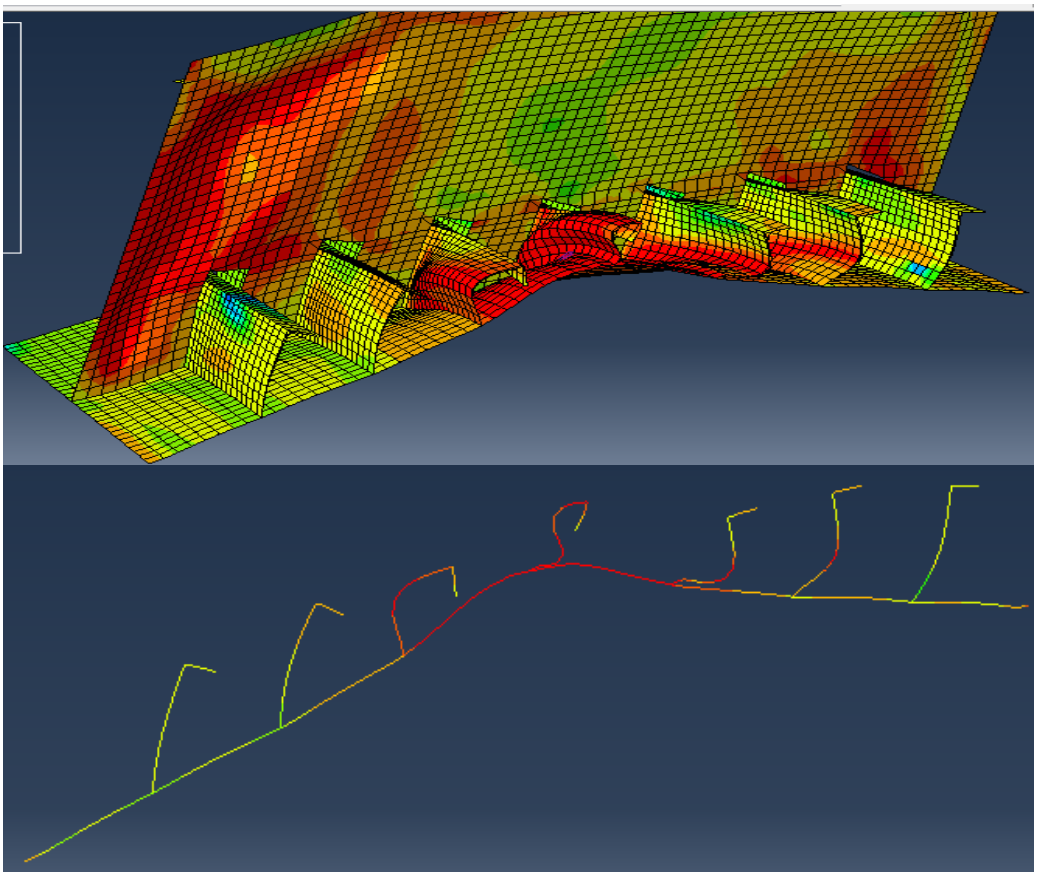

Figure 123 Plot of deformation subjected to limit load 47.876 MPa –L grillage- case 3

Appendix D: Behavior of frames with and without tripping bracket for different web angle inclination

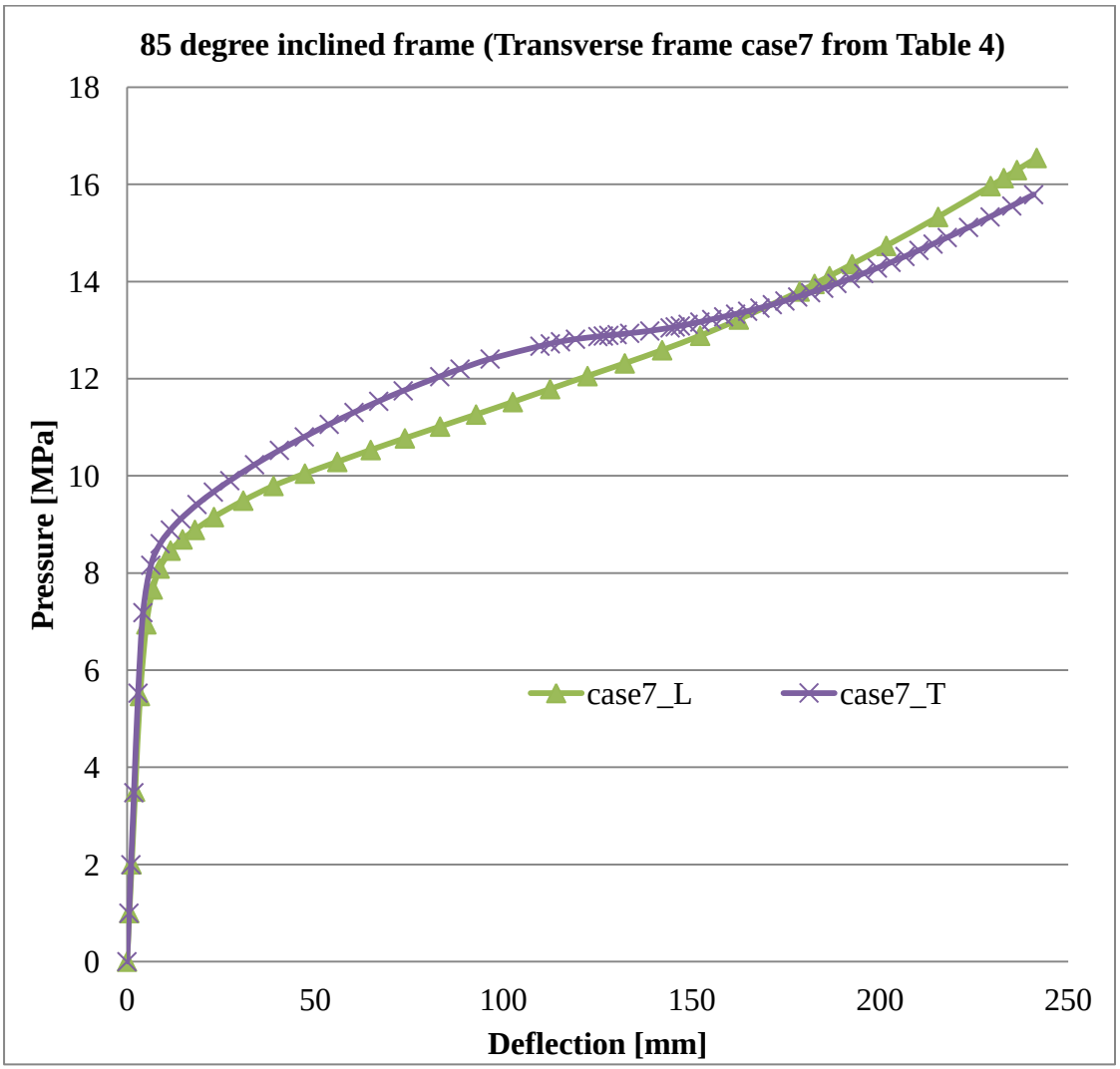

Figure 124 Load deflection curve of transverse frame case 7 – 85 degree web inclination

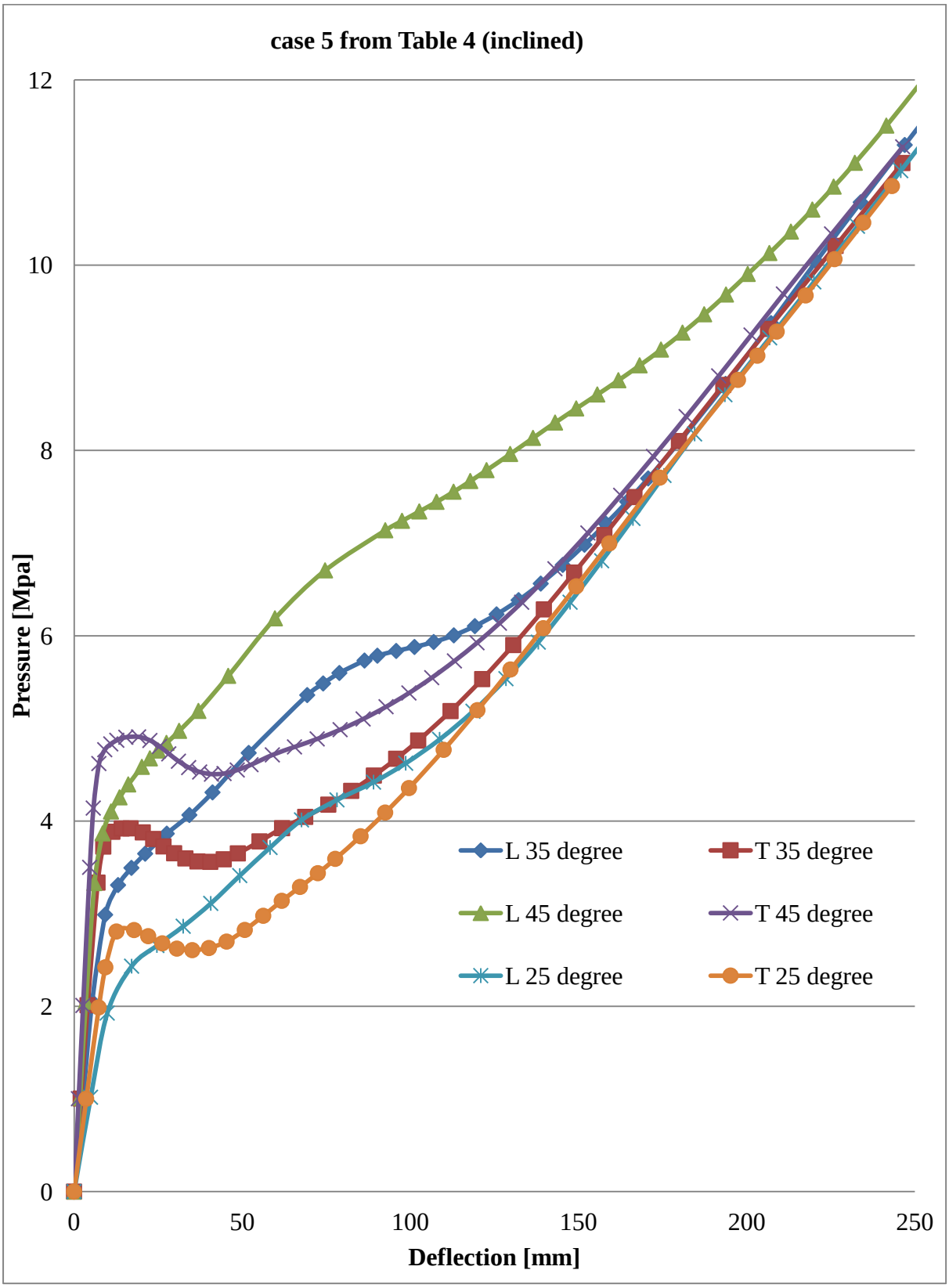

Figure 125 Load-deflection curve of transverse frame case 5- for different web angle inclination

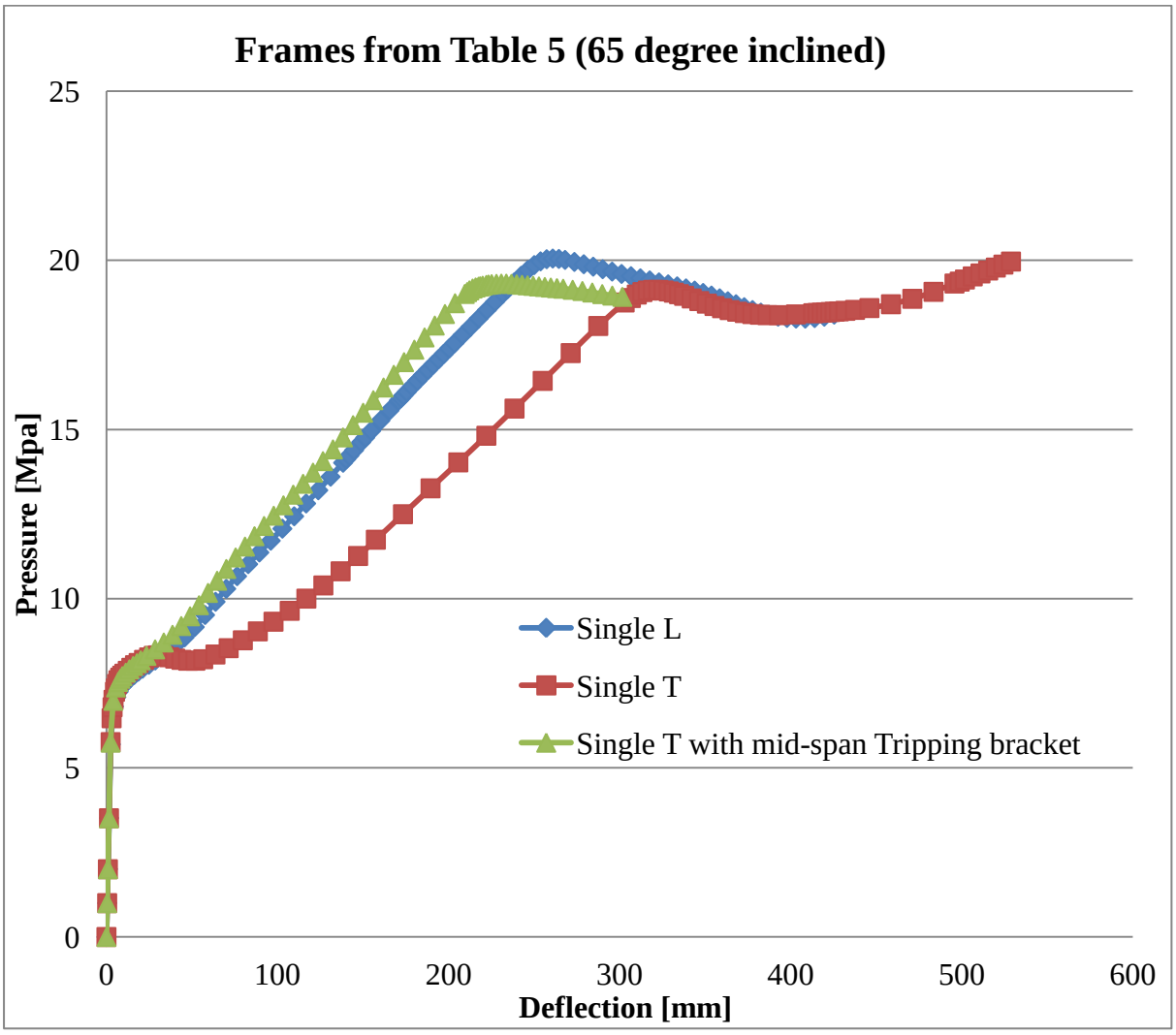

Figure 126 Load deflection curve of frame from table5- 65 degree web angle inclination

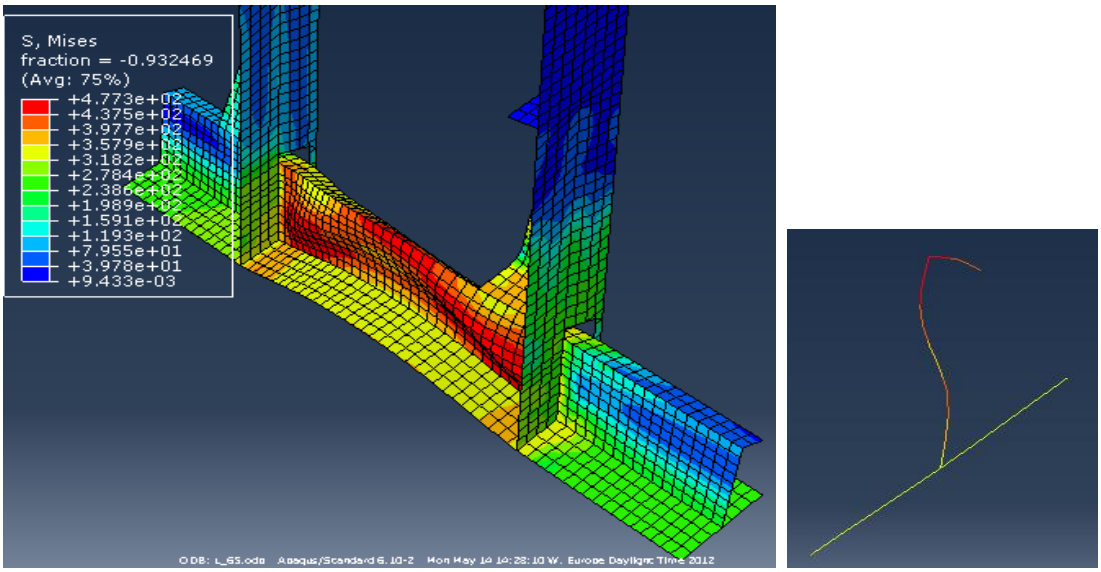

Figure 127 Plot of deformation (with Von Mises stress contour) and section at mid-span for 65 degree inclined single L frame subjected to load 15.262 MPa.

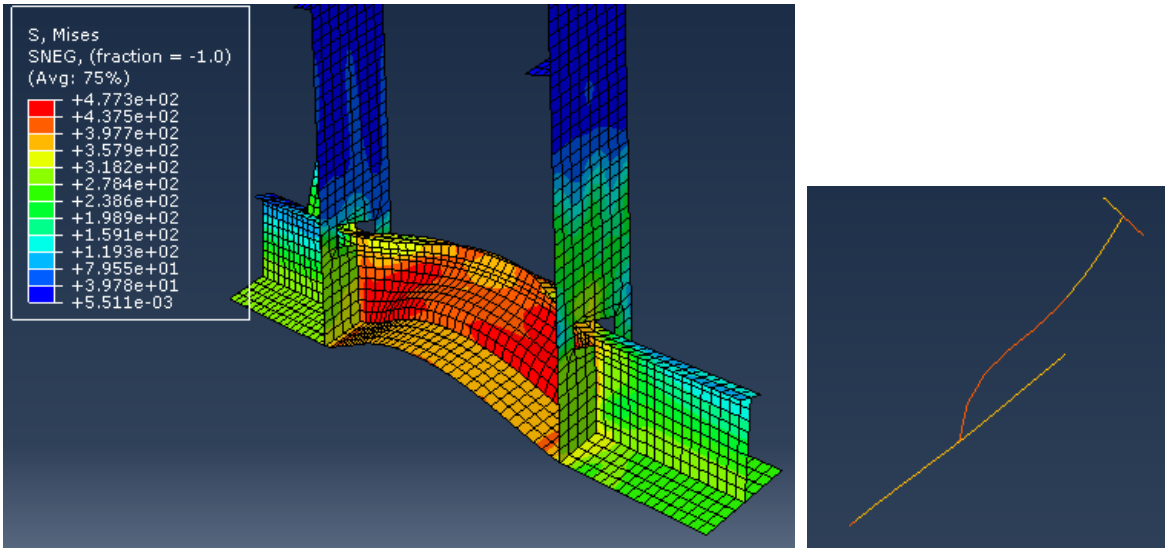

Figure 128 Plot of deformation (with Von Mises stress contour) and section at mid-span for 65 degree inclined single T frame subjected to load 14.8144 MPa.

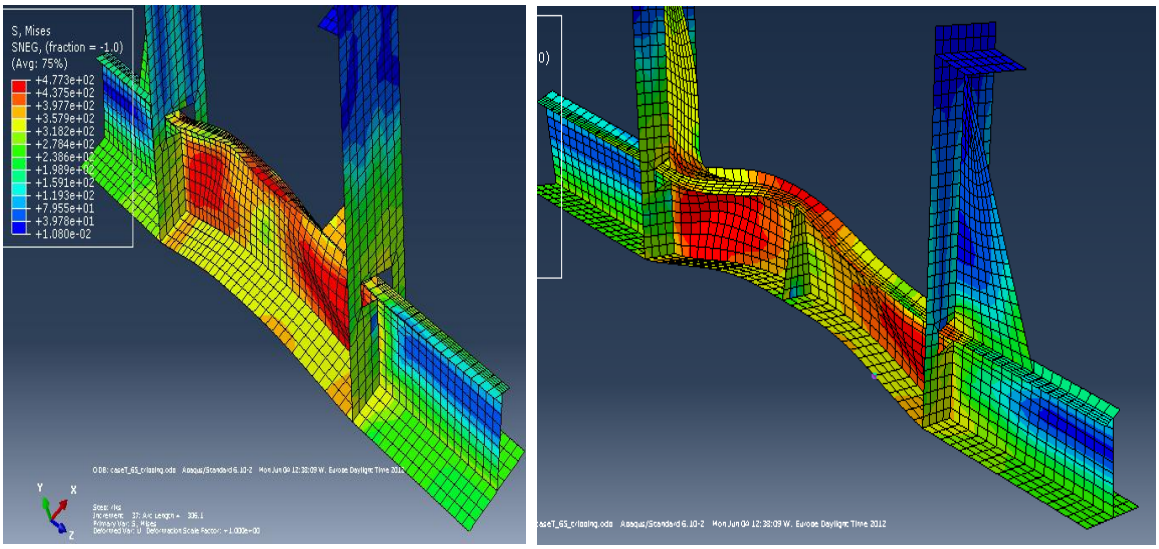

Figure 129 Plot of deformation (with Von Mises stress contour) for 65 degree inclined single T frame with mid-span tripping bracket subjected to load 14.8144 MPa.

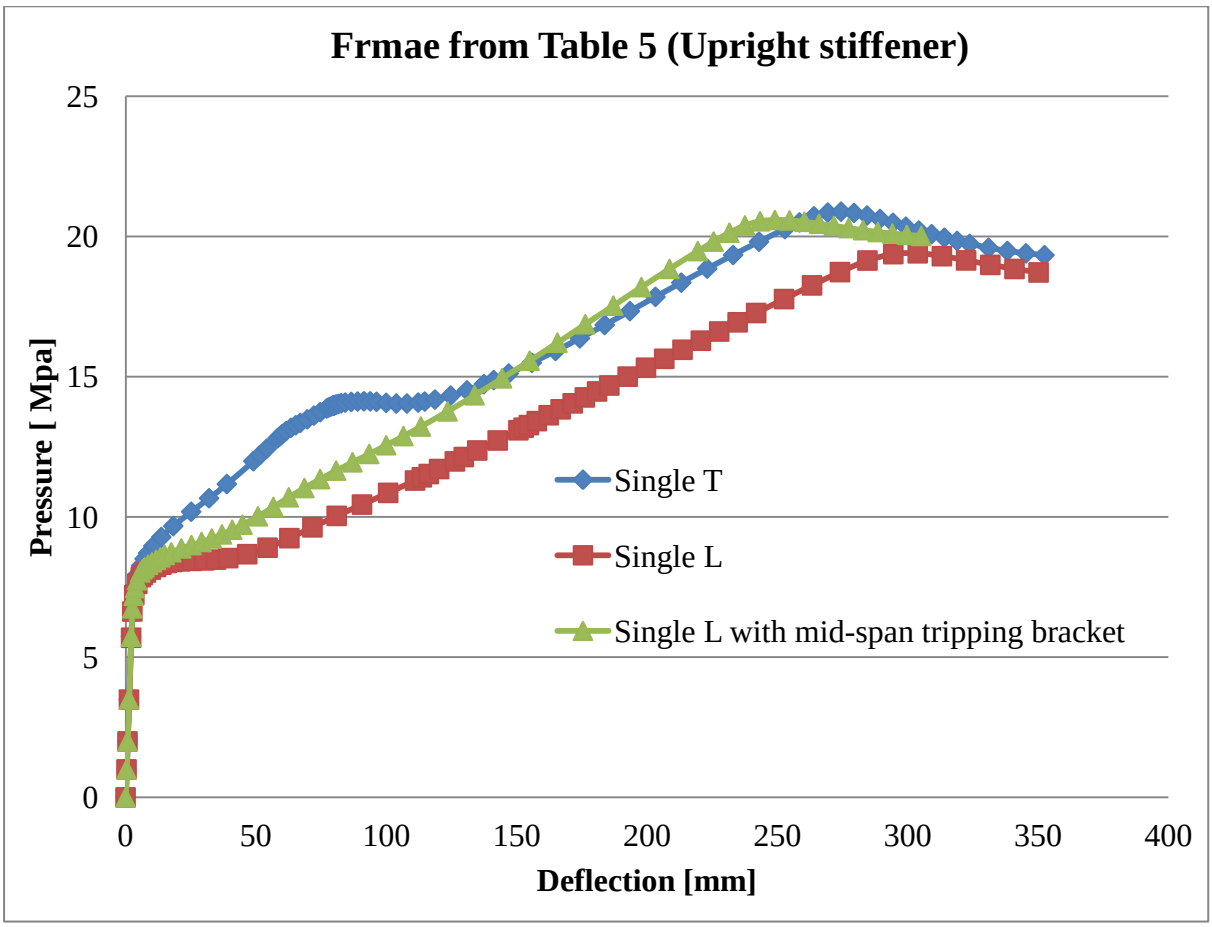

Figure 130 Load deflection curve of frame from table5

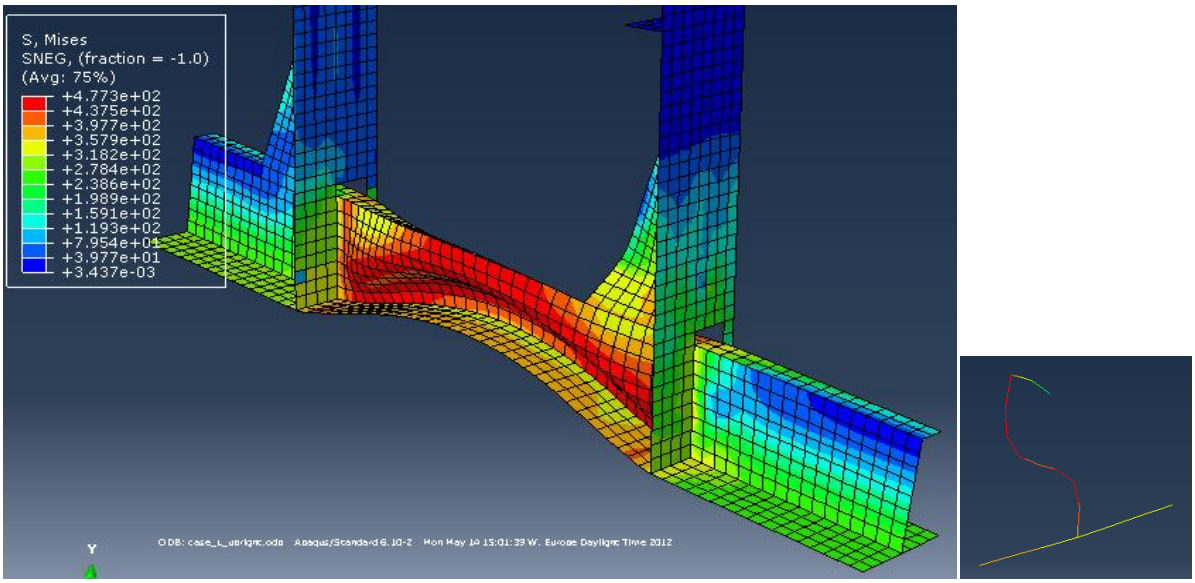

Figure 131 Plot of deformation (with Von Mises stress contour) and section at mid span for upright single L frame subjected to load 15.0049 MPa.

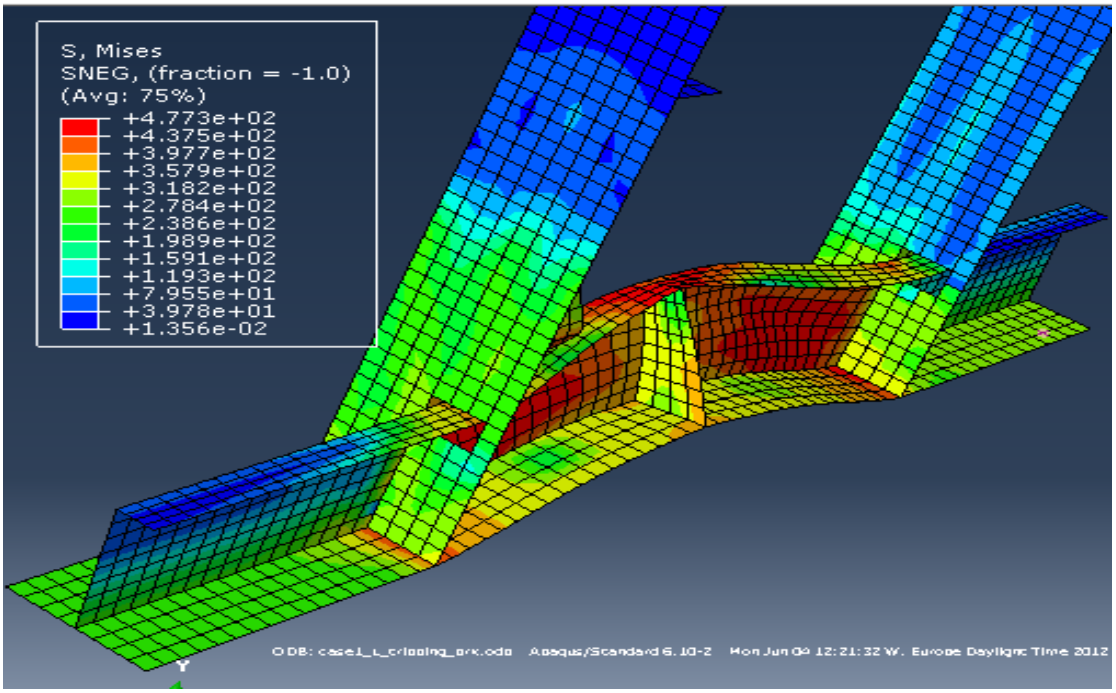

Figure 132 Plot of deformation (with Von Mises stress contour) for upright single L frame with mid-span tripping bracket subjected to load 15.57 MPa.

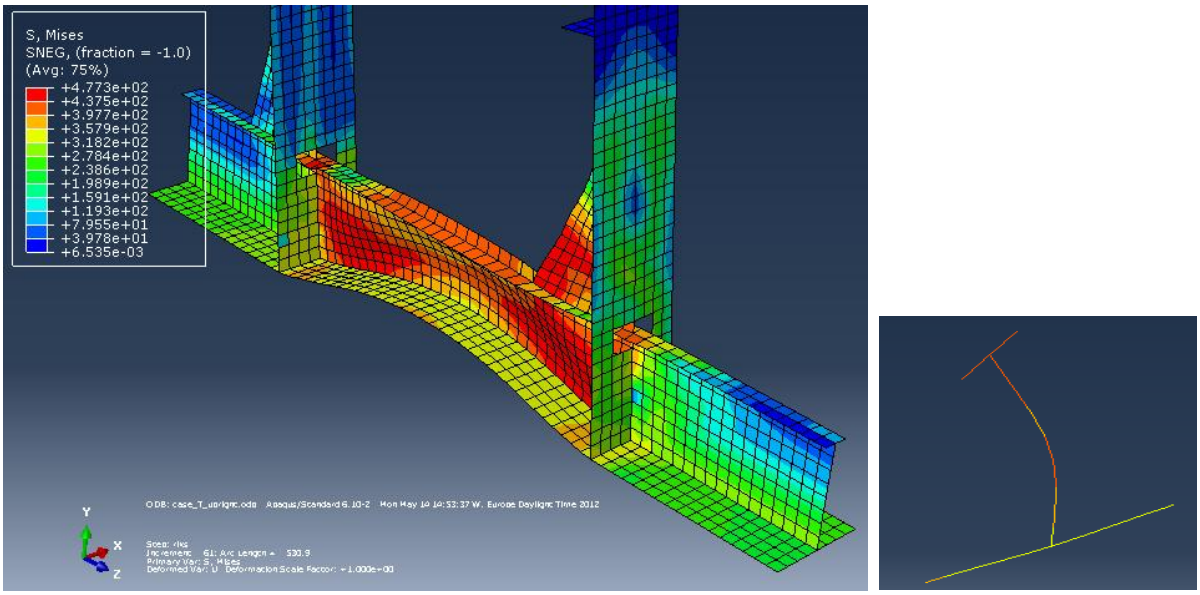

Figure 133 Plot of deformation (with Von Mises stress contour) and section at mid span for upright single T frame subjected to load 15.1149 MPa.